INFORMATION TO USERS

This manuscript has been reproduced from the microfilm master. UMI films the text directly from the original or copy submitted. Thus, some thesis and dissertation copies are in typewriter face, while others may be from any type of computer printer.

The quality of this reproduction is dependent upon the quality of the copy submitted. Broken or indistinct print, colored or poor quality illustrations and photographs, print bleedthrough, substandard margins, and improper alignment can adversely affect reproduction.

In the unlikely event that the author did not send UMI a complete manuscript and there are missing pages, these will be noted. Also, if unauthorized copyright material had to be removed, a note will indicate the deletion.

Oversize materials (e.g., maps, drawings, charts) are reproduced by sectioning the original, beginning at the upper left-hand corner and continuing from left to right in equal sections with small overlaps. Each original is also photographed in one exposure and is included in reduced form at the back of the book.

Photographs included in the original manuscript have been reproduced xerographically in this copy. Higher quality 6" x 9" black and white photographic prints are available for any photographs or illustrations appearing in this copy for an additional charge. Contact UMI directly to order.

UMI

A Bell & Howell Information Company
300 North Zeeb Road, Ann Arbor MI 48106-1346 USA
313/761-4700 800/521-0600

AN INNOVATIVE APPROACH IN MAGNETIC CARRIER TECHNOLOGY

Qingxia Liu

Department of Mining and Metallurgical Engineering

McGill University, Montreal

August, 1996

A Thesis Submitted to the

Faculty of Graduate Studies and Research

in partial fulfillment of the requirement of the degree of

Doctor of Philosophy

To my wife Bo Zhang

and my lovely son Meichen Liu

ABSTRACT

Magnetic carrier technology (MCT) has found a wide range of applications, including biological cell separation, waste remediation, and raw material recovery. The challenge to MCT is to develop a new method for the preparation of magnetic carriers with the following features: high density of reactive functional groups, diversity of functionalities, and durability of surface films. In this thesis, two novel methods, molecular self-assembly and silanation, were developed for the preparation of magnetic carriers.

In molecular self-assembly, 16-mercaptohexadecanoic acid ($HOOC-C_{15}H_{30}-SH$, i.e. MHA) was anchored onto the γ-Fe_2O_3 surface through chemical bonding between the carboxylic head group of the surfactant and iron on the surface, leaving the thiol or disulfide groups reactive. The molecular orientation of MHA self-assembled on γ-Fe_2O_3 was studied by x-ray photoelectron spectroscopy (XPS), diffuse reflectance infrared Fourier transform spectroscopy (DRIFTS) and film flotation. The self-assembled MHA film on γ-Fe_2O_3 was immobilized and resistant to acid and base attack. Magnetic carriers prepared as such showed a strong affinity to Ag^+ and Cu^{2+} ions in an aqueous solution.

In the preparation of magnetic carriers by silanation using 3-amino-propyltriethoxy silane (APTES), XPS, DRIFTS, and zeta-potential measurements indicated that direct silanation of APTES from either water or toluene solutions on bare magnetic particles was successful. In acid solutions, APTES films silanized on bare magnetic particles from toluene were more stable compared to the ones silanized from water. Both films were unstable in alkaline solutions. To improve the stability of silanized films, a thin silica layer was coated onto the magnetic particles using the sol-gel process, followed by dense liquid silica coating. Magnetic carriers with amino groups were prepared by the silanation of silica coated magnetic particles using APTES in toluene. Stability tests indicated that the silanized films on silica coated magnetic particles were more stable than the ones silanized on bare magnetic particles.

Magnetic carriers with reactive amine groups were proved to be effective for removal or recovery of heavy metal ions such as Cu^{2+} and Zn^{2+} from aqueous solutions. Loaded metal ions on magnetic carriers were completely stripped off by 0.01 M nitric or hydrochloric acid. The possible recycling of magnetic carriers could offset the high price of magnetic carriers and lower the cost associated with industrial applications. Applications of magnetic carriers with reactive amine and thiol groups in biological cell separation, immobilization of enzymes, magnetic fluids, and waste remediation were also discussed.

RÉSUMÉ

La téchnologie des porteurs magnétiques (MCT) a donné lieu à de nombreuses applications, dont la séparation de cellules biologiques, la remédiation des déchets, et la récupération de matières premières. Le défi dans le domaine des MCT est de développer des nouvelles méthodes de préparation de ces porteurs magnétiques répondant aux critères suivants: simplicité de préparation, diversité des groupes fonctionels, et durabilité (robustesse) du film de surface. Deux méthodes, auto-assemblage moléculaire et "silanation" ont été développées pour la préparation de porteurs magnétiques.

Dans le cas de l'auto-assemblage moléculaire, l'acide 16-mercaptohexadecanoïque ($HOOC-C_{15}H_{30}-SH$, i.e. MHA) est ancré à la surface des particles de γ-Fe_2O_3. L'ancrage se fait par réaction chimique entre le groupe carboxylique et γ-Fe_2O_3 à la surface de la particule, laissant les groupes "thiolique" ou "di-thiolique" libres pour des réactions ultérieures. L'orientation moléculaire du MHA à la surface des particles de γ-Fe_2O_3 a été déterminée par spectroscopie photo-éléctrique à rayons X (XPS), spectroscopie infrarouge à transformée de Fourier par réflexion diffuse (DRIFTS), et flottation. Le film de MHA auto-assemblé à la surface des particules de γ-Fe_2O_3 est fermement immobilisé et résistant aux attaques acides et basiques. Les porteurs magnétiques ainsi préparés ont démontré une forte affinité pour des ions métalliques tels que Ag^+ et Cu^{2+} en solution acqueuse.

La préparation des porteurs magnétiques par "silanation" a utilisé le 3-amino-propyltriethoxy-silane (APTES). Des mesures par XPS, DRIFTS, et potentiel zéta ont démontré que la "silanation" directe (i.e., sans traitement préliminaire de la surface des particules) de l'APTES à la surface des particules magnétiques est possible dans le cas de solution acqueuse et dans le cas de solution à base de toluène. Dans le cas de solution acides, les films obtenus par "silanation" directe sur les particules magnétiques sont plus

stables pour la "silanation" dans le toluène que pour la "silanation" dans l'eau. Dans le cas de solution alkalines, les films sont instables pour les deux solvents. Afin d'améliorer la stabilité des films obtenus par "silanation", une dense mais fine couche de silica a été déposée à la surface des particules magnétiques en utilisant la méthode sol-gel, suivie d'une déposition de silica liquide dense. Des porteurs magnétiques avec fonction amine ont été préparés par "silanation" d'APTES dans une solution de toluène de particules préliminairement enrobées de silica. Les tests de stabilité sur les films ainsi préparées sur des particules préliminairement enrobées de silica ont montré une stabilité supérieure à celle obtenue lors de préparation par "silanation" directe sur les particules non enrobées.

Les porteurs magnétiques dotés de groupes réactifs amine ont montré leur efficacité pour l'élimination ou la récupération en solution acqueuse d'ions métalliques tels que Cu^{2+} ou Zn^{2+}. Les ions métalliques absorbés sur les porteurs magnétiques peuvent être complètement détachés de la surface des porteurs en les traitant par une solution d'acide hydroclorique (ou nitrique) à 0.01 M. L'opportunité de recyclage des porteurs magnétiques pourrait compenser le coût élevé de ces porteurs, et réduire les coûts associés à une application industrielle de ces porteurs. L'application des porteurs magnétiques avec groupes réactifs amine et thiol dans les domaines de la séparation de cellules biologiques, l'immobilisation des enzymes, les fluides magnétiques et les traitements des déchets sont aussi discutés.

Acknowledgments

I would like to express my sincerest gratitude and appreciation to my supervisor, Dr. Zhenghe Xu, for his guidance, encouragement, and invaluable advice throughout the course of this research. His wonderful suggestions for the organization of the thesis, fruitful discussions on modern colloid and surface chemistry, and critical reading of the manuscripts are also greatly appreciated.

I would also like to thank Professor J. A. Finch for his keen insight, enthusiasm and constant support during the program. Appreciation also goes to Professor A. R. Laplante for his kind support and help in enriching my knowledge of mineral processing.

I would like to thank Dr. S. H. R. Brienne and Dr. M. K. Shi for their helpful discussions and comments on DRIFTS and XPS analysis. Thanks also go to Yong Din and Ou Mao for their help in TGA and VSM measurements, respectively. I am indebted to S. R. Rao for his helpful discussion during the reading of manuscripts. Thanks also go to Ms. M. Riedeau and Mr. R. Langlois for their technical expertise in the laboratories, and Mr. J. Broomberg for his help in translating the abstract. I wish to thank Professor B. Lennox and Dr. Antonella Badia for providing us with the 16-mercaptohexadecanoic acid.

I would like to thank all the members of the mineral processing group for those valuable discussions, formal and informal, and their friendship. The financial support from Natural Sciences and Engineering Research Council of Canada is also acknowledged.

TABLE OF CONTENTS

LIST OF FIGURES

LIST OF TABLES

LIST OF APPENDICES

CHAPTER 1 INTRODUCTION

Stringent environmental legislation regarding the discharge levels of priority pollutants, such as heavy metals, is posing challenges to many industries, including mining and metallurgy, electroplating, paper making, textile, dye and pesticide manufacture, petroleum refining, and nuclear and agricultural industries (Patterson, 1995; Rao, et al., 1995). For example, the acid mine drainage (AMD) which is defined as the ground surface-water draining from a mining site is one of the most severe environmental problems facing the mining industry today. When sulfide minerals, particularly pyrite and pyrrhotite, are exposed to oxygen in water, they are oxidized to produce sulfuric acid. This acid, in turn, leaches out metals from other minerals into the surface or ground water. In Canada, many of the waterways around mining sites are contaminated, often from mines that have been closed for decades. The two provinces with the most extensive metal mining base, Ontario and Quebec, have over 2,000 abandoned mine sites, many of which may pose an acid drainage problem (Wang, et al, 1996). Depending on the sites, water from the AMD contains a different degree of metal contaminants. Above certain "threshold toxicity" levels, these contaminants can have a significant impact on the quality of surface and ground water. The toxic nature of many metal ions, even at trace levels, has been recognized for many years. For example, Cu(II), Cr(VI), and Zn(II) are found to interfere with biological oxidation by consuming enzymes required to oxidize organic matter. The accumulation of mercury in predatory fish, such as tuna and swordfish, due to contaminated water from paper processing and caustic-soda manufacturing, constitutes a major health hazard to humans. Many catastrophes, such as the one in Minamata Bay, Japan, have resulted in the death of humans from eating fish contaminated with mercury (Nemerow and Dasgupta, 1991). Biochemical transformations similar to those for mercury may convert arsenic, selenium, and tellurium to organic compounds much more toxic than their inorganic forms (McBride and Wolf, 1971). Clearly, it is necessary to develop technologies effective for removing various pollutants from contaminated water in order to preserve the high quality of living environments.

A wide range of technologies have been developed or considered for the treatment of industrial effluents in order to meet mandatory discharge standards. The most commonly used techniques are chemical precipitation (as either hydroxides, oxides or sulfides), adsorption, ion exchange, reverse osmosis, and ion flotation (also known as foam separation) (Rousseau, 1987). A brief review of these existing processes for heavy metal removal is given below.

1.1. EXISTING TECHNOLOGIES FOR HEAVY METAL REMOVAL

1.1.1 Precipitation

Precipitation is a well known process capable of removing heavy metals from aqueous solutions (Stumm and Morgan, 1995). In hydroxide precipitation, for example, the solution pH is raised by adding sodium hydroxide or lime to a regime where the solubility of the metal hydroxide is exceeded, thus resulting in the precipitation of heavy metals. Hydroxide precipitation is an effective method for the removal of large quantities of metals from contaminated water. The simplicity of the process has led to its extensive use in industry. Notable among problems associated with precipitation processes are solid-liquid separation and the ultimate disposal of the solid product which often contains a high water content, voluminous sludge. The inappropriate disposal of unstable precipitates may cause secondary contamination of water, since metal ions can be leached out from the sludge back into the aqueous environment. In addition, a polishing step is required for most precipitation processes in order to achieve low residual levels of metal ions in processed water. Precipitation of base metals as sulfides and oxides (e.g. ferrite) is preferred but often costly (Finch, et al., 1994; Huang, et al., 1988). The production of secondary resources could, however, offset the processing cost (Demopoulos, 1994). For example, gypsum, a valuable material for the construction industry, could be produced from the neutralization of acid mine drainage of high sulfate concentrations using lime. It is worth mentioning that only a few metals can precipitate to form a valuable solid product.

1.1.2 Adsorption

This process is based on the adsorption of soluble contaminants in solution onto a solid adsorbent. Adsorption of metal ions onto activated carbon, sandstone, fly ash, natural minerals (e.g. clay) and other surface reactive adsorbents has been widely used in waste water treatment and significant progress has been made in the past two decades. This method is capable of removing most toxic species, including Cu(II), Cr(VI), Pb(II), and Zn(II). Khalfaoui, et al. (1995) and Alaerts et al. (1989) reported that coconut shell-based activated carbon was effective for the removal of Cr(VI) from acidic electroplating wastewater. Huang et al. (1989) studied the adsorption characteristics of Zn(II) onto various hydroaluminosilicates and demonstrated a high zinc removal efficiency by adsorption. Most adsorption processes have only been tested at the pilot plant level, and the applicability to full scale treatment is effective only in the recovery of gold cyanide from its pregnant leaching solution (Marsden and House, 1992). Since most adsorption processes are performed in a column packed with adsorbents, a prefiltration step is needed for most industrial applications in order to remove finely-divided solids which may, otherwise, clog the channels available for transporting liquid. Regeneration of the adsorbent and the cost for carbon replacement are also issues to be concerned with.

1.1.3 Ion Exchange

The ion-exchange process relies on the exchange of certain undesirable cations or anions in wastewater with sodium, hydrogen, chloride, etc. in porous polymer resins of either a styrene or an acrylic matrix. The ion exchange process continues until the solution being treated exhausts the resin exchange capacity. When this point is reached, the exhausted resin must be regenerated by other chemicals which replace the ions captured in the ion exchange operation, thus converting the resin back to its original composition for reuse in the next cycle. The ion exchange resins were originally developed to reduce the hardness of domestic water (Nordell, 1951). Applications of industrial ion-exchange are expanding rapidly in different fields, ranging from the purification of low-cost commodities to the treatment of high-cost pharmaceutical

derivatives and precious metals such as gold and platinum (Bolto and Weiss, 1977; Appelbaum, 1968; Mehmet and Te Riele, 1984). Clogging and regeneration of resins, similar to that encountered in the adsorption process by activated carbon, may also be experienced in this process. In practice, wastewater to be treated by ion exchange is generally pre-filtered to remove suspended solids which could mechanically clog the resin bed.

1.1.4 Reverse Osmosis

When an ideal semipermeable membrane (one that is permeable to solvent but not solute) is placed between two compartments, one containing the pure solvent and the other a solution (solvent and solute), the solvent passes through the membrane to the solution side. This phenomena is called osmosis. The chemical potential from the solute concentration gradient causes the transport of solvent. The pressure that must be applied to the solution side to stop the solvent flux is called the osmotic pressure. Reverse osmosis is a membrane permeation process capable of separating solvent from a solution by forcing the solvent through the semipermeable membrane under a applied pressure greater than the osmotic pressure of the solute. To be used in the reverse osmosis process, the membrane must be (1) highly permeable to solvent, (2) highly impermeable to solute, (3) capable of withstanding the applied pressure without failure, (4) as thin as possible but with sufficiently high mechanical strength, (5) chemically inert and creep resistant, and (6) readily fabricated into configurations of high surface-to-volume ratios (Nemerow and Dasgupta, 1991). Reverse osmosis has found many practical applications including the preparation of high-purity water as a successor to distillation and as a precursor for ion exchange in ultrapure water systems; concentration of whey, milk, and maple sap in the food industry; recovery of salts, such as $NiSO_4$ from rinse water; concentration and partial fractionation of lignosulfonates in wood pulping; and the concentration and recovery of metals from many industrial effluents (Parekh, 1988). The apparent limitations of this approach are concerns with membrane lifetimes, loss in flux rate, relatively small amount of effluent that can be treated and limited types of materials that can be removed. Some solutions (strong oxidizing agents, solvents, and other organic

compounds) can cause dissolution of the membrane. Fouling of membranes by suspended solids in wastewater is another concern. For charged membranes the ion exchange between the feed solution and the membrane can cause shrinking or swelling of the membrane, which, in turn, affects the transport properties of the membrane (Parekh, 1988).

1.1.5 Ion Flotation

Ion flotation was first introduced by Sebba (1959). The basic principles of the technique were described in a number of publications (1960, 1962a, b, 1963, 1964, 1965). The method involves the removal of surface-inactive ions from aqueous solutions by the addition of surfactants capable of forming ion-surfactant pairs, and the subsequent passage of gas bubbles through the solutions. Due to the surface active nature of the surfactant, the ion-surfactant pairs are concentrated on the bubbles, and floated to the surface of the solution where they are removed as foams. In general, an ionic surfactant (known as collector in mineral processing) of opposite charge to the surface-inactive contaminants is used to induce an electrostatic force between them, thus forming ion-collector pairs. It is, however, possible to use a nonionic surfactant (i.e. neutral molecules) capable of forming coordination bonds with contaminants as a collector. One of the examples is the removal of Cu (II) ions by neutral dodecylamine molecules (Pinfold, 1972). Numerous investigations have been conducted to determine the propensity of various surfactants in removing metal ions from dilute solutions. Ion flotation has been applied to a wide range of problems other than base metal recovery, including waste water treatment, removal of radioactive elements from water, and the recovery of precious metals (Rubin, et al., 1966; Charewicz and Gendolla, 1972; Davis and Hass, 1972; Berg and Downey, 1980; Nicol, et al., 1992). The major advantage of ion flotation over activated carbon adsorption is that air bubbles are relatively inexpensive to produce and no desorption step is required. However, a stoichiometric ratio of surfactant molecules to ions to be floated is needed in ion flotation. The process can, therefore, be quite expensive and may only be used to float ions in solutions of low concentration.

1.1.6 SiroFloc/Heavy Metal Process

The Sirofloc/Heavy metal process was developed recently. In this process, magnetic seeds (magnetite) were added as nucleation centers for hydroxide precipitation. The loaded magnetite was separated using a magnetic separator and then treated with acid to generate a small volume of concentrated effluent with the magnetite ready for reuse in the next cycle (Dixon, 1992). Apparently, this process is suitable for metals that can readily form precipitates on magnetite, but fails if homogeneous bulk precipitation prevails or if the precipitation of metals is not effective. An inherent difficulty of this approach is to select conditions under which all unwanted species precipitate, otherwise, a multistage treatment may be required.

In summary, each technique reviewed above has its own limitations in industrial applications. For example, the high percentage of suspended solids in solution interferes with the adsorption, ion exchange, and reverse osmosis processes. The cost of surfactant in ion flotation is a concern. Obviously, there is a need to develop a versatile technique suitable for effective removal or selective recovery of metals from industrial effluents at a relatively low cost.

1.2 MAGNETIC CARRIER TECHNOLOGY

For the selective recovery or removal of heavy metals from voluminous industrial effluents of high metal concentrations and suspended solids, the use of magnetic carrier technology (MCT) is of particular importance, as the technique combines the advantages of technical flexibility, economic value, and environmental acceptability.

MCT originated in the early 1940s from the study on wastewater treatment where the objective was to adsorb organic matter onto small magnetite (Fe_3O_4) particles and to subsequently separate the loaded magnetite from the process liquor by magnetic separation (Urbain and Stemen, 1941). In its broadest application MCT refers to the tailoring of physical, chemical and surface properties of magnetic carriers to enable

selective or non-selective attachment of molecules, macromolecules, biological cells, colloidal particles and metal ions to the carriers. Magnetic particles (carriers) with their load of target species such as metal ions, biological cells and toxic organic matter can be captured by exposing them to a magnetic field gradient, thus allowing them to be separated efficiently from the streams. The application of MCT in the removal of contaminants is shown schematically in Figure 1.1.

The target species, such as heavy metals loaded onto the surface of magnetic carriers, can then be stripped off by acid washing, thus enriching the concentration of metal ions for the subsequent recovery by electrowinning. The magnetic carrier, after stripping off loaded metal ions, can be reused. A hypothetical process for heavy metal removal using MCT is shown schematically in Figure 1.2.

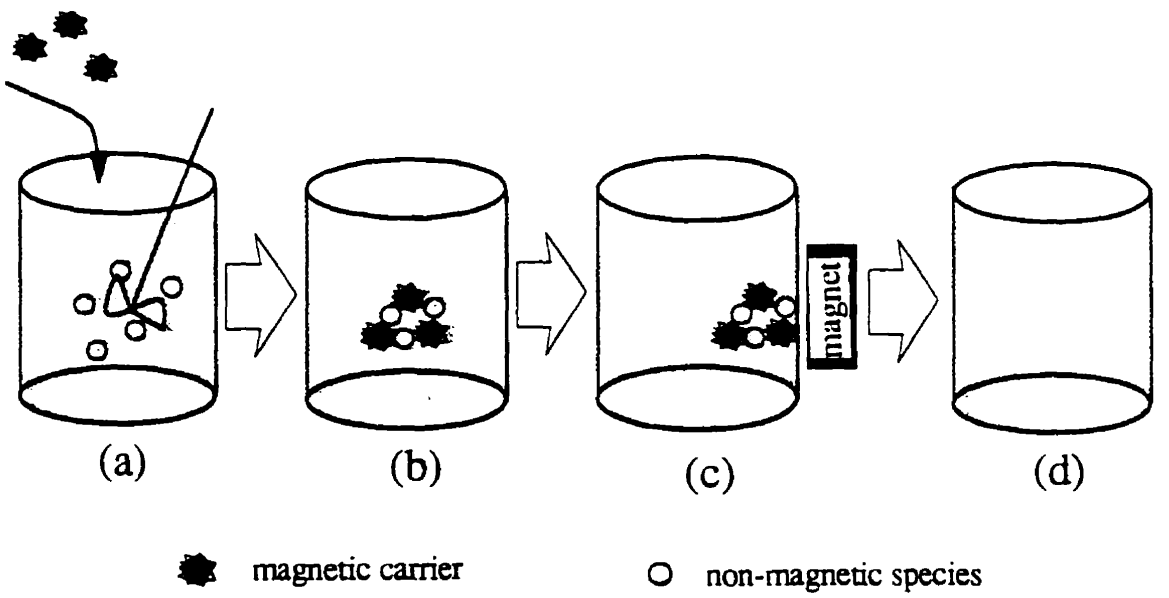

Figure 1.1 Schematic representation of magnetic carrier technology. (a). Magnetic carriers with reactive functional groups on the surface are added to a solution containing non-magnetic species to be removed or recovered; (b). Non-magnetic species attached to the magnetic carriers; (c). Magnetic carriers with their load of selected species are attracted by an external magnetic field and then separated from the stream; (d). Purified solution after removal of non-magnetic species.

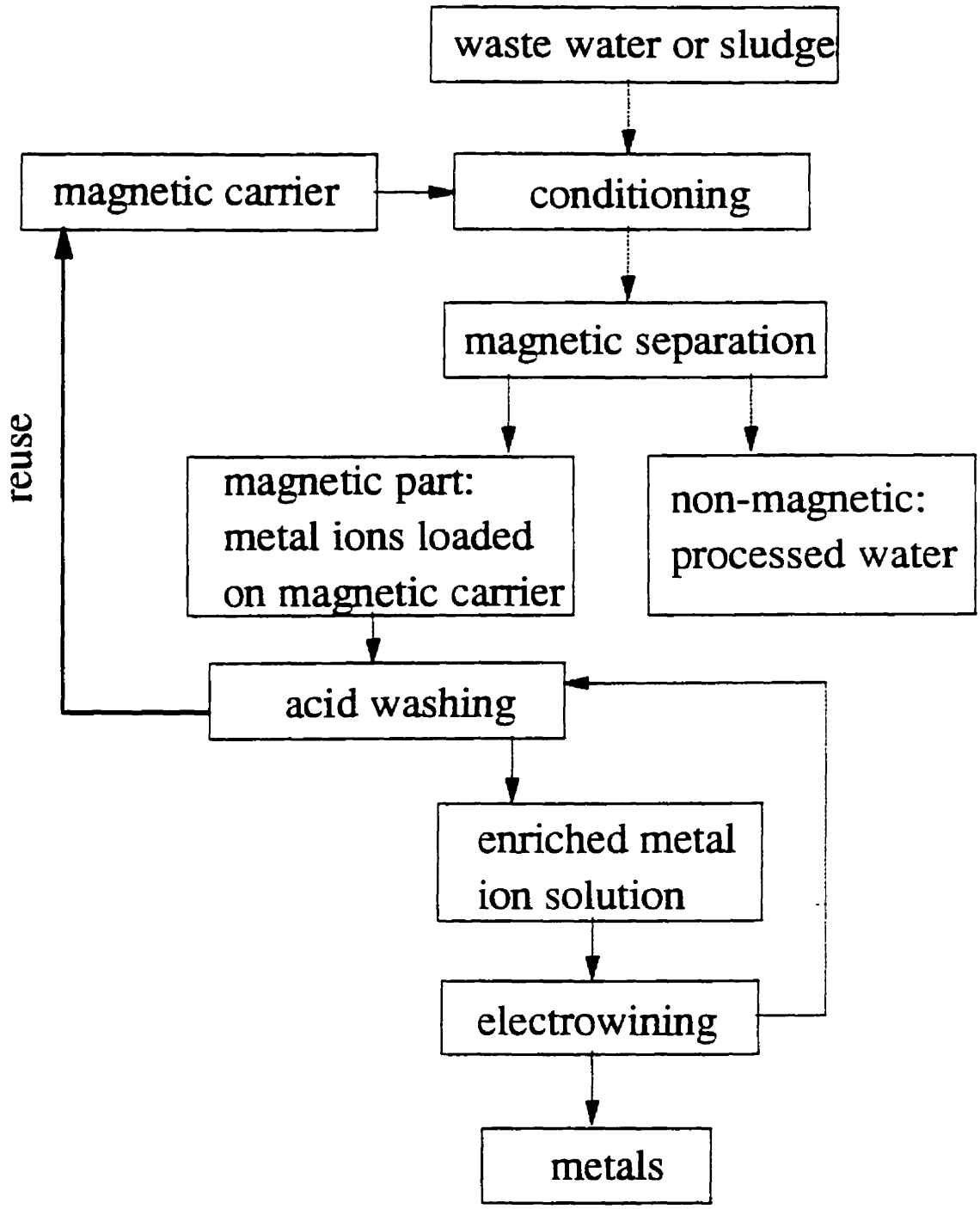

Figure 1.2 Flow diagram for recovery/removal of metal ions using MCT.

Magnetic carrier technology has the following features:

1. selective removal or recovery of target metal ions using functionalized magnetic carriers;
2. high loading efficiency of nanosized magnetic carriers due to their large specific surface areas;
3. high solid-liquid separation efficiency by magnetic separation; suitable for large volumes of industrial effluents;
4. less interference from particulates often present in the industrial effluent;
5. economic benefits from recovering metals and recycling the magnetic carriers.

In order to incorporate MCT into industrial processes, it is essential to prepare magnetic carriers with the following properties:

- reactive functional groups on the surface capable of capturing metal ions from solution, and also allowing the loaded metal ions to be stripped off;
- robust thin organic film on the surface which can tolerate harsh conditions encountered in industrial processes;
- suitable magnetization for magnetic separation;
- high density of functional groups for high loading efficiency;
- ability to be redispersed and reused in subsequent cycles;

In essence, MCT involves the preparation of functionalized magnetic carriers and their subsequent removal from the streams after loading target species. An integrated interdisciplinary approach for the manufacture and surface hybridization of appropriate carriers with careful attention to the constraints imposed by the subsequent applications is, therefore, required. In this respect MCT can be regarded as a prime example of using colloid and surface engineering principles to yield a step change in technology. The challenge to MCT in a variety of applications, such as biological cell removal, raw material and metal ion recovery, is to develop a new method for the preparation of magnetic carriers with the above mentioned features, which is the focus of this thesis.

1.3 METHODS FOR THE PREPARATION OF MAGNETIC CARRIERS

Many methods have been developed to prepare magnetic carriers. These include polymer adsorption and polymerization (Ugelstad, 1992), bilayer formation of amphilphiles (Huang, 1990; Wooding, et al., 1992; Menager and Cabuil,1995), silanation by organofunctional silane (Whitehead, et al., 1987; Albert, et al., 1989), and ligand complexation on magnetic particles (Briggs, et al., 1977). Either a single reaction or several steps are required in order to prepare desirable magnetic carriers. Generally, a probing molecule or reactive functional group on magnetic carriers has a specific affinity to targeted biological cells or metal ions as shown in Figure 1.3. The interaction between fabricated magnetic particles and target molecules can be described by a key-and-lock relationship. Such specific interactions as antibody-antigen, biotin-streptavidin and ligand-metal have been incorporated into MCT for selectively removing the target cells from biological system and metal ions from industrial effluents (Thomas, et al., 1992; Spinke, et al., 1993; Nunez, et al., 1995). The following is a brief summary of the current status of various methods for preparing magnetic carriers.

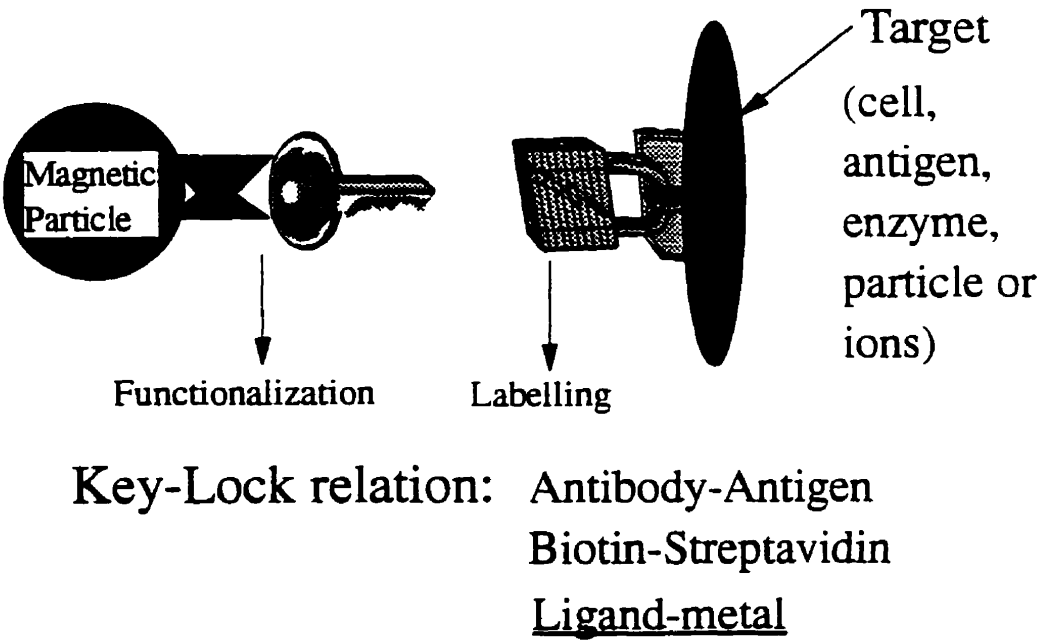

Figure 1.3 Schematic diagram for designing magnetic carriers for target species.

1.3.1 Polymer Adsorption and Polymerization

Polymer adsorption and surface polymerization have been used to fabricate magnetic carriers. Co-precipitation of Fe^{2+} and Fe^{3+} with polymers under similar conditions to those used in the production of synthetic magnetite has also been used to prepare magnetic resins. This technique can produce submicron magnetic particles with chitosan (Yen, et al., 1981), dextran (Molday and Mackenzie, 1982; Molday, 1984) and polypyrrole (Qi, 1995) functionality. The density of functional groups on polymer-coated magnetic particles is, in general, lower than those prepared by molecular bilayer assembly. This limitation is associated with the dangling and coiling of polymer molecules on the surface. As a result the subsequent uptake of target cells or particles will be retarded for steric reasons (Albert, et al., 1989).

1.3.2 Molecular Bilayer Assembly Using Amphiphiles

In many applications, a magnetic carrier has been prepared by building two layers of surfactants on colloidal magnetite (nanometer size in most cases) as shown in Figure 1.4a (Huang, 1990). The inner layer surfactant has a functional group with an affinity for magnetite. The outer layer of surfactant can be built on top of the inner layer through hydrophobic association between hydrocarbon chains. The functional group of the outer layer orients outwards from the magnetite and provides the capability for coupling with the target species. Since the functional group of the outer layer can be tailored, the selectivity of the coupling can be controlled. A similar bilayer molecular architecture has been engineered on the surface of magnetic particles using a phosphate lipid through the formation of liposomes (Menager and Cabuil, 1995). This type of magnetic carrier with phosphate lipids on the surface has the feature of biological compatibility and could be used in drug delivery and drug encapsulation. The main drawback of magnetic carriers prepared as such is that the outer layer can be unstable when in contact with metal ions in application, resulting in the loss of capacity and functionality. This can be overcome by self-assembling a monolayer using a bolaamphiphile with two functional groups at both ends of a alkylchain. By controlling the relative reactivity of the two functional groups

with the surface, one functional group can anchor chemically onto the magnetic particles and the other remains reactive as shown in Figure 1.4b. Exploration of this approach is one of the objectives of this thesis.

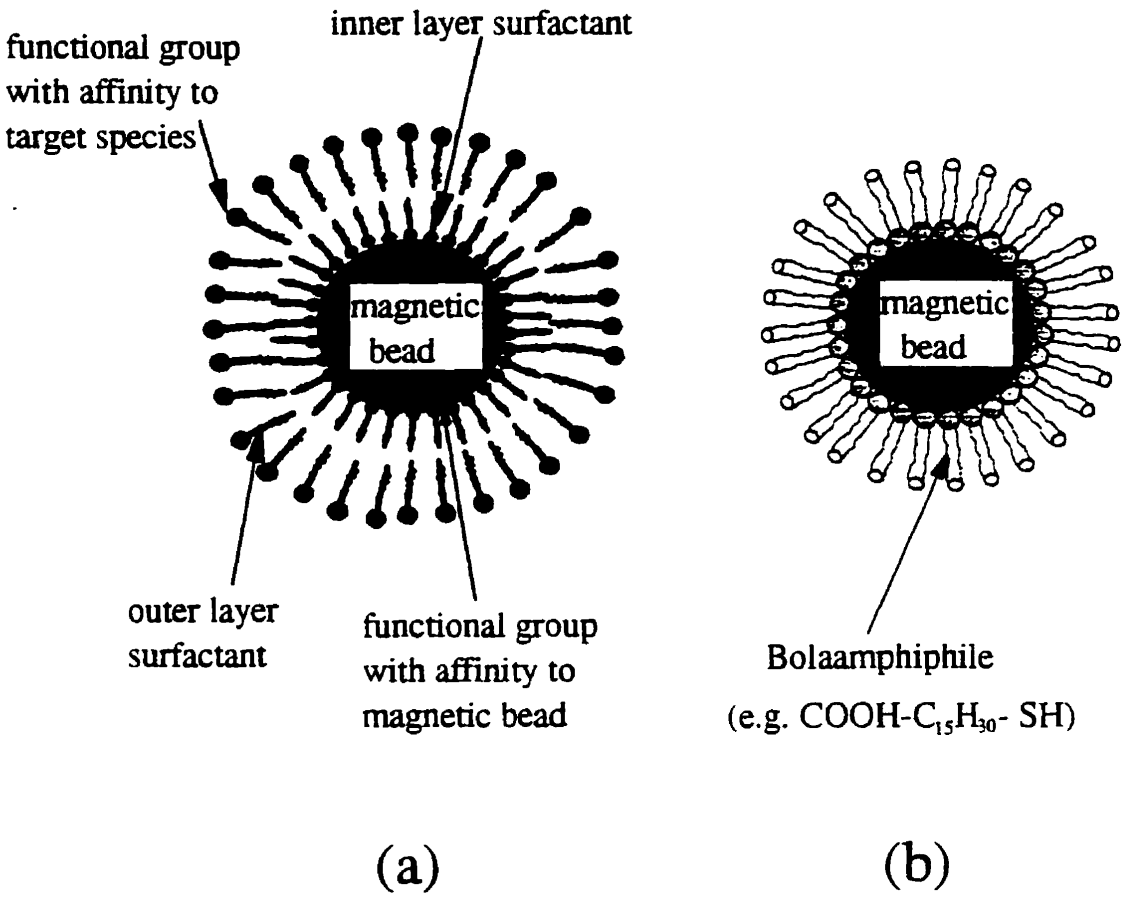

Figure 1.4 Schematic pictures for (a) Bilayer assembly using amphiphiles on magnetic particles; (b) Monolayer assembly using bolaamphiphiles on magnetic particles.

1.3.3 Silanation Using Silane Coupling Agents

The most widely used techniques for covalently placing reactive organic groups on inorganic surfaces is through the reaction of inorganic surface with silane coupling agents which have dual functionalities, inorganic group at one end and organic group at the other (Plueddemann, 1982). The inorganic functional group (silanol) can condense

with surface hydroxyl groups on the substrate through chemical bonding, and the organic functional group at the other end retains the reactivity with the target species in solution (Plueddemann, 1982). Silanation of magnetic particles (Fe_3O_4) with 3-amino-propyltriethoxy silane (APTES) or 3-mercapto-propyltriethoxy silane (MPS) for the preparation of magnetic carriers and their applications in biological separation were patented by Whitehead, et al. (1987). They confirmed the presence of silanes on iron oxide particles based on the following observations: After treating the silanized particles with 6N HCl solutions, the iron oxide was dissolved and a white, amorphous residue was left in solution which was not present if the unsilanized iron oxide was similarly digested. The acid insoluble residue was believed to be polymerized silane. However, there is no detailed report in this patent on (i) how the stability of silanized films was; (ii) how the silane coupling agents reacted with the surface: and (iii) how the reaction conditions, such as the type of solvents, reaction and post curing temperatures, were controlled. Stable silanized films have been reported to form on some oxides such as aluminum, zirconium, tin, titanium, and nickel (Arkles, 1992). The films formed on oxides of boron, iron, and carbon were found less stable, and alkali metal oxides and carbonates did not form stable bonds with silane coupling agents (Arkles, 1992). It is well documented that the most stable thin organic films formed by silanation are those on silica (Plueddemann, 1982). Therefore, an approach to improve the stability of silanized thin organic films on magnetic particle by silanation is to coat the magnetic particles with a thin layer of silica before silanation, which will be pursued in this thesis.

1.4 OBJECTIVES OF THIS WORK

The overall objective of this research is to develop new methods for preparing magnetic carriers that have potential uses in the recovery or removal of metal ions from industrial effluents. Specifically, this program is designed to:

1. develop a novel method for preparing magnetic carriers by molecular self-assembly and silanation;

2. characterize the functionality and coating density of the prepared carriers using surface sensitive techniques such as diffuse reflectance infrared Fourier transform spectroscopy (DRIFTS), X-ray photoelectron spectroscopy (XPS), zeta-potential measurement, thermal gravimetric analysis (TGA), and film flotation;
3. examine the stability of organic thin films on prepared magnetic carriers;
4. determine the selectivity and efficiency of magnetic carriers in the removal of different metal ions such as silver, copper, and zinc from solution;
5. investigate the stripping off of metal ions from magnetic carriers by acid washing;
6. evaluate the possibility of recycling and regenerating magnetic carriers, which completes the testing of hypothetical approach given in Figure 1.2.

1.5 STRUCTURE OF THE THESIS

Molecular self-assembly and silanation are the two methods that have been adopted for the preparation of magnetic carriers in this work. This thesis contains eight chapters.

Chapter one introduces the traditional physical-chemical methods for heavy metal removal. The comparison of these methods with the magnetic carrier technology (MCT) is made and the advantages of using MCT are presented. The current state of preparing magnetic carriers is reviewed, followed by the objectives and the structure of the thesis.

Chapter two reviews some characterization techniques used in this thesis. These include infrared spectroscopy, X-ray photoelectron spectroscopy, thin film flotation and zeta-potential measurement, and thermal gravimetric analysis. Examples of these techniques applied to the thin organic film characterization and to the study of mineral flotation system are given. The vibrating sample magnetometer is also briefly discussed as it is used to characterize the magnetization of magnetic carriers.

Chapter three introduces a novel method for the preparation of magnetic carriers using molecular self-assembly of bolaamphiphiles (16-mercaptohexadecanoic acid, $SH\text{-}C_{15}H_{24}$-

COOH) on magnetic particles (γ-Fe_2O_3). The self-assembled layers on the magnetic carriers are characterized by X-ray photoelectron spectroscopy (XPS), diffuse reflectance infrared Fourier transform spectroscopy (DRIFTS), and vibrating sample magnetometer (VSM). The molecular orientation of the surfactants on particles was inferred from the critical surface tension values determined by film flotation and confirmed by infrared spectroscopy. The packing density of the surfactant molecules in self-assembled monolayer is derived from XPS analysis and thin film flotation. The stability of self-assembled monolayer is studied by leaching test.

Chapter four presents the results of the preparation of magnetic carriers by direct silanation on bare magnetic particles using silane coupling agent, 3-aminopropyltriethoxy silane (APTES). The effects of solvents and curing temperatures on silanation are discussed. The stability of the silanized films is examined.

Chapter five describes the techniques for thin layer silica coatings on magnetic particles, including sol-gel and dense liquid silica processing. A novel two-step silica coating process, sol-gel followed by dense liquid silica is developed, which produces a stable, densely packed thin silica layer on the surface. Silica-coated magnetic particles are more amenable for the silanation.

Chapter six discusses the silanation of silica coated magnetic particles using APTES in toluene. The improved stability of silanized films on such surfaces are demonstrated.

Chapter seven presents the examples of the applications of prepared magnetic carriers in heavy metal removal. Stripping off metal ions from loaded magnetic carriers and reuse/regeneration of magnetic carriers are described.

Chapter eight presents the overall conclusions and recommendations for future work.

In appendices the recipes for silica coatings by sol-gel and dense liquid silica processes are presented.

CHAPTER 2 CHARACTERIZATION TECHNIQUES

2.1 INTRODUCTION

The nature of the surfactant used and its orientation on the magnetic particles governs the functionality of the magnetic carriers. However, the chemical bonding between the functional groups of the surfactant and the particle surfaces determines the stability of the thin organic films on the magnetic carriers (Ulman, 1991). An understanding of the interactions between the surfactant molecules and the magnetic particles is essential for controlling the orientation of molecules on the surfaces, and hence the functionality of the magnetic carriers. Surface characterization techniques are often used to elucidate the orientation of surfactant molecules on the surface and to examine the nature of the chemical bonds between the functional groups of the surfactant and the particle surfaces. A brief discussion on characterization techniques used in this study is, therefore, given in this chapter.

Most surface analytical techniques are based on the interactions of electromagnetic "particles" or "waves" with samples, which generates a signal radiation detected or/and analyzed by proper detectors. Based on the sources of excitation and the modes of emission, various analytical techniques such as X-ray photoelectron spectroscopy (XPS), secondary ions mass spectroscopy (SIMS), and infrared spectroscopy (IR) have been developed. The various spectroscopic techniques are shown schematically in Figure 2.1. Among the techniques widely used today, using electrons as an excitation source results in the highest spatial resolution (e.g. Auger electron spectroscopy); using photons as the excitation source features the highest energy resolution (e.g. XPS); while using ions as the excitation source gives the highest sensitivity (e.g. SIMS).

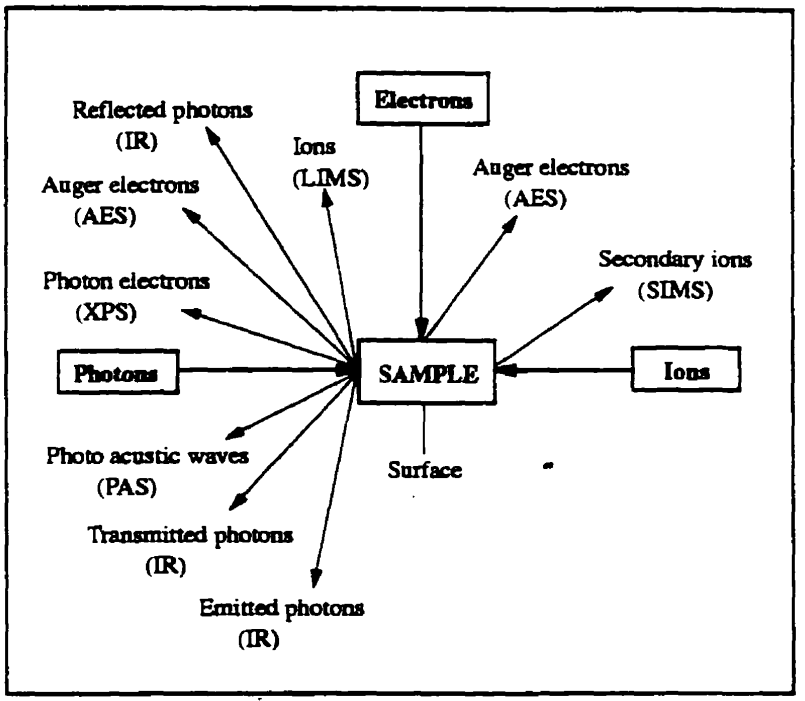

Figure 2.1 Schematic picture of spectroscopic techniques

Many of these techniques have been extensively used to study physiochemical interfacial properties of thin organic films on metal oxides. For example, the orientation and packing of surfactant molecules in thin organic films on metal oxides have been studied by infrared spectroscopy with various sampling methods (Hair, 1967). The chemical composition and monolayer structure of surface films have been determined by X-ray photoelectron spectroscopy (XPS) (Briggs and Seah, 1990). The complementary techniques such as scanning tunneling microscope (STM), atomic force microscope (AFM) and ellipsometry have also been used to study the topography and thickness of surface films at the molecular scale (Sarid, 1991; Azzam and Bashara, 1977; Birzer and Schulzer, 1986). Some traditional techniques have also found their way into modern surface science. Contact angles measured by a goniometer with different probing liquids, for example, were used to evaluate wetting properties (Lee, 1993), surface-free energies (Fowkes, 1964; Van Oss, 1994), and to get information on surface forces (Xu, et al., 1996). Some of these techniques are not suitable to study surface films on fine powder samples, and each technique has its own merits and drawbacks. A judicious combination

of different analytical techniques is, in most cases, needed to draw a complete picture of surface coatings.

In order to perform meaningful surface analysis and interpret the results, it is necessary to understand the nature of interactions between the excitation beam and samples and the production/detection of signals. It is beyond the scope of this thesis to give a detailed description of the physical background for every surface analytical technique; but a brief discussion of the techniques used in this work should be useful and is thus given as follows.

2.2 FOURIER TRANSFORM INFRARED (FTIR) SPECTROSCOPY

Infrared spectroscopy is widely used in determining the chemical structure of organic molecules. This technique is based on the absorption of infrared radiation by organic molecules which causes the changes in vibrational and rotational energy states of the molecules. For a simple molecule, the amount of energy required to change the vibrational energy level from one state to another is related to the molecular vibrational frequency (ν) by Planck's Law:

$$E = h\nu \tag{2.1}$$

where the vibrational frequency is derived from ordinary mechanical model (Simple Harmonic Oscillator Model) and is given by:

$$\nu = \frac{1}{2\pi}\sqrt{\frac{K}{\mu}} \tag{2.2}$$

where K is the force constant of the bond between two atoms (N/m); and μ is the reduced mass related to the masses of the individual atoms in the bond by:

$$\mu = \frac{m_1 m_2}{m_1 + m_2} \tag{2.3}$$

in which m_1 and m_2 are the mass of atoms 1 and 2, respectively.

The radiation frequency can also be expressed in wavenumber ($\bar{\nu}$) as:

$$\bar{\nu} = \frac{1}{2\pi c}\sqrt{\frac{K}{\mu}} = 5.3\times 10^{-12}\sqrt{\frac{K}{\mu}} \qquad (2.4)$$

where $\bar{\nu}$ is the wavenumber of absorption peak (cm^{-1}) and c is the velocity of light in cm/s.

It can be seen from equation (2.4) that higher radiation energy is needed to cause a change in vibrational energy state of the molecules with a bond of greater force constant and/or smaller masses of atoms. Thus, IR bands will appear at higher wavenumbers for stronger bonds and/or a smaller mass of the bonded atoms. For example, IR bands for C-C, C=C, and C≡C appear at wavenumbers of ca. 1429, 1667, and 2222 cm^{-1} respectively, because the force constant of a carbon/carbon bond is in the order of single < double < triple. Similarly, the bands of metheylene antisymetric and symmetric stretching modes appear at higher wavenumbers for gauche conformations of alkane chains in monolayer than that for well packed ones in trans conformations. Compared to stretching vibrations, the bending vibration requires less energy, and thus corresponding bands appear at lower wavenumbers. The difference in the absorption of radiation energy for various vibrational modes gives rise to a pattern of IR bands (i.e. spectrum).

The instrument used in the past were dispersive spectrometers that consisted of a polychromatic radiation source, a monochromator and a detector. This type of apparatus has now been superseded by Fourier Transform infrared (FTIR) spectrometer which has a number of advantages. The most significant advantages are the high sensitivity and fast spectra acquisition in addition to high accuracy and precision in wavelength determination. A few sampling techniques are often used in FTIR spectrometer including transmission, external and internal reflection, diffuse reflection and photo-acoustic spectroscopy.

2.2.1 Transmission Infrared Spectroscopy

In the transmission mode, the radiation passing through the sample is detected. For powder samples, KBr is often used as the matrix or dilutent in preparing the sample pellets since KBr is transparent in the middle IR range. The possible problems in this method are the interactions of chemicals to be detected with KBr and the need for dry powder samples. The low surface sensitivity has limited this technique to the bulk characterization.

In the reflection technique, three types of sampling modes are available for different applications: external reflectance, internal reflectance and diffuse reflectance.

2.2.2 External Reflectance Infrared Spectroscopy

In this mode, the single IR beam is directed to a highly reflective sample surface and the reflected IR radiation is detected. External reflectance spectroscopy is particularly useful for studying the structure of thin organic films on the surface that strongly reflects the incident beam. For substrates of relatively low reflectivity, the sensitivity of the technique is reduced. The advantages of external reflectance IR spectroscopy are that the incident beam can be polarized and the incident angle can be controlled to probe the orientation of molecules on the surface as shown in Figure 2.2. Two beams, i.e., incident (i) and reflected (r), form a plane called the plane of incidence. The angle θ of incident beam to the normal of the surface is known as the incidence angle. When the electrical field of IR

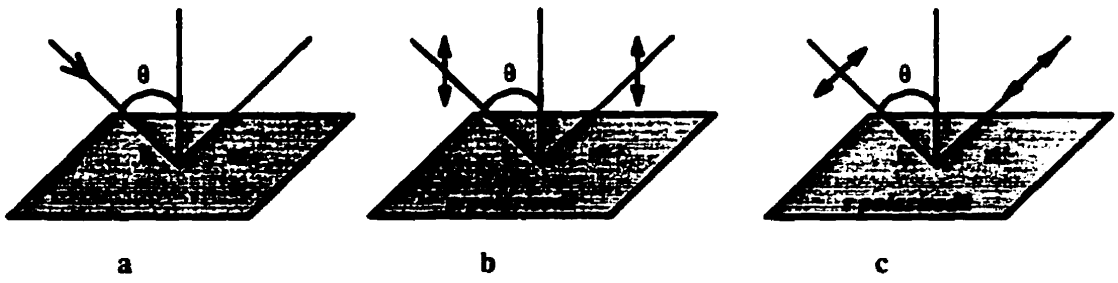

Figure 2.2 Optical schematic of an external reflectance.

radiation is polarized to have a component parallel to the plane of incidence, p-polarization is obtained (Figure 2.2b). If the electrical field vectors are oriented perpendicular to the plane of incidence, the radiation is s-polarized (Figure 2.2c).

The first application of this technique to metal surfaces was reported by Grenler (1966). Adsorption and orientation of xanthates and other thiol collectors on copper metal and cuprous sulfide (chalcocite) electrodes, with and without applied potential, have been investigated by Mielczarski and co-workers (1987; 1989; 1990; 1991; 1993). The formation of mono and multilayers of surfactants on semiconductors (low adsorption substrate) was detected and the orientation of the individual molecular groups and the nature of chemical bonding between the adsorbed species and surfaces were identified by using the external reflection spectroscopy at different incident angles with both p- and s-polarized radiation. Equilibrium structures of n-alkanoic acids on aluminum (Golden et al., 1982) and fluorite surfaces (Sivamohan, et al., 1990) have been studied using this technique, and the relation between film structure and solution concentration of surfactants was established. The oxidation species on iron plate were also identified by reflection infrared spectroscopy (Poling, 1969). Unfortunately, this technique is not very useful for powder samples.

2.2.3 Internal Reflectance Infrared Spectroscopy

Internal reflectance is sometimes referred to as attenuated total reflection (ATR) or multiple internal reflection. A typical setup for an ATR FTIR experiment is shown in Figure 2.3. A Brewster-angle rotating Ge polarizer can be placed in the IR beam, in front of the C face of the ATR crystal that can be made of Si, Ge, or ZeSe. The radiation is incident on the crystal in such a manner that total reflection occurs at the crystal-sample interface. ATR is more sensitive than other modes of FTIR, since the multiple reflection path enhances the signal. Also, it can be modified for in-situ studies. Using this technique, Couzis and Gulari (1993) studied the adsorption dynamics and the structure of adsorbed sodium laureate on an alumina surface from its aqueous solution. Recently, the amount and the state of fatty acids adsorbed on the crystal surface have been performed by Kellar

et al. (1993). With this technique, large amounts of powder samples are often required for full coverage of the crystal surface, and the intimate contact between the crystal and samples has to be controlled carefully. When hard materials are analyzed, attention has to be paid to avoid scratching the crystal with the sample.

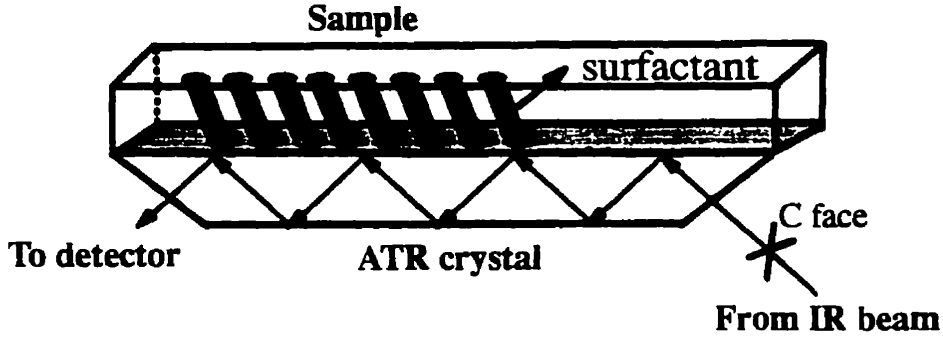

Figure 2.3 Typical setup of ATR FTIR experiment.

2.2.4 Diffuse Reflectance Infrared Fourier Transform Spectroscopy (DRIFTS)

Diffuse reflection results from the multiple scattering and partial absorption of the light flux impinging on (ideally) a matte-finish surface. Optical configuration of a diffuse reflectance cell is shown in Figure 2.4. A small cup, about 10-15 mm in diameter and 3-4 mm deep, is used to hold the sample. Microcups, about 2-3 mm in diameter, may be used whenever there is only a limited amount of sample available. In this technique, the IR beam is focused on the sample by an ellipsoid mirror, and the diffusely reflected beam is collected with a large aperture mirror to direct the beam to the detector. This technique is preferred for fine powder samples and is surface sensitive. Another important feature of DRIFTS is the dependence of the effective penetration depth on the absorption and scattering coefficients of the sample. Our experimental results indicated that for strongly absorbing materials such as magnetite, the IR signal is fairly weak because of the low reflectance, and the technique is less valuable.

DRIFTS has been used extensively to study the interaction of silane coupling agent with silica and to characterize the thin films formed on the silica (Blitz, et al., 1988; Bogart and Leyden, 1994). The adsorption densities of alcohol on silica powders were determined using quantitative diffuse reflectance FT-IR (Horr, et al., 1992). The orientation of xanthate molecules on the pyrite surface was also analyzed by DRIFTS (Cases, et al., 1993). In this thesis work, DRIFTS is used to characterize the thin organic films on nanosized magnetic particles.

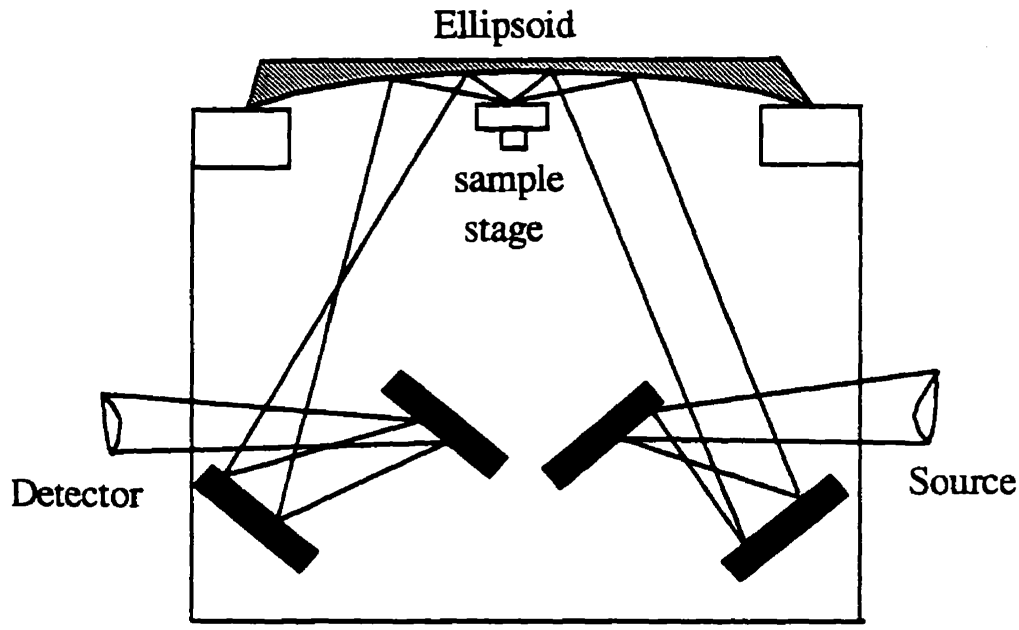

Figure 2.4 Optical configuration of a diffuse-reflectance cell.

2.3 X-RAY PHOTOELECTRON SPECTROSCOPY (XPS)

In XPS, X-rays of a given energy are used to eject electrons (called photoelectrons) from core and valence energy levels of atoms on a solid surface. The kinetic energies of the emitted electrons are analyzed by the electron spectrometer. The block diagram of XPS instrument is shown in Figure 2.5.

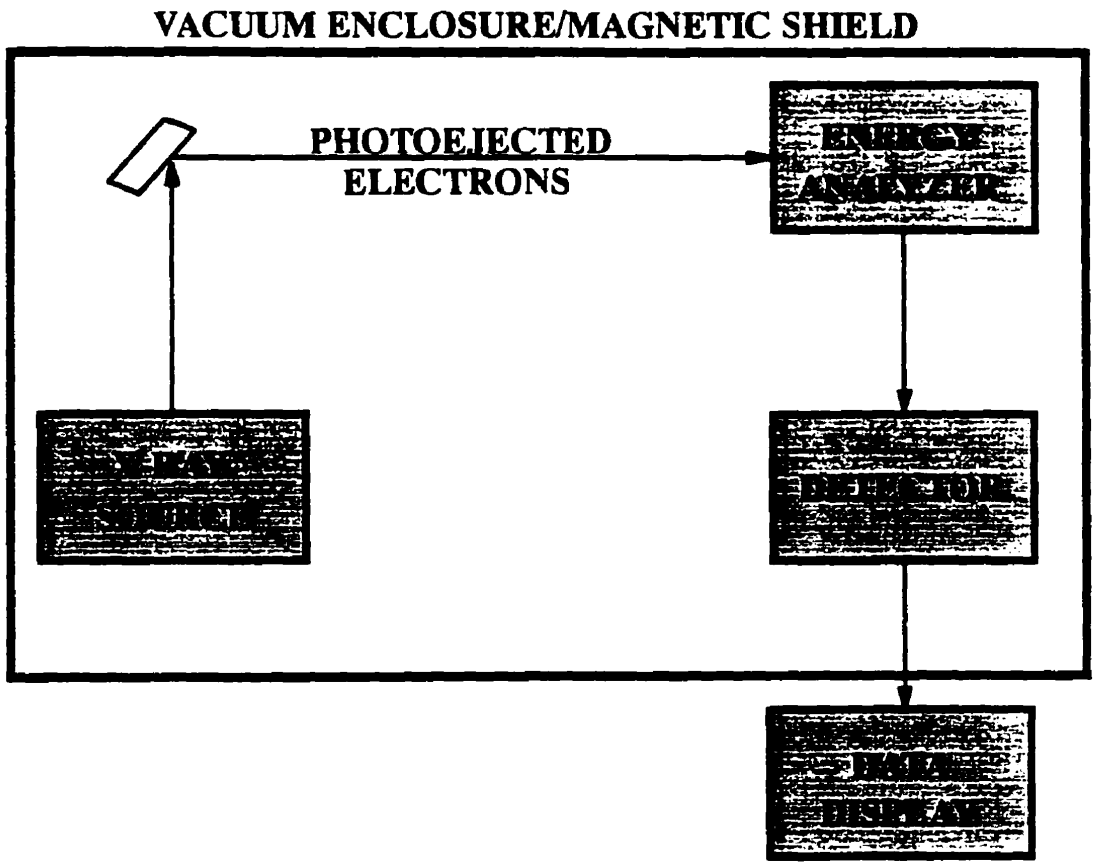

Figure 2.5 Schematic representation of photoelectron generation in XPS.

The energy levels of core electrons for a given element are sensitive to the structure and bonding of the element, even though core electrons are not necessarily involved in chemical bonding. The value of the core level binding energy determines the type of atoms present in the solid, while the chemical shifts give information on the chemical environments of the elements. If oxygen interacts with hydrogen to form a hydrogen bond on the surface, for example, the binding energy of oxygen will shift to a lower value compared to that without hydrogen bonding. It is well known that the strong electronegativity of oxygen attracts the electron cloud around hydrogen, thus reducing the binding energy of oxygen nuclei to electrons, which accounts for observed chemical shifts. An analogue of this chemical shift is the appearance of two different oxygen bands at 531 eV and 528 eV for the oxygen in silica and in iron oxide, respectively. Similarly, the band position of carbon bound to oxygen in carboxylic groups will appear at a higher binding

energy value than that bound to hydrogen or carbon in hydrocarbon chains as shown in Figure 2.6. It is evident that XPS analysis can provide information of the chemical environment of an element on a solid surface.

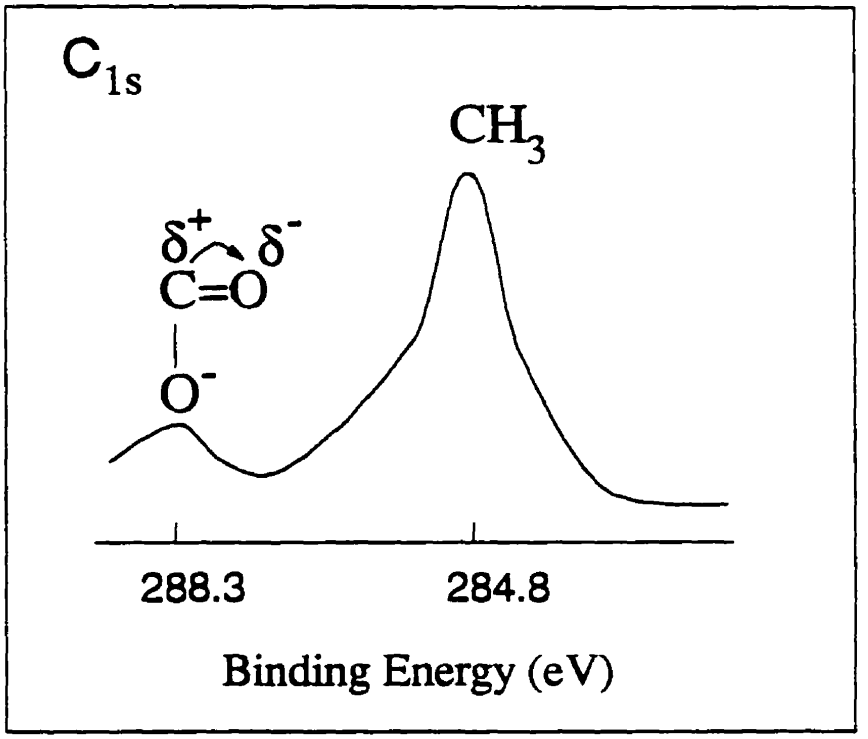

Figure 2.6 Schematic illustration of chemical shift in XPS. The binding energy of carbon bound to hydrogen appears at 284.8 eV, whereas the binding energy of carbon bound to oxygen in carboxylic groups appears at 288.3 eV. Therefore, the chemical environment of elements present on the surface can be determined from the chemical shift.

XPS has been widely used to study the interactions between the surfactant and metal oxides (Moses, et al., 1978). Extensive research has also been devoted to the study of sulfides oxidation by using XPS (Fornasiero, et al, 1994; Prestidge, et al, 1995). More recently, a variable take-off angle (defined as the angle between the sample surface and the direction of emission of the photoelectrons) technique has been used to probe the orientation of molecules on the surface (Horner, et al., 1992). Information on the structure

of thin organic films as a function of depth was obtained by collecting spectra at different take-off angles, since the sampling depth increases with the take-off angle. As a result, XPS signals from the bulk materials reduce as take-off angles become smaller, representing a more surface sensitive condition. Surface chemical composition can also be obtained from XPS analysis. For example, in the XPS spectrum of narrow scans, the integrated band area for each element, normalized by the sensitivity factors of corresponding elements and the experimental number of cycles, can provide a relative concentration of elements on the surfaces. It should be noted, however, that the XPS is an ultrahigh vacuum technique. In some cases, the charging is a problem for non-conducting samples.

2.4 THIN FILM FLOTATION

The wettability is an important characteristic of a surface in colloid and surface science. One of the commonly used methods to determine the surface wettability is to measure the contact angle. It has been well documented that a smaller water contact angle represents a more hydrophilic surface, or vice versa. Based on this observation, it becomes clear that the contact angle measurement can be used to identify the orientation of molecules on the surface. A typical example is a water contact angle larger than 90 degrees for a monolayer of octadecanethiol on a gold surface, indicating the terminated methyl group being exposed to the environment (Bain, et al, 1989). A zero water contact angle for a monolayer of 16-mercpatohexadecanoic acid ($HS\text{-}C_{15}H_{30}\text{-}COOH$) on a gold substrate indicates that the carboxylic group is towards the environment (Bain, et al, 1989). The homogeneity of the surface or monolayer can also be determined by the hysteresis of the contact angle (Xu, et al., 1996). The apparent limitation of contact angle measurement, as an analytical tool, is that only flat and smooth surfaces can be studied.

Based on the wetting theory that a particle will be wetted and sunk in a liquid if interfacial tension of liquid-air is lower than that of solid-air (provided the density of liquid is lower than the particle), an alternative method, thin film flotation, has been developed to determine the surface wettability of powder samples (William and Fuerstenau, 1987). A

typical setup of a thin film flotation experiment is shown in Figure 2.7. A given amount of particles are placed gently on the top of the solution of various surface tensions prepared from a methanol-water mixture. At a given surface tension of liquid, the wettable particles sink to the bottom of the beaker, while unwettable particles remain floating on the top. After a period of time, usually twenty minutes for wetting and settling of wettable particles, the weight fraction of unwettable particles is determined, from which a film flotation curve can be obtained by plotting the weight percentage of unwettable particles (lyophobic part) as a function of solution surface tension (Figure 2.8). The slope of the curve reflects the uniformity of the surface. The steeper the curve, the more homogeneous the surface. Also obtained from this curve is the critical surface tension (CST) where all particles are wetted. The lower the critical surface tension, the more hydrophobic the surface.

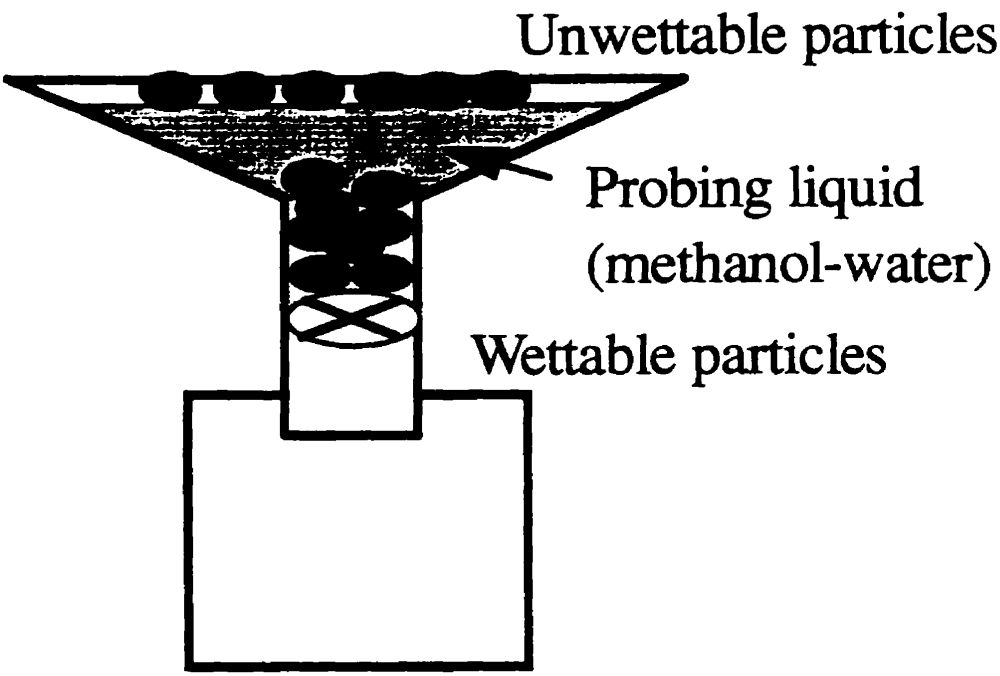

Figure 2.7 Typical setup of thin film flotation experiment.

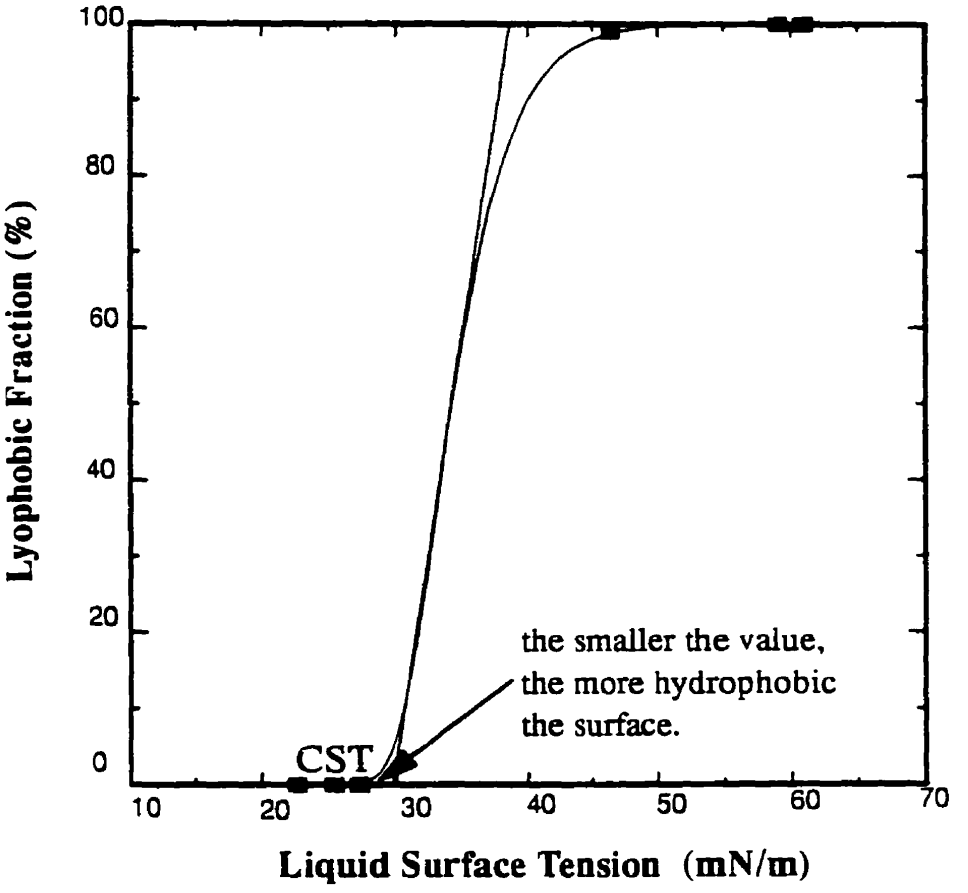

Figure 2.8 A typical thin film flotation curve.

A surface with different terminal functional groups will have different CST values. For example, it has been reported that the CST value for a methyl terminated monolayer formed using $C_{22}H_{45}SH$ on a gold surface is ca. 19 mJ/m^2, and for a chlorine group terminated monolayer is ca. 40 mJ/m^2 (Ulman, 1991). The latter is less hydrophobic due to the greater polarity of chlorine compared to that of methyl, thus giving a higher CST value. Considering the correlation between the polarity of terminated functional groups and the surface wettability, the orientation of molecules on the surface can be derived from the thin film flotation measurements.

2.5 ZETA-POTENTIAL MEASUREMENT

It is well known that most substances carry an electric charge when brought into contact with a polar medium such as electrolyte aqueous solutions. The existence of surface electric charges can be easily demonstrated by applying an external electrical field to quiescent fine particle suspensions. It is conceivable that the charged particles move in the external electrical field due to electrostatic forces. The nature of an electrode toward which a particle moves determines the sign of the average surface charge carried by this particle. For example, a particle moving toward a positive electrode carries a negative surface charge, and vice versa. The transport velocity at a given electrical field strength, called electrical mobility, determines the magnitude of the surface charge. The electrokinetic potential (zeta-potential, ζ) is the potential drop across the mobile part of the electrical double layer which is responsible for electrokinetic phenomena or motion of colloidal particles in an electric field. It is assumed that the liquid adhering to the solid (particle) surface and the mobile liquid are separated by a plane called the shear plane or slipping plane. The electrokinetic charge is the charge on the shear plane. It is worth mentioning that the surface potential is not accessible by direct experimental measurement; however, it can be calculated from the experimentally determined surface charge. In the absence of specifically adsorbing ions, the zeta-potential calculated from electrophoretic measurements is often lower than the surface potential (ψ_o) calculated from diffuse double layer theory. The zeta-potential reflects the potential difference between the shear plane and the bulk phase. At certain conditions, the surface charge will become zero which is called the point of zero charge (PZC). The point at which the zeta-potential value is zero is called the isoelectric point (IEP) of colloidal particles. The adsorption density and the orientation of the molecules on a surface can be inferred by measuring the changes of IEP before and after adsorption.

Parks (1965) has compiled and critically reviewed the literature on the measurements of isoelectric points for a large number of solid oxides and hydroxides. He has shown that the IEP for an oxide depends on the valence (Z) and radius (R) of the cations. IEP is the

highest for the divalent (Z=2) metal oxides such as MgO (pH_{iep} = 12); is in the medium pH range for trivalent metal oxides (Z=3) such as Al_2O_3 (pH_{iep} = 9) or α-Fe_2O_3 (pH_{iep} = 8.5), and is the lowest (most acidic) for metals of valence 4 or higher (e.g., for SiO_2 pH_{iep} = 2.1). Oxidation often reduces the IEP of metal oxides. For example, for the various oxides of molybdenum, as the valence of Mo increases from Mo_2O through Mo_2O_5 and MoO_3, the IEP decreases from about 12 down to about 0.5 (Bolger, 1983). The reverse occurs for sulfide minerals: higher IEP of an oxidized pyrite than that of an unoxidized one is a typical example (Fornasiero, et al, 1994). Evidently, the measurement of zeta-potential could offer such information on surface properties in a polar solution as adsorption, surface dissociation, oxidation/reduction, etc.

As a surface analytical tool, Sprycha et al. (1995) have used the electrophoretic mobility measurements to characterize monodispersed colloidal particles of silica, and silica coated with alumina and polymers. The IEP of alumina-coated silica is shifted towards the value for pure alumina, confirming the dense coating of alumina on the surface. The silica particles sulfonated with acid dyes carry a relatively constant, negative charge over the entire pH range, mainly due to the strong acidic nature of the dyes that contain many sulphate groups. Similar zeta-potential changes of air bubbles in the presence of various types of surfactant were also observed by Laskowski et al. (1989) as shown in Figure 2.9. As the anionic surfactant, such as sodium dodecylsulphate (SDS), adsorbs at the air-water interface, the zeta-potential of air bubbles becomes more negative, indicating that sulphate groups are exposed to the aqueous environment. With cationic surfactants, such as dodecylamine (DDA), on the other hand, the zeta-potential of air bubbles becomes positive, indicating that the positively charged amino groups are towards the solution. These examples clearly demonstrate that from the zeta-potential measurements the adsorption and orientation of molecules on the surface can be inferred.

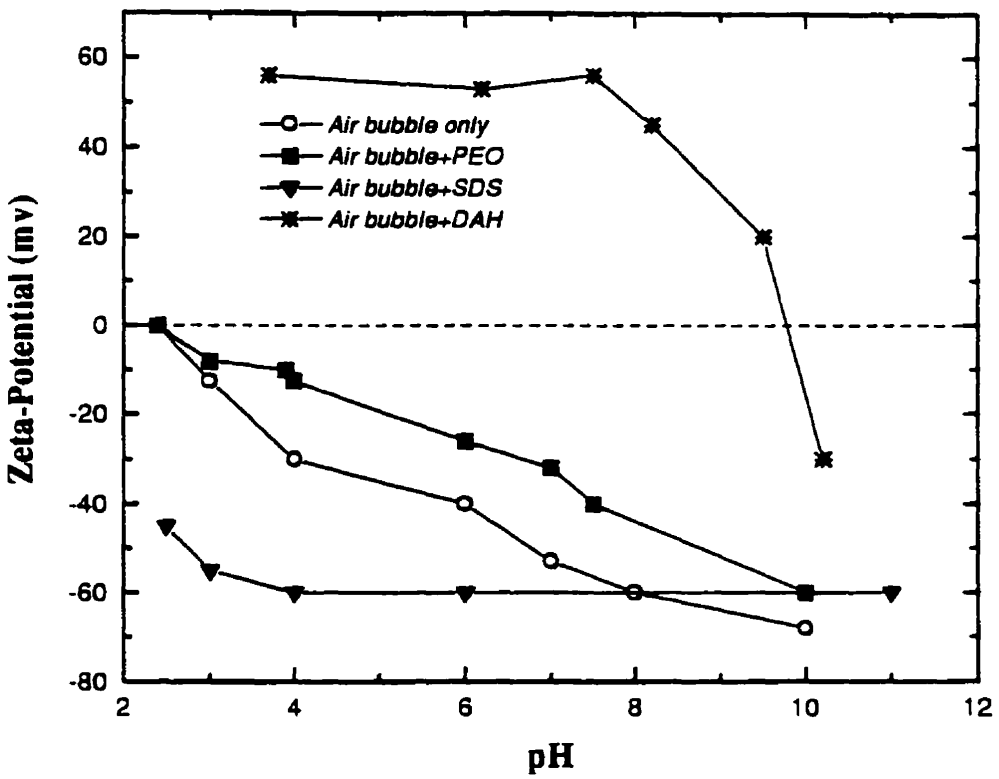

Figure 2.9 Zeta-potentials of air bubbles as a function of pH in the presence of different surfactants at the concentration lower than the critical micelle concentration. PEO is a nonionic surfactant with formula of $C_{12}H_{25}(OCH_2CH_2)_{23}OH$. SDS is an anionic surfactant with formula of $C_{12}H_{25}SO_4Na$. DDA is a cationic surfactant with formula of $C_{12}H_{25}NH_2$. Hydrophobic attraction between the air bubble and the hydrocarbon chain is a key factor in controlling the orientation of surfactant molecules (after Laskowski, et al., 1989).

2.6 THERMAL GRAVIMETRIC ANALYSIS (TGA)

TGA is a technique by which physicochemical properties (moisture, crystalline water, and/or volatile components) of a substrate and/or surface reaction products can be probed as a function of temperature, whilst the substrate is subjected to a controlled heating rate (Skoog and Leary, 1992). The mass of the sample in a controlled atmosphere is recorded

continuously as a function of temperature or time during heating. The amount and the rate of weight loss at elevated temperatures are related to the chemical structure and composition of given samples. In general, a higher temperature is required to decompose more stable materials. For example, the decomposition temperature of PMMA (polymethyl methacrylate) ca. 400 °C is lower than PTFE (polytetrafluoroethylene) ca. 600 °C, the latter being well known as more stable than the former.

Thermal gravimetric analysis has been used to characterize the thin organic film coatings on metal oxides (Qi, 1996). The underlying idea is that most metal oxides decompose at a higher temperature than the thin organic films. Therefore, the net weight loss in the temperature regime in which metal oxides remain stable can be attributed to the decomposition of thin organic films. Figure 2.10 shows thermal gravimetric analysis (TGA) of SiO_2, γ-Fe_2O_3, polypyrrole coated SiO_2, polypyrrole coated γ-Fe_2O_3 and polypyrrole samples (Qi, 1996). For all the sample analyses, the temperature was initially held at 100 °C until trace amounts of water were completely evaporated. This ensured that the mass loss during the subsequent temperature scanning arised solely from either the core material or the polymer. It is evident that at the temperature above 600 °C, both SiO_2 and γ-Fe_2O_3 showed negligible mass loss, while polypyrrole coated SiO_2 and γ-Fe_2O_3 have a 33% and 19% mass loss, respectively. In contrast, the polypyrrole samples alone showed a 100% mass loss. Therefore, the mass loss for polypyrrole coated samples is attributed to the decomposion of coated polypyrrole layers on the surface. The more weight losses for polypyrrole coated SiO_2 suggested that the more polypyrroles were coated on the surfaces. These findings indicated that TGA is a useful technique to characterize the thin organic film coatings on metal oxides. In this thesis, TGA is used as a complementary technique to examine the thin organic film coatings on magnetic particles (γ-Fe_2O_3).

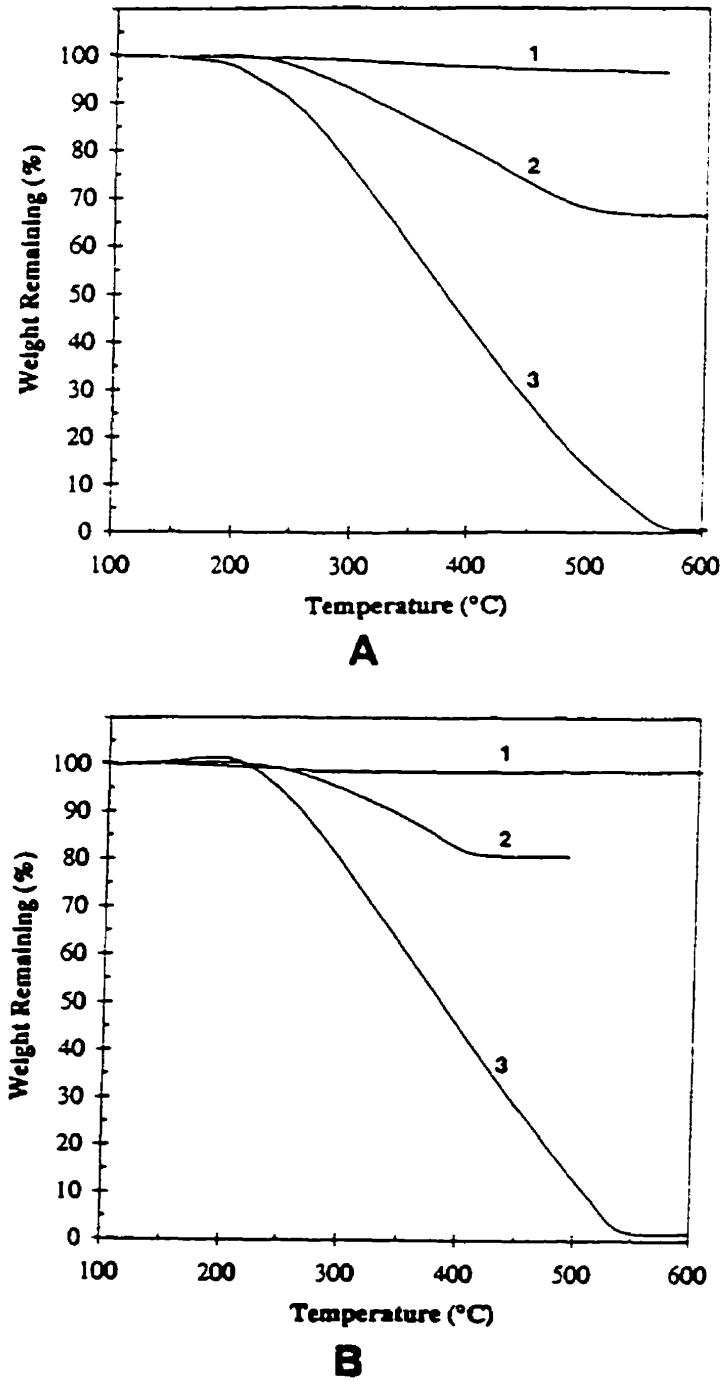

Figure 2.10 Thermal gravimetric analysis of (A): SiO_2 (1); polypyrrole coated SiO_2 (2); polypyrrole alone (3); and (B): γ-Fe_2O_3 (1); polypyrrole coated γ-Fe_2O_3 (2); and polypyrrole alone (3).

2.7 VIBRATING SAMPLE MAGNETOMETER (VSM)

In order to incorporate MCT into industrial applications, it is important to minimize the reduction of the magnetic properties of the carriers. For this purpose, the characterization of magnetic properties of prepared carriers is, therefore, essential in MCT. One of the methods to obtain a magnetization curve of a magnetic specimen is to use a vibrating sample magnetometer (VSM). In a typical VSM shown in Figure 2.11, the specimen is made to vibrate in a direction perpendicular to that of the magnetic field at a fixed frequency, typically about 80 Hz. The pick-up coils, with an alternating inductive signal, are placed with their axes perpendicular to the main magnetizing field to minimize spurious signals arising from field fluctuations. A finely-tuned signal detecting system is used to reduce background signals to a minimal level. Usually a small permanent magnet is attached to the up part of the vibrating system. This small magnet moves inside its own pick-up coils and induces a reference signal against which the signal produced by the sample can be measured accurately. The magnetization of specimen is obtained by processing the induced signal from a pick-up coil at varying magnetic fields. A relatively high sensitivity can be achieved with this configuration. It should be noted that VMS is a technique to determine the bulk magnetic properties of samples. It does not provide any information regarding the chemical composition.

The typical magnetization curves of three different materials are shown in Figure 2.12. Ferromagnetic materials, such as magnetite, respond strongly to a magnetic field. But diamagnetic materials, such as silica, respond opposite. The different responses reflect the different extent to which the magnetic dipoles align under an imposed magnetic field. For a sample of monodispersed particles, the magnetization curve can be described by (Cullity, 1972)

$$M(T) = M_s\left[\coth\left(\frac{\mu B}{kT}\right) - \frac{kT}{\mu B}\right] \qquad (2.5)$$

where μ is the magnetic moment of the individual particles, T the absolute temperature, k the Boltzman constant, and M_s the saturation magnetization of the sample ($M_s = \mu N$,

where N is the number of particle/weight of sample). If the magnetization curve passes through the origin without any hysteresis, then the sample is considered to be superparamagnetic. The magnetic particles (γ-Fe_2O_3) are known to be a spinel type

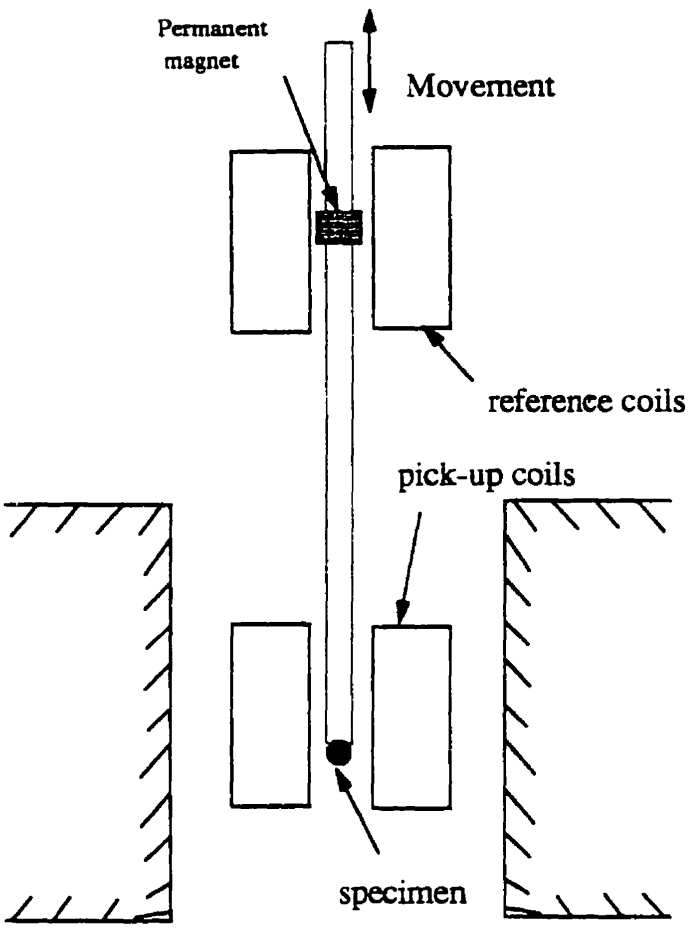

Figure 2.11 Schematic picture of vibrating-sample magnetometer.

ferrimagnet with a Neel temperature well above 600 °C (Morrish, 1980). However, as the particles become smaller and reach a critical size (~20 nm in most cases), the bulk magnetic characteristics of retentivity and coercivity vanish. Such particles are also called superparamagnetic and are in a state in which thermal fluctuations supersede the Weiss anisotropy (Bean and Livingston, 1959). The superparamagnetic feature of nanosized magnetic particles permits them to be redispersed without magnetic aggregation after

removing the external magnetic field. It is, therefore, important to use superparamagnetic particles as core materials in preparing magnetic carriers in order to reuse them in the next cycles without any aggregation.

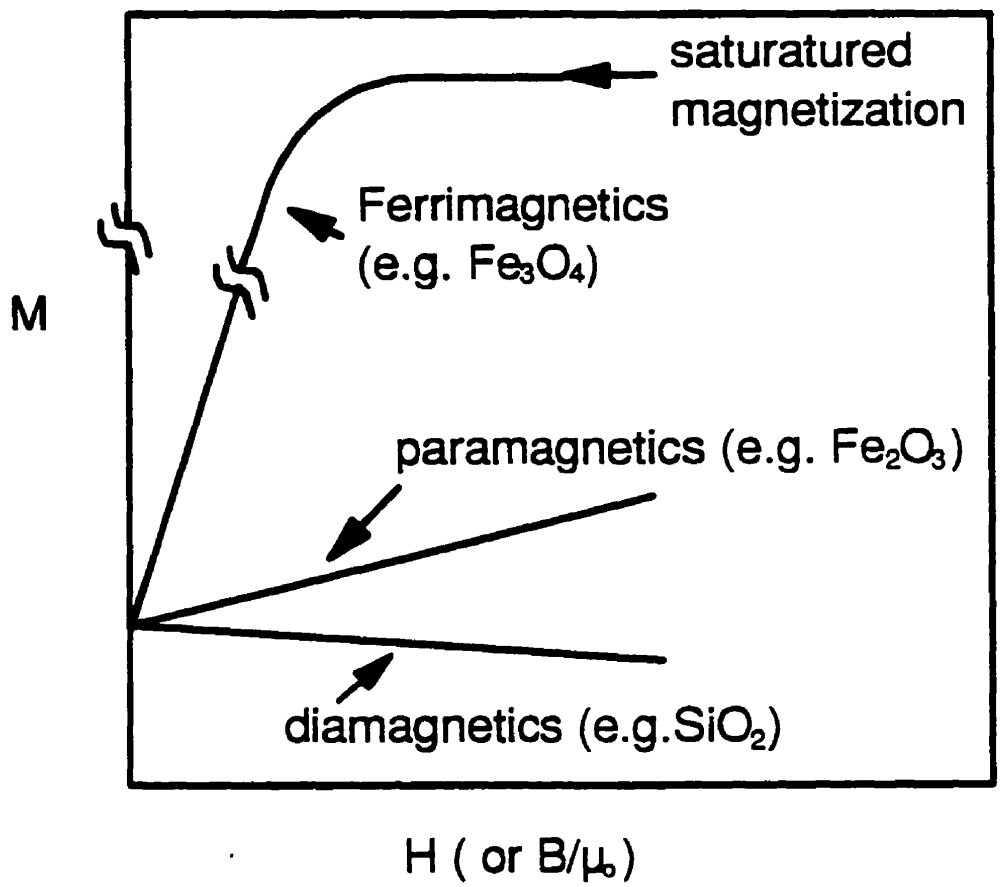

Figure 2.12 General magnetization curve for different materials. M is the particle magnetization (A/m); H is the field intensity (A/m).

2.8 SUMMARY

Several analytical techniques used in this thesis for characterizing surface films are briefly reviewed. XPS is suitable for determination of surface chemical environments and compositions, while DRIFTS can furnish an insight into the molecular orientation and chemical bonding of surface coatings. Some classical techniques such as contact angle, zeta-potential, and thin film flotation can be very useful in modern surface science. While contact angles measured by goniometer with different probing liquids on flat surfaces can be used to evaluate wetting properties, surface free energies, molecular orientation in surface films, zeta-potential measurements and thin film flotation are preferred for powder samples. TGA can be used as a complementary technique to examine the thermal stability of thin organic film coatings on metal oxides such as γ-Fe_2O_3. The characterization of magnetic properties of magnetic particles by VSM is also described.

CHAPTER 3 PREPARATION OF MAGNETIC CARRIERS (I): MOLECULAR SELF-ASSEMBLY

3.1 SELF-ASSEMBLY OF AMPHIPHILES AND BOLAAMPHIPHILES

Amphiphilic molecules possess polar head groups and non-polar chains. To minimize unfavorable solvophobic (solvent-hating) interactions, they spontaneously aggregate to form a variety of microstructures in a solvent at a given concentration (Evans and Wennerstrom, 1994). Bolaamphiphiles consist of two functional head groups on both ends of an alkyl chain. By controlling the reactivity of the functional groups to the substrate, desired monolayers can be coated onto the surface using either amphiphiles or bolaamphiphiles through molecular self-assembly as shown in Fig. 3.1 (Fuhrhop and Kon, 1994). The molecular orientation of amphiphile or bolaamphiphile on a substrate is determined by the reactivity of the polar groups with the substrate, while the packing of the molecules is related to van der Waals attractions between the alkyl chains. The bonding nature and packing density of surfactants on the surface are responsible for high durability of these films.

The surface coatings of surfactants on various types of substrates by molecular self-assembly have found a wide range of applications in varying areas, including non-linear optical devices, waveguides, microstructure electronics, optical and biological sensors, material protection (corrosion resistance), raw material recovery, and tribology (Ulman, 1991), to name a few. The preparation and characterization of self-assembled (SA) monolayers of various organic surfactants on flat metals or metal oxides have been reported in a number of publications. The systems studied include alkylsilane surfactant on hydroxylated surfaces, such as silica and aluminum oxide, alkanethiolates on gold, silver,

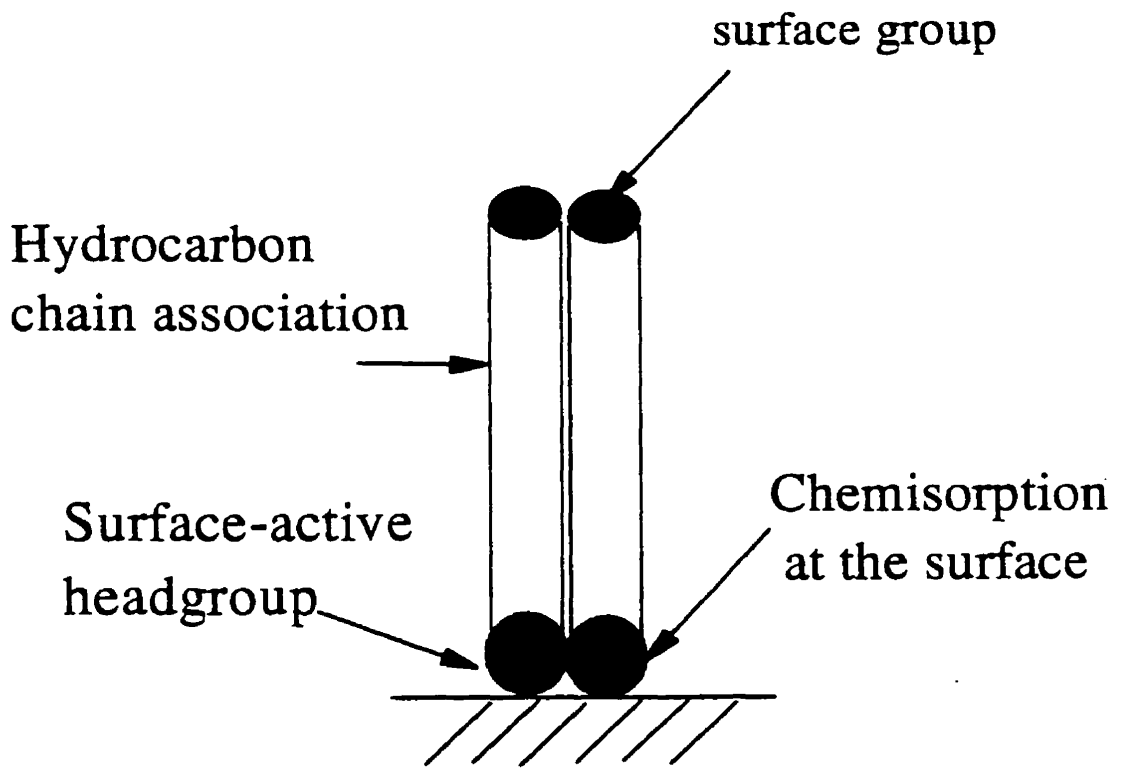

Figure 3.1 Schematic representation of molecular self-assembly. Orientation of molecules on the surface depends on the affinity of the polar group to the substrate, and the packing of molecules on the surface is related to van der Waals interactions between the hydrocarbon chains. By controlling the reactivity of the functional group with the substrate, desired monolayer coatings on the surface can be prepared through molecular self-assembly.

and copper, alcohol and amines on platinum, and carboxylic or hydroxamic acids on aluminum oxide and silver oxide (Pomerantz, et al., 1985; Allara and Nuzzo, 1985; Schlotter, et al., 1986; Laibinis, et al., 1989; Bain, et al., 1989; Walczak, et al., 1991; Parikh, et al., 1994; Folkers, et al., 1995). In more recent publications, bolaamphiphiles have been used to manipulate the architecture of thin organic films on flat metal or metal oxides such as gold, silica and aluminum oxide (Allara, et al., 1983; Ihs and Liedberg, 1991; Uvdal, et al., 1992; Smith, et al., 1992). However, few publications have described the preparation and characterization of SA monolayers using bolaamphiphiles on metal or metal oxide powders, particularly of nano-sized magnetic iron oxides.

In this chapter, preliminary studies describing the SA coatings on nano-sized magnetic particles (γ-Fe_2O_3) using 16-mercaptohexadecanoic acid (MHA) are reported. Comparative studies using stearic acid, citric acid, and 3,3'-dithiodipropionic acid (DTDPA) were also described to elucidate the reactivity of polar groups with γ-Fe_2O_3. Based on the previous studies, it is expected that the carboxylic head group (-COOH) of MHA anchors on the surface of magnetic particles so that the thiol (-SH) on the other end remains reactive for different uses. The magnetic particles fabricated as such are anticipated to have potential applications in biological cell separation, precious metal recovery, and as fillers in polymer matrices. Details of the applications will be described in chapter seven.

3.2 MATERIALS AND EXPERIMENTS

3.2.1 Materials

Magnetic particles (γ-Fe_2O_3, 99+%) from Alpha Chemicals were further dried in a vacuum oven at 12 psi and 120 ^{o}C for 24 hours prior to the self assembly experiments. The purpose of drying the particles was to remove physisorbed water from the surfaces. The average particle size was found by transmission electron microscopy (TEM) to be about 30 nm. Specific surface area measured by BET method is about 44.2 m^2/g. Stearic acid (99%), citric acid (99%), 3,3'-dithiodipropionic acid (99%), chloroform (HPLC grade), and hexane (HPLC grade) from Aldrich were used as received. The procedures as reported in literature (Pale-Grosdemange, et al., 1991) were used in synthesizing 16-Mercaptohexadecanoic acid (99%). All other chemicals were reagent grade. Water, purified with the Millipore system, was used in all experiments. All glassware was cleaned with "Piranha solutions" (1/3 H_2O_2/H_2SO_4) at 70 ^{o}C for about 20 minutes, and then rinsed with distilled water until the pH of effluent was neutral (pH = 6-7). *Note: "Piranha solutions" react violently with many organic materials and should be handled with extreme care.*

3.2.2 Experiments

A) Procedures for SA

Surfactant solutions (3 mM) were prepared in chloroform. γ-Fe_2O_3 powder (50 mg) was gently mixed with 25 mL of surfactant solution in a 40 mL vial, whilst bubbling nitrogen through the solution. The vial was then sealed and shaken for 24 hrs using a laboratory shaker (New Brunswick Scientific Inc., USA). The treated particles were separated from solution by a hand magnet and rinsed repeatedly with chloroform, followed by dry hexane to remove unbound surfactant. The particles were then dried in a vacuum oven (12 psi) at 40 ^{o}C for 12 hrs, and stored under nitrogen for characterization.

B) XPS

XPS spectra were obtained on an ESCALAB Mark-II instrument with a MgKα anode (hv=1253.6 eV) at a take-off angle normal to the sample. The source x-ray was not filtered and the instrument was calibrated against the C_{1s} band (284.8 eV). The spectra were recorded using a band-pass energy of 20 eV corresponding to an energy resolution of 1.2 eV. The powder samples, placed in a copper cup, were maintained under a background pressure of $1x10^{-9}$ torr for ~1 hour in the sample chamber before spectral acquisitions. The spectra presented here were corrected for background charging by determining the C_{1s} (284.8 eV) signal both at the outset and at the end of a series of narrow scans for each sample. No significant charging was detected during the scan. Band-fitting and spectral deconvolution were performed using the program Surf-Soft.

C) DRIFTS

The coated samples were characterized by diffuse reflectance infrared Fourier transform spectroscopy (DRIFTS: Nicolet advanced diffuse reflectance accessory) using a Bruker IFS 66 FTIR spectrometer equipped with a narrow-band MCT detector. A sample of finely crushed KBr was used as the background. DRIFTS spectra were obtained using 100 scans at nominal resolution of 4.0 cm^{-1} and presented without base-line correction.

D) Film Flotation

The surface wettability of the coated particles was characterized by film flotation, from which the critical surface tension was derived. In these experiments, methanol was used to adjust the surface tension of the liquid. Twenty milligrams of coated particles were placed gently on the solution-air interface and left for about 20 minutes. The particles remaining on the air-liquid interface were skimmed off. The sunk and floated particles were weighed separately after filtration and drying. The floated (lyophobic) fraction was plotted against the surface tension of the liquid. Two additional surface tension values for a complete wetting (100% sunk) and nonwetting (0% sunk) condition can be found from this plot, and the difference between these two values serves as a measure of the surface heterogeneity, in this case, of self-assembled layers.

E) Stability of Surface Film

It is well known that the nanosized magnetic particles used in this work are leachable in acidic solution. Therefore, the leaching of Fe from magnetic particles with and without treatment in acidic solution can be used as an indication of the packing and stability of the surface films. If densely packed surface films are formed and are stable, the leaching of Fe will be negligible. To examine the nature of various surfactants on γ-Fe_2O_3 and to investigate the susceptibility of the self-assembled layers to harsh environments, leaching experiments were conducted by placing 15 mg of treated particles in acidic media (pH=2.8) for 20 hrs. The slurry was then centrifuged using a Sorvall® RC-5B refrigerated superspeed centrifuge (Du Pond Instruments) at 12000 rpm for 30 minutes. The supernatant was then collected and analyzed for iron concentration by atomic absorption spectroscopy (Perkin Elmer 310, USA). The settled solids were washed and centrifuged three times with Millipore water, then dried in a vacuum oven at 60 °C before taking DRIFTS spectra. The changes in the DRIFTS spectra before and after leaching were used as an indication of the detachment of the surfactant from the surface.

F) VSM

A vibrating sample magnetometer (VSM) was used to characterize the magnetic properties of γ-Fe_2O_3 particles with or without surfactant monolayer coatings. The VSM was calibrated against single nickel crystal before each measurement.

3.3 RESULTS AND DISCUSSION

3.3.1 Orientation and Packing of Bolaamphiphiles on γ-Fe_2O_3

XPS analysis: XPS spectra of γ-Fe_2O_3, with and without self-assembled layers, are shown in Figure 3.2. The band positions in XPS spectra are given in Table 3.1. The bands at 724.3, 710.7 and 529.8 eV attributed to iron (Fe_{2p}) and oxygen (O_{1s}) of untreated γ-Fe_2O_3 are consistent with those reported previously (Moulder, et al., 1992). No significant spectral changes in the Fe_{2p} band were observed when γ-Fe_2O_3 was treated with either stearic acid or MHA. The bands corresponding to O_{1s} (spectra a and b) became broader slightly and skewed towards higher binding energy, probably due to the contributions of conjugated oxygen from carboxylic acid interacting with surface iron. The most significant spectral change is, however, the appearance of two C_{1S} bands at 288.3 and 284.6 eV for γ-Fe_2O_3 powders treated by stearic acid and MHA. In the latter case, a sulphur band (S_{2p}) at 163.3 eV was also observed. These spectral changes indicate the presence of stearic acid and MHA on γ-Fe_2O_3.

It is well documented (Moulder, et al., 1992) that the band at 288.3 eV is characteristic of carbon in a carboxylic environment (C-O), while the band at 284.6 eV is characteristic of carbon in a hydrocarbon chain (C-C). The ratio of the area under C_{1s} band of higher

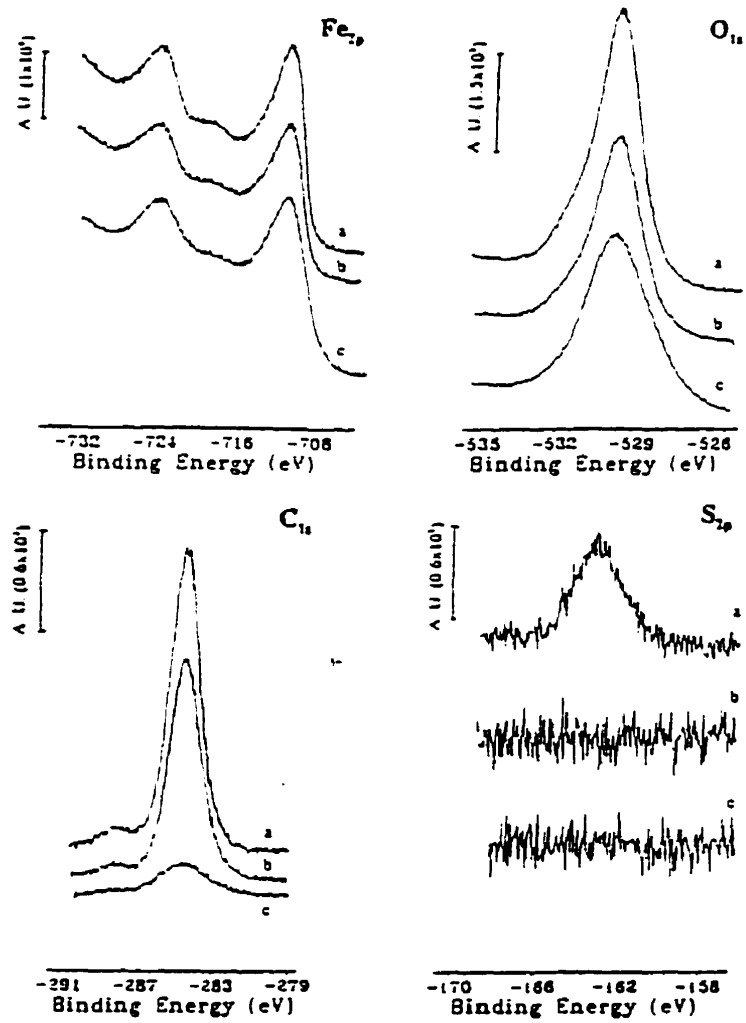

Figure 3.2 XPS spectra of narrow scans for the elements of interest on γ-Fe_2O_3 surfaces with self-assembled (a) MHA; (b) stearic acid; and (c) untreated.

binding energy to that of lower binding energy was calculated to be ca. 1:17 and 1:15 for γ-Fe_2O_3 treated with stearic acid and MHA respectively. These values are in excellent agreement with those derived from molecular structure. A similar calculation showed that the ratio of the area under C_{1s} band (at 284.6 eV) to that of Fe_{2p} (at 710 eV: normalized by the sensitivity factors of the elements and the experimental number of cycles) was 3.7 and 3.6 for γ-Fe_2O_3 particles coated with stearic acid and MHA respectively. Considering a 5 to 8 nm sampling depth of XPS technique and a length of 2.4 nm for a fully extended stearic acid molecule, the carbon to iron ratio of 3.7 suggests that a densely packed surfactant monolayer is assembled on γ-Fe_2O_3 particles. The ratio for MHA (3.6) is almost

the same as for stearic acid, indicating that the monolayer packing of MHA is similar to that of stearic acid on γ-Fe_2O_3 particles. (Note: MHA contains 15 carbons while stearic acid contains 17 carbons in the hydrocarbon chain).

Table 3.1. Binding energy (eV) of x-ray photoelectrons at band maxima[a]

System	Binding energy (eV)			
	S_{2p}	O_{1s}	Fe_{2p}	C_{1s}
γ-Fe_2O_3	nd[b]	529.8	724.3 710.7	nd
γ-Fe_2O_3 + stearic acid	nd	531.4 529.6	724.3 710.7	288.3 284.6
γ-Fe_2O_3 + MHA	163.3	531.4 529.6	724.3 710.7	288.3 284.6

[a] Band positions are accurate to ± 0.7 eV. [b] nd, not detected.

The S_{2p} band at 163.3 eV for γ-Fe_2O_3 coated by MHA is characteristic of -SH or -S-S- groups. For comparison, the band positions of different sulfur groups reported in literature (Volmer-Uebing and Stratmann, 1992) are given in Table 3.2. It is evident from

Table 3.2. Binding Energies of the S_{2p} (eV) in organic and inorganic molecules [a]

	Fe-S	R-SH	R-S-S-R	$R\text{-}SO_2^-$	$R\text{-}SO_3^-$	$Fe_2(SO_4)_3$
Binding energy	161.5 ±0.5	163.8 ±0.2	163.9 ±0.2	166.6 ±0.5	168.6 ±0.6	168.8 ±0.2
FWHM [b]	2.0	2.0	2.0	2.2	2.2	2.2

a: from Volmer-Uebing and Tratmann (1992); b: full-width at half maximum.

Table 3.2 that the binding energy of S_{2p} is expected to increase as the thiol or disulfide group is further oxidized, appearing at around 166~168 eV. These bands were not observed in our experiments, suggesting that our experimental procedure does not induce a significant oxidation of thiol group to sulfate, which is consistent with literature results. XPS is, however, unable to distinguish whether the sulfur on γ-Fe_2O_3 is in the form of thiol or disulfide as the band positions for these two states are within the resolution limit

of the instrument used here. It is not clear from the XPS results presented above whether the thiol or carboxylic groups of MHA is anchored on the surface. Therefore, the complementary techniques, such as DRIFTS and film flotation, were used to elucidate the orientation of MHA molecules on the surface.

DRIFTS: Infrared spectra of γ-Fe_2O_3 particles with and without MHA self-assembled layers were obtained using the DRIFTS, a surface-sensitive technique suitable for powder samples. The high (3100 to 2700 cm^{-1}) and low (1800 to 1200 cm^{-1}) wavenumber regions of the spectra, which contain diagnostic spectral features, are shown in Figure 3.3. For comparison, the spectrum of the MHA compound dispersed in KBr is also included in this figure. The assignment of the bands is given in Table 3.3. Four distinct bands at 2923, 2851, 1527 and 1432 cm^{-1} for γ-Fe_2O_3 treated by MHA (spectrum b) are due to the molecular vibrations of asymmetric and symmetric stretching of CH_2 and COO^- groups (Smith, et al., 1992) respectively, confirming the self-assembly of MHA on γ-Fe_2O_3. There is no band observed in the spectral region above 3000 cm^{-1} where characteristic bands of CH_3 stretching vibrations appear. This is in agreement with the molecular structure of MHA which does not contain a CH_3 group. Two bands assigned to CH_3 stretching vibrations were observed in this spectral region for γ-Fe_2O_3 treated with stearic acid (spectrum c). It is worth mentioning that direct spectral feature of thiols (i.e. C-S-H) was not observed. The weak infrared adsorption by C-S and S-H stretching vibrations appears to be the reason for these two bands being undetected. (Note: The C-S band at 600-700 cm^{-1} overlaps with the iron oxide vibrational bands.) Two distinct spectral differences between the spectrum of bulk MHA (spectrum a) and that of MHA on γ-Fe_2O_3 (spectrum b) were observed. In the low wavenumber region, the carbonyl band at 1702 cm^{-1} for bulk MHA was shifted to lower wavenumber, 1527 cm^{-1}, and associated with this shift is the appearance of a new band at 1432 cm^{-1} when the MHA was present on γ-Fe_2O_3. This spectral change indicates that binding between the carboxylic group and metal on γ-Fe_2O_3 occurred, transforming a carboxylic acid functionality to a carboxylate functionality with

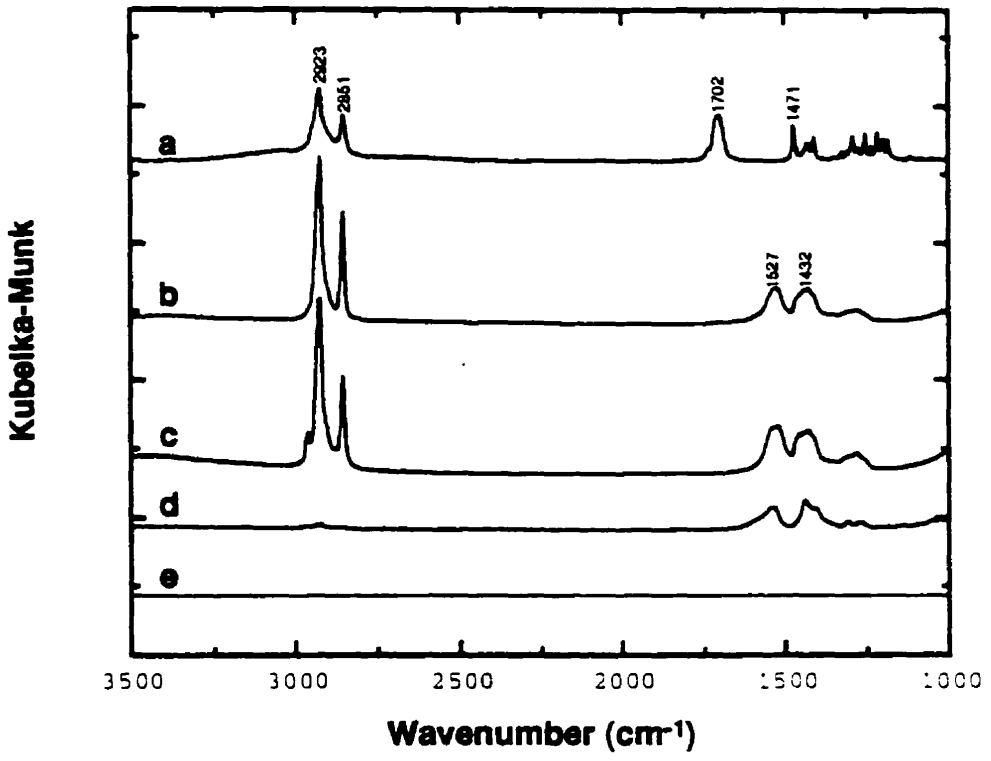

Figure 3.3. Infrared spectra in the high and low-frequency regions for (a) MHA in KBr; (b) MHA on γ-Fe_2O_3; and (c) Stearic acid on γ-Fe_2O_3; (d) DTDPA on γ-Fe_2O_3; (e) γ-Fe_2O_3.

both oxygen atoms interacting with the metal on the surface (Smith, et al., 1992). A similar shift and split were observed when stearic acid was self-assembled on γ-Fe_2O_3. It is worth mentioning at this point that this spectral feature is different from that of MHA self-assembled on gold substrates where the carboxylic group did not react with the surface and remained exposed to the environment (Smith et al., 1992). In this case, the reactivity of the thiol with gold is stronger than that of the carboxylic acid. In contrast, our observations confirm the stronger reactivity of carboxylic group with γ-Fe_2O_3 than the thiol group, leaving the thiol group exposed to the environment. The above experimental evidence demonstrated that by controlling the relative reactivity of polar groups of a bolaamphiphile with a substrate, the surface of desired functional groups can be fabricated

using the self-assembly method. It is important to note the absence of the band at 1703 cm^{-1} (spectrum b) assigned to the C=O stretching mode of the carboxyl group, indicating that all carboxyl groups on MHA are intimately bound to the γ-Fe_2O_3 surface. This finding suggests that MHA only forms a monolayer on γ-Fe_2O_3.

Table 3.3. Vibrational mode assignments and band positions (cm^{-1}) for MHA dispersed in KBr and self-assembled on γ-Fe_2O_3.

	MHA in	
Mode Assignment	KBr	monolayer
$\nu_a(CH_2)$	2923	2923
$\nu_s(CH_2)$	2851	2851
ν(C=O)	1702	nd[a]
$\nu_a(COO^-)$	nd	1527
$\nu_s(COO^-)$	nd	1432

[a] nd, not detected.

In the high wave number region, the band positions for CH_2 stretching are almost the same for both bulk and self-assembled MHA. However, the CH_2 stretching bands for MHA on γ-Fe_2O_3 are sharper with a narrow band width at half band height, indicating more ordered (crystalline) polymethylene chains and hence confirming the formation of a densely packed surfactant monolayer as derived from XPS spectra. It should be noted that the relative geometrical orientation (i.e. tilt angle of alkyl chains) of MHA on γ-Fe_2O_3 powder cannot be determined directly using the DRIFTS technique.

Film Flotation: The results of film flotation using γ-Fe_2O_3 with and without surface coatings are shown in Figure 3.4. The untreated γ-Fe_2O_3 particles are readily wetted by water as expected for high energy surfaces of oxides. A similar result was obtained for the γ-Fe_2O_3 particles treated with citric acid, on which hydrophilic carboxylic acid groups are exposed to water. The γ-Fe_2O_3 particles treated with 3,3'-dithiodipropionic acid (DTDPA) showed a moderate hydrophobicity with 20% of particles floating on the air-water

interface (Figure 3.4c). In contrast, the particles treated with stearic acid and MHA are strongly hydrophobic, all the particles floating on the air-water interface.

The critical surface tensions of 27 and 33 mN/m at the low limit (0%), and 32 and 43 mN/m at the high limit (100%) of film flotation curves were obtained for the γ-Fe_2O_3 particles treated with stearic acid and MHA, respectively. For stearic acid coated γ-Fe_2O_3 particles, the critical surface tension for complete wetting (27 mN/m) approached the surface tension of normal hydrocarbon liquids (25 mN/m), or CH_3 terminated crystalline monolayers (22 mN/m) (Ulman, 1991; Israelachvili, 1992), confirming a compact monolayer on γ-Fe_2O_3 terminated with methyl groups. The small difference (5 mN/m) between surface tensions for complete wetting and nonwetting conditions (Figure 3.3 a) implies a homogeneous surface, i.e., suggests the formation of a relatively uniform monolayer. Considering the findings from XPS analysis that MHA had the same surface coverage as stearic acid, it can be concluded that the densely packed monolayers of MHA were self-assembled on γ-Fe_2O_3.

The critical surface tension of MHA-coated γ-Fe_2O_3 particles remained low (33 mN/m), confirming that hydrophilic carboxylic groups anchored onto the surface with relatively hydrophobic thiol or/and disulfide groups exposed to the environment. This finding also suggests that the original hydrophilic nature of magnetic particles was shielded, confirming a fully packed surface coating. It should be noted that this value is slightly higher than that for stearic acid coated particles, which can be attributed to the relatively polar nature of thiol or disulfide groups compared to methyl groups. The difference between the two limiting critical surface tension values (10 mN/m) increased slightly, showing an increase in surface heterogeneity of MHA coated particles compared to stearic acid coated particles. It is possible that some of thiol groups were oxidized to disulfide (Zhong and Porter, 1994). The presence of these two sulfur species with different polarity may have contributed to the increased surface heterogeneity.

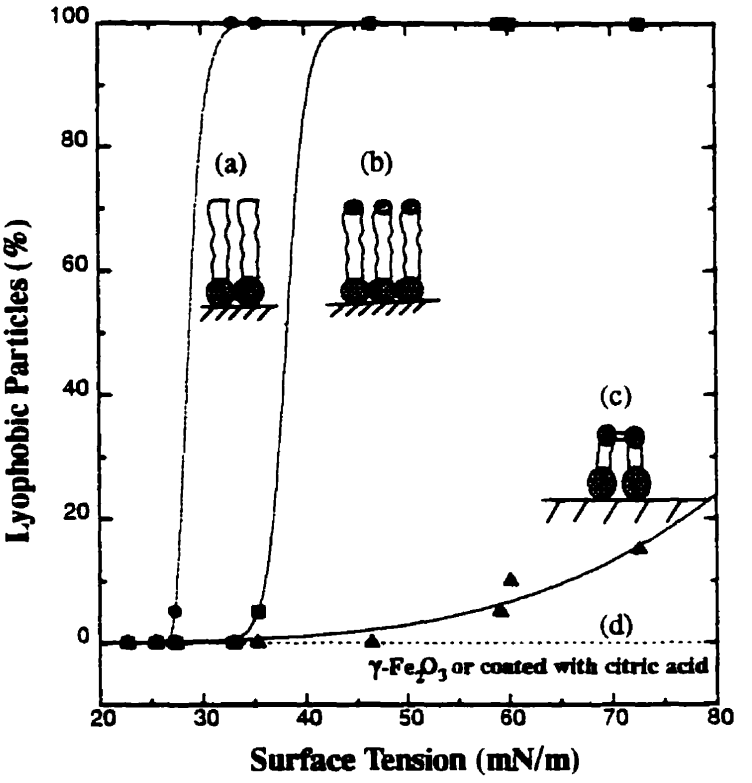

Figure 3.4 Partition curve of the film flotation using γ-Fe_2O_3 self-assembled with (a) stearic acid; (b) MHA; (c) DTDPA; and (d) citric acid and untreated.

It is interesting to note the significant difference in surface wettability of γ–Fe_2O_3 particles coated with MHA and DTDAP. As shown in Figure 3.4 c, two carboxylic groups of DTDPA are expected to anchor to γ–Fe_2O_3 particles with a disulfide group being exposed to water. Therefore, thiol or/and disulfide are the terminating group for both MHA and DTDPA coated γ–Fe_2O_3 particles. A higher wettability of DTDPA-coated particles compared to MHA-coated particles seems to be related to a lower DTDPA surface coverage, suggesting that long chain hydrocarbon association of amphiphiles is required to self-assemble a densely packed monolayer, such as MHA on γ-Fe_2O_3. The architecture of self-assembled surfactant layers using MHA is schematically shown in Figure 3.4 and 3.5.

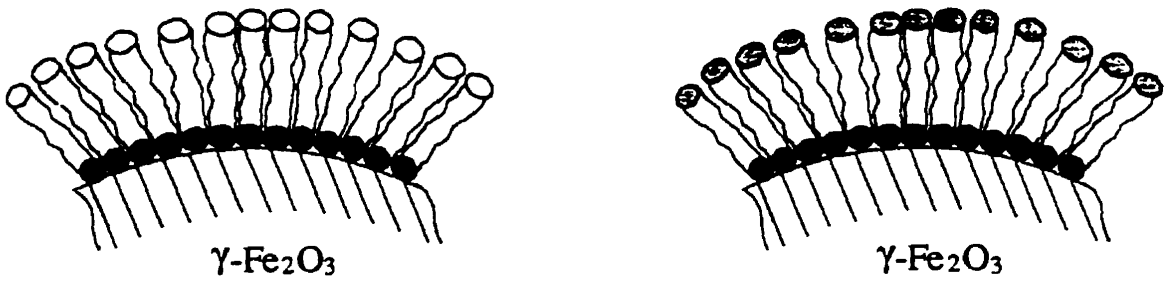

Figure 3.5. Schematic representation of γ-Fe_2O_3 coated with (a) MHA monolayer with thiol group on surface; (b) Oxidized MHA monolayer showing disulphide functionality.

3.3.2 Stability of Self-assembled Monolayer

The leaching results for magnetic particles with and without surface coatings are given in Table 3.4. It can be seen that about 30.1 mg Fe per gram of particles was leached out from bare magnetic particles. In contrast, Fe was not detected in the acidic leachate of magnetic particles treated with MHA and stearic acid. After the leachate was removed and the powder dried, the same critical surface tension values as unleached particles were obtained. Also, there is no significant change in DRIFTS spectra before and after acid leaching. Similar results were also obtained from the base leaching (pH = 10.1). These findings further confirm that the monolayer formed on magnetic particles by MHA and stearic acid is tightly packed to prevent the leaching solutions from reaching the bare magnetic particles. It also suggests that the monolayer coatings with stearic acid and MHA are stable in both acidic and basic solution.

Compared with MHA and stearic acid monolayer coatings, Fe was detected from the acidic leachate of DTDPA coated particles. This implies that either the surface is not fully covered by DTDPA molecules or the films formed by DTDPA are unstable and may be detached in acidic solution. As discussed previously, DTDPA has two carboxylic groups with short hydrocarbon chains. From infrared spectrum (Figure 3.3 d) it is evident that

these two carboxylic groups reacted with the surface, as indicated by the absence of an IR band of the free carboxylic group (1702 cm^{-1}). It is unlikely that DTDPA formed a densely packed monolayer mainly due to geometric constraints between the two carboxylic groups and weak hydrocarbon chain association. Thus, uncovered surface sites by DTDPA molecules are subject to attack of acidic solution, releasing Fe into the leachate. These observations confirm the packing information derived from DRIFTS and film flotation experiments.

Table 3.4 The amount of iron leached out from magnetic particles with and without surface coatings[a].

system	Fe ions (mg/gram particle)
γ-Fe_2O_3	30.1
γ-Fe_2O_3 with DTDPA	13.2
γ-Fe_2O_3 with MHA	nil
γ-Fe_2O_3 with stearic acid	nil

a: Leaching was conducted in acidic solutions (pH = 2.8).

3.3.3 Magnetic Properties of Prepared Magnetic Carriers

The room temperature magnetization curves for theγ-Fe_2O_3 particles, obtained with a VSM, are shown in Figure 3.6. A saturation magnetization of 52.7 $A.M^2/Kg$ at 1 Tesla was obtained for untreated γ-Fe_2O_3 particles, representing a strong magnetization. Only a marginal decrease in the saturation magnetization (2 $A.M^2/Kg$) was observed when γ-Fe_2O_3 particles were coated with MHA. A common feature of these two magnetization curves is their small hysteresis and coercivity of magnetization, indicating that these particles are close to superparamagnetic at room temperature. This magnetization characteristics

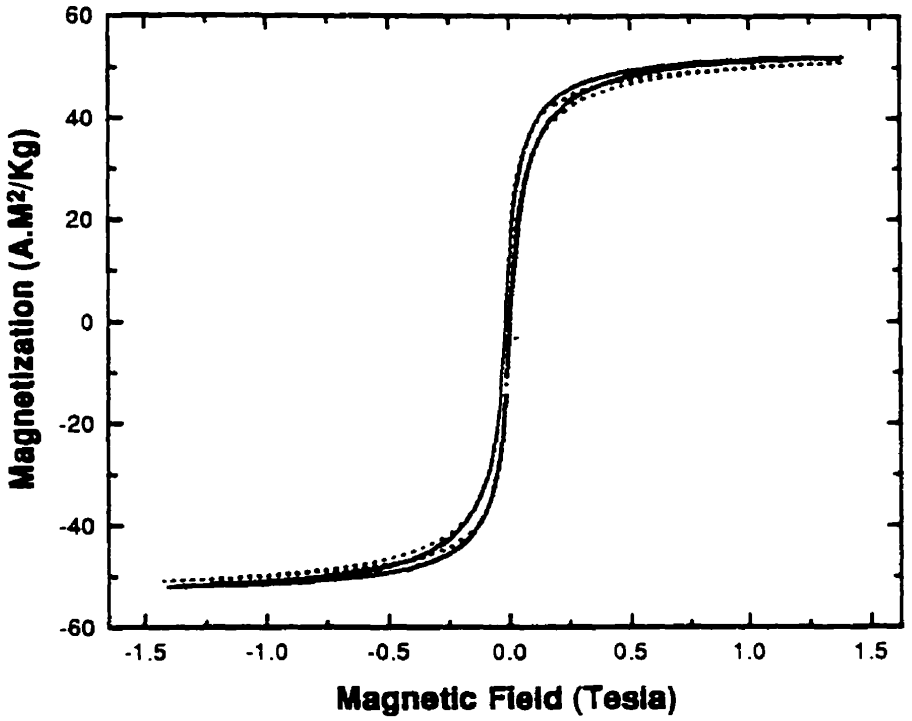

Figure 3.6 Room temperature magnetization curve of γ-Fe_2O_3 obtained with a vibrating sample magnetometer: solid line for untreated and dotted line for MHA-coated particles.

suggest that nano-sized γ-Fe_2O_3 particles do not become permanently magnetized after exposure to an external magnetic field. This property permits the particles to be redispersed without magnetic aggregation. Hence, the magnetic carrier prepared as such can be reused or recycled in practice.

3.4 SUMMARY

Using XPS, DRIFTS and film flotation, it has been shown that 16-mercaptohexadecanoic acid (MHA) was anchored onto γ-Fe_2O_3 surface through chemical bonding between the carboxylic head group of MHA and iron on the surface, leaving the thiol or disulfide groups reactive. The self-assembled MHA film on γ-Fe_2O_3 was densely packed and resistant to acid and base attack. In contrast, DTDPA with a short alkyl chain

resulted in disordered, loosely packed films due to the geometric constraints between the two carboxylic groups and weak hydrocarbon chain associations. It was concluded that magnetic carriers with desired functionalities can be prepared using bolaamphiphiles through molecular self-assembly.

CHAPTER 4 PREPARATION OF MAGNETIC CARRIERS (II): DIRECT SILANATION USING 3-AMINO-PROPYLTRIETHOXY SILANE

4.1 INTRODUCTION

In the previous chapter, the preparation of magnetic carriers with reactive thiol or disulfide groups by a novel method, molecular self-assembly using a bolaamphiphile, was described. This method appears attractive due to the high stability of the monolayers and high density of surface functional groups. However, for achieving a desired monolayer coating, the reactivity of the two functional groups with the substrate has to be significantly different. An ideal case would be that one functional group anchors chemically on the surface while the other is unreactive to the surface. This requirement limits the type of functional groups that can be directly introduced onto magnetic particles.

To search for a more general approach for preparing magnetic carriers, direct silanation using silane coupling agents seems to be an attractive choice. A typical silane coupling agent has the structure $Y\text{-}(CH_2)_n\text{-}Si\text{-}X_3$, where X represents the alkoxy or halide groups and Y, an organic functional group, including amine, thiol, carboxyl, phosphate, vinyl, cyanide, and methacrylate (Plueddemann, 1982). The $Si\text{-}X_3$ group can be readily hydrolyzed in the presence of water and a catalyst to form silanol groups (Si-OH) which couple readily with surface metal hydroxyl groups (M-OH), forming Si-O-M bonds upon dehydration. As a result, the organic functional groups remain reactive on the surface. A schematic representation of hydrolysis of silane coupling agents and silanation on an inorganic substrate, such as metal oxides, is shown in Figure 4.1. It seems feasible to prepare magnetic carriers by silanizing the magnetic particles using silane coupling agents.

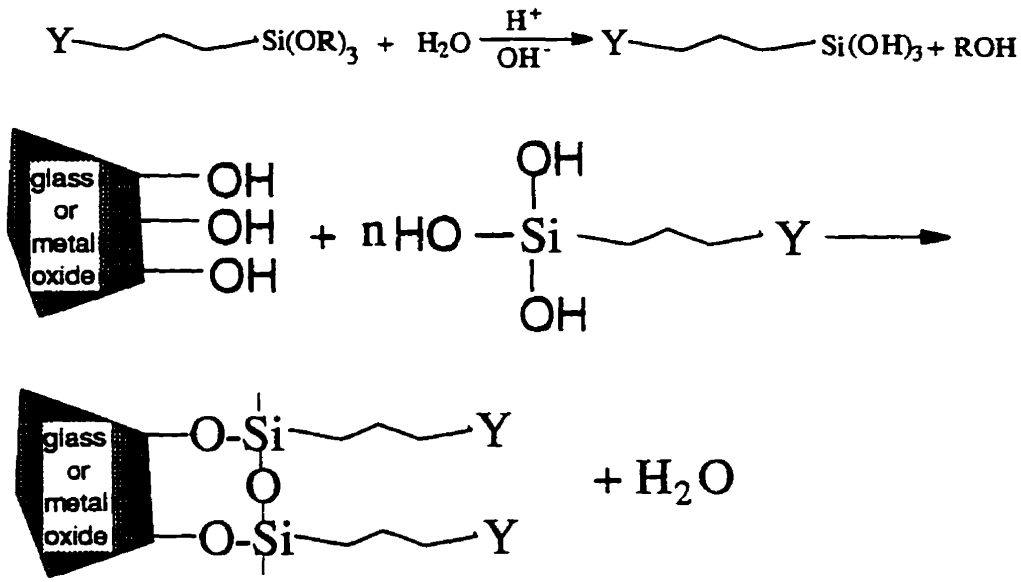

Figure 4.1 Schematic representation of the hydrolysis of silane coupling agents and silanation on a metal oxide surface. Silane coupling agents are hydrolyzed in the presence of water and catalyst to form a silanetriol that can condense with surface hydroxyls to form a chemical bond (Si-O-surface).

Silanation was initially introduced to improve the adhesion between different polymers and between a metal or glass fiber and polymeric resin (Plueddemann, 1982). A large volume of literature is available on the silanation using silane coupling agents to tailor surface properties of various substrates (Leyden, 1986; Mittal, 1992). The silanation has now been extended to such applications as the modification of silica surfaces for use in synthetic transformations (Angeletti, et al., 1988), molecular recognition (Heckl, et al., 1990), chromatographic separations (Buszewski and Lodkowski, 1991), preconcentration of trace metals (Plueddemann, 1985), and immobilization of artificial membranes and biomolecules (Markovich, et al., 1991; Muramatsu, et al., 1987; Battistel, et al., 1991; Matteucci and Caruthers, 1981).

An attempt has also been made by Whitehead et al (1987) to directly silanize magnetic particles. The functional groups they proposed include aminophenyl, amino, hydroxyl, aliphatic, and mixed functional groups. They mainly described the preparation and potential applications of magnetic carriers prepared from direct silanation, but gave no

detailed information on the characteristics of the silanized films, in particular the film stability and possible "leaching" of iron from the substrate in acidic solutions.

In this chapter, the preparation of magnetic carriers by the direct silanation of magnetic particles using 3-aminopropyltriethoxy silane (NH_2-CH_2-CH_2-CH_2-Si-$(OCH_2CH_3)_3$, APTES) is studied. APTES was used mainly due to the interest of making magnetic carriers with reactive amino groups, through which heavy metals in industrial effluents can be removed or recovered. The silanized organic films were characterized by x-ray photoelectron spectroscopy (XPS), diffuse-reflectance Fourier transform infrared spectroscopy (DRIFTS), surface electrokinetics, and solution analysis of leachates. The characteristics investigated include the state of the amino groups, the binding of silane on magnetic particles, and the stability of the silanized films.

4.2 THEORETICAL CONSIDERATION OF SILANATION

The formation of thin organic films on various substrates by silanation using silane coupling agents is a multistep, complex process. A triangle relationship among substrate, silane, and solvent, with the parameters to be considered is shown in Figure 4.2. Among these complicated interactions, the type of solvents and experimental conditions, such as surface pretreatment, reaction time and temperature, silane concentration and curing temperature, have the most significant effect on the structure and stability of the silanized films. A brief discussion on the effect of these factors on the silanation will, therefore, be useful for designing the silanation experiments.

4.2.1 Surface Characteristics

Surface characteristics have significant effects on the condensation of silane coupling agents with the surface and the stability of the silanized films. Extensive literature is available on the effect of silica pretreatment on silanation (Hair and Tripp, 1995; Vrancken, et al. 1995; Bogart and Leyden, 1994). It is well known that a silica surface

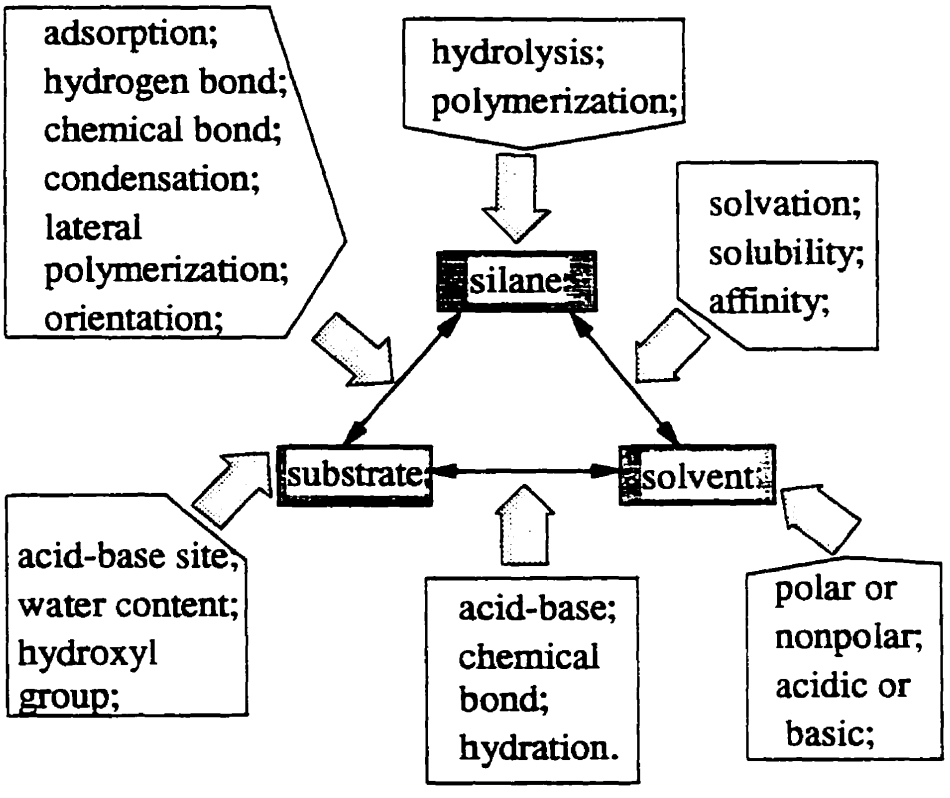

Figure 4.2 Schematic representation of various interactions in silanation.

contains different types of silanol groups such as isolated, geminal, silanetriol, and hydrogen bonded silanols as shown in Figure 4.3 (Iler, 1979; Bergna, 1994). Silanetriols (Q^1) and silanediols (geminal, Q^2) are known as having one and two bridging oxygens

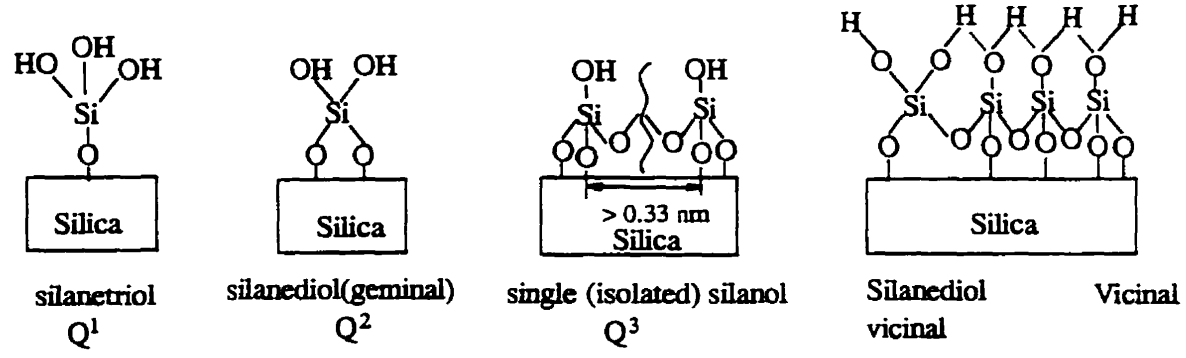

silanetriol Q^1 | silanediol(geminal) Q^2 | single (isolated) silanol Q^3 | Silanediol vicinal | Vicinal

Figure 4.3 Schematic illustration of various silanols on silica surface.

(Si-O-) bonded to a central silicon, respectively (i.e. Q^1 has three hydroxyl groups bonded to a central silicon and Q^2 has only two hydroxyls). An isolated silanol (Q^3) has an OH group, located at a distance sufficiently far from neighboring hydroxyl groups to prevent hydrogen bonding, bonded to a central Si atom with three bridging oxygens.

These surface silanols (Q^1, Q^2 and Q^3) have different reactivities with water and silane coupling agents. It is well documented that water can physically adsorb on the hydrogen bonded silanol, while isolated silanols show a weak affinity for water, but strong reactivity with silane molecules (Flinn, et al., 1994). The nature and hence reactivity of surface silanols with silane coupling agents also change with temperature. It has been reported that heating silica at 150 °C removes all physisorbed water, while heating at 400 °C reversibly reduces hydrogen bonded silanols and increases the amount of free silanols. Heating between 400 and 800 °C irreversibly eliminates adjacent hydroxyl groups and reduces the amount of free silanols, thus inhibiting the silanation reaction (Vrancken, et al., 1995). Above 800 °C, it is believed that few hydroxyl groups remain amongst hydrophobic siloxane bridges. The result is the progression of surface hydrophobicity and the degradation of reactivity to silane coupling agents as shown in Figure 4.4.

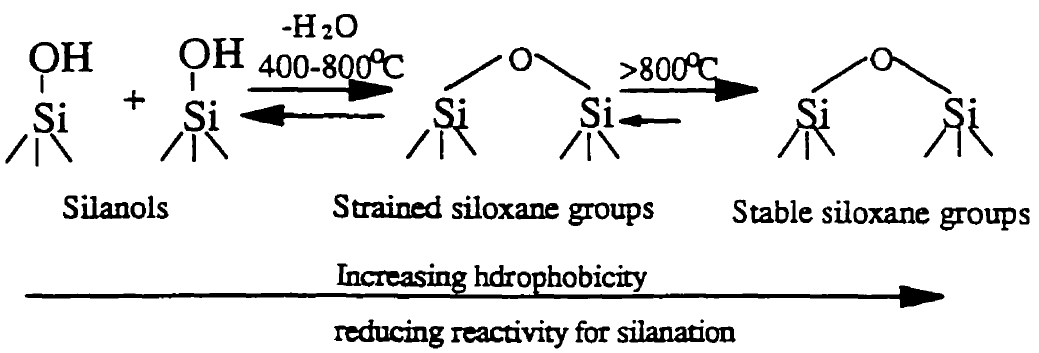

Figure 4.4 Schematic representation of the changes of surface silanols at various temperatures.

For magnetic particles (γ-Fe_2O_3), few references are available to show the effects of such pretreatment on the state and the density of surface hydroxyls. Simmons and Beard (1987) studied the acid-base properties of hydrated oxides on iron metal surface. They found a surface hydroxyl concentration of 2.6 OH/nm^2, which is lower than that (ca. 4.2

OH/nm^2) for silica (Vrancken, et al., 1995; Zhuravlev, 1993). Fowkes, et al. (1988) reported that the FeOH on γ-Fe_2O_3 can react with either acidic or basic molecules, indicating the amphoteric nature of the surfaces. In the work presented in this chapter, all samples are pre-dried at 120 °C in a vacuum oven in order to remove physisorbed water while avoiding the removal of metal hydroxyl groups necessary for silanation.

4.2.2 Solvents: Water vs. Toluene

Some recent publications on the silanation of silica with APTES in organic solvents mainly focused on the effect of experimental parameters such as reaction time, temperature, and silane concentrations on surface coverage (Vandenberg, et al., 1991). The effect of surface water and curing temperatures on APTES-silica reactions was also investigated extensively (Vrancken, et al., 1992). When an anhydrous organic solvent was used, a trace amount of water on the substrate surface was found essential for an initial hydrolysis of alkoxy groups of silanes to produce precursors for subsequent condensation and lateral polymerization on the surface. In the presence of excess water, on the other hand, the formation of the H-bonds between the amino moieties or water and silanols on silane molecules stabilized the silanols and prevented lateral cross-linking on the surface. In toluene, H-bonding between the silane amino groups and surface silanols has been postulated to occur preferentially, thus enabling the free silane silanols to cross-link on the surface (Kallury, et al. 1994).

Kurth and Bein (1995) have studied the formation of thin films and monolayers of APTES on alumina and gold substrates using reflection-absorption FTIR spectroscopy, ellipsometry, contact angle, and quartz-crystal microbalance measurements. They found that adsorption of APTES from aqueous solutions yields a film thicker than a monolayer, suggesting the formation of oligomeric species on the surface. The deposition of APTES from its vapor on silica substrate resulted in a film of approximately two or three layers thick. In a humid environment the film thickness increased steadily with exposure time. Bogart and Leyden (1994) studied the effect of humidity on the modification of Cab-O-Sil using alkoxysilane in the presence of alkane amine in dry toluene (25 °C for reaction, 140

°C for curing). They found that the adsorbed water influenced the surface silane coverage both in the presence and absence of an amine catalyst. The advantage of using an amine as a catalyst became less obvious with increasing surface adsorbed water, which resulted in a decrease in surface silane coverage. Cab-O-Sil fused silica, equilibrated at 50% relative humidity and reacted in the presence of an amine catalyst, showed the highest silane coverage for short chain alkyltrialkoxysilanes, whereas low surface moisture was favorable for reaction with long chain alkyltrialkoxysilanes. Chen and Braner (1982) also studied the effect of amine catalysts on the bonding of methacryoxypropylsilane to silica surfaces. The stability of the modified surface was investigated by aging the samples in water for approximately 280 hours. Silica silanized from nonaqueous solutions in the presence of an n-propylamine catalyst was found to contain much larger amounts of silanes as compared to the reaction without the amine catalyst. The films formed in nonaqueous solutions were more stable than those in aqueous solutions. These findings indicate that the solvents and the presence of trace amount of water on the surface have significant effect on the properties of the silanized films.

Two major types of solvents: anhydrous organic solvent (e.g. toluene) and water, have been used in previous silanation studies. Compared to organic solvent, water is more economic and non toxic. Therefore, for most industrial applications, silanation is performed in aqueous media. In this study, we are investigating the effect of solvents on the silanation of magnetic particles (γ-Fe_2O_3) using APTES. Two solvents, water and toluene, are examined to see whether a desirable surface film can be fabricated on magnetic particles.

4.2.3 Hydrolysis Kinetics

The hydrolysis of silane coupling agents is an essential step for the adsorption and the condensation of silane molecules with surface hydroxyl groups. In order to better control the silanation reaction, it is necessary to understand the mechanism and rate of hydrolysis and condensation.

The hydrolysis of alkoxy silanes is generally considered to be nucleophilic substitution at silicon of the silane molecule in the presence of acid or base, which catalyzes the hydrolysis as shown in Figure 4.5. The hydrolysis proceeds through a stepwise process. In the first step the monosilanol (Si-OH) is formed, followed by bisilanol ($Si-(OH)_2$) and silanetriol ($Si-(OH)_3$). It was reported that the hydrolysis of alkoxy silane followed pseudo-first-order kinetics where the rate appeared to be acid- and base-catalyzed (Blum, et al., 1992). The formation of monosilanol was the slowest, thus the rate determining step (Blum, et al., 1992).

The hydrolysis of alkoxy silanes is affected by many factors, including water content, temperature, solvent, catalyst, and the type and concentration of silanes used. In general, an increase in water content and temperature enhances the hydrolysis. Blum, et al. (1992) reported that the hydrolysis of 3-aminopropyltrimethoxy silane (APTES) in an acetone and water mixture increased with water content. The hydrolysis rate of alkoxy groups also depends on the type of organofunctional group at the other end. The hydrolysis of the alkoxy group is slower in alkyl silane than in aminoorganosilane due to the self-catalysis of amino groups. Plueddemann (1982) reported that the alkoxy groups in aminoorganosilanes such as APTES were hydrolyzed almost immediately in water at alkaline pH. Contributing factors may be the hydrophilic nature of organofunctional groups and their impact in self-catalysis. In our experiments, the reaction time is kept at about 3 hours to ensure the complete hydrolysis of APTES in the solvents used.

4.2.4 Surface Condensation

In the solution containing hydrolyzed silane coupling agents, two possible condensation reactions may occur when a substrate is present. The monomeric or oligomeric silanols may either react with each other to form a polymer or couple with surface silanols (i.e. condensation on the substrate) to form a silanized film. This condensation process is influenced by many factors including (i) the rate at which the active species are formed, (ii) their relative ability to be attracted to the particulate surface, (iii) their orientation with respect to the surface, and (iv) the type of layers formed on the surface. In most

applications, silane molecules are first adsorbed on the surface by either physical

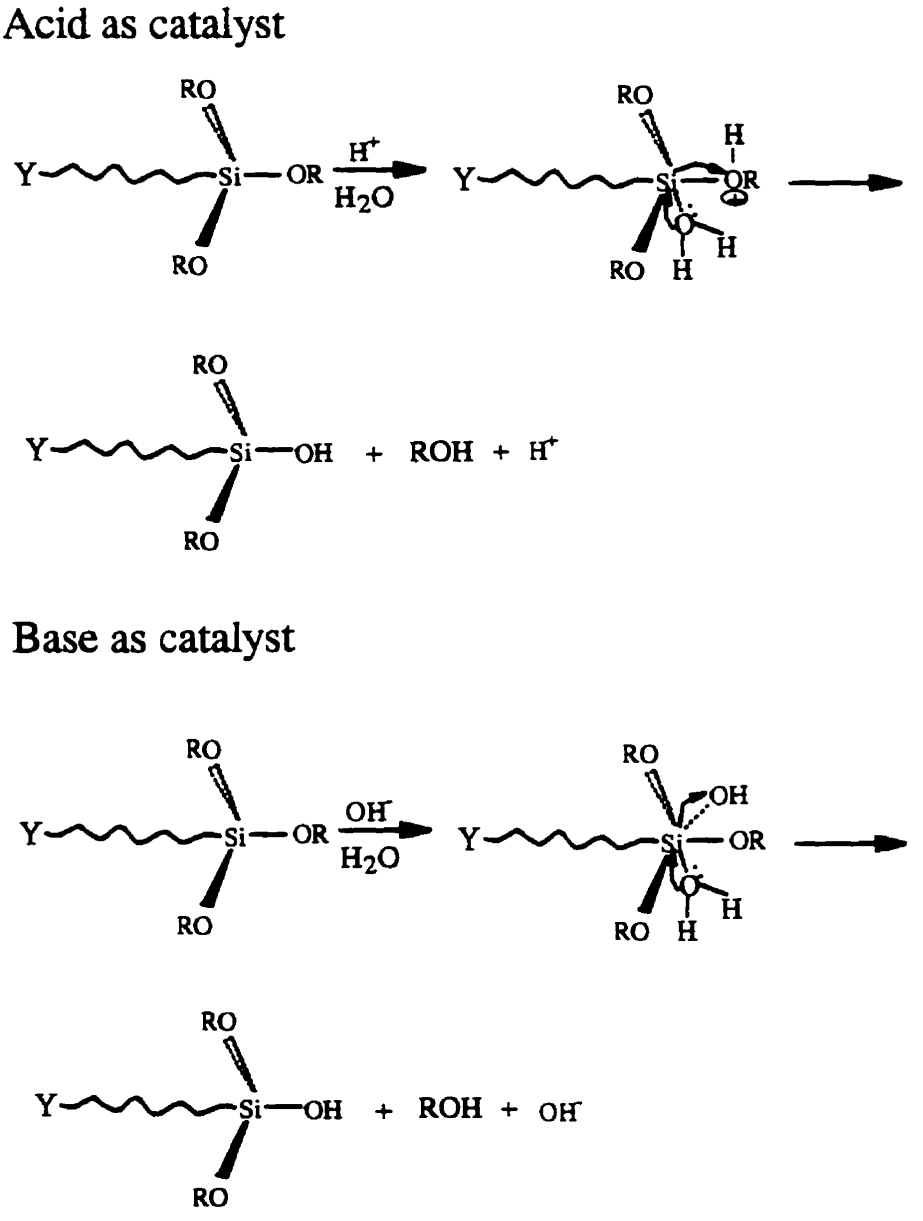

Figure 4.5 The hydrolysis of alkoxy silane in the presence of acid or base as catalyst. Only the first step of hydrolysis is shown. As the hydrolysis proceeds, the silanetriol monomer will form.

adsorption or hydrogen bonding with surface hydroxyl groups, followed by dehydration to form covalent bonds (Si-O-surface) accompanied by lateral cross-linking on the surface. The released water molecules may act as a promoter for further hydrolysis of alkoxy groups. Condensation reactions may continue to form multilayers on the surface, depending on the orientation of the molecules in the first layer. For example, some APTES could be attached on the surface through amino groups by forming hydrogen bonds between the hydrogen of surface silanols and the nitrogen of the amino groups, leaving APTES silanol groups free at the other end for further condensation. Due to the favorable condensation reaction between silanol groups of APTES and surface silanols, most APTES molecules are chemically bonded in the first layer, while physisorbed species, probably as oligomers, are the major part in the outer layers. Most of these physisorbed species can be washed away with a suitable solvent while the chemisorbed species on the surface remain attached

Blum, et al. (1992) studied the adsorption of aminopropyltrimethoxyl silanes (APTMS) onto silica from a 10:1 acetone-water mixture and showed that maximum loading (0.7 mmol APTMS/100 m^2) was achieved at a silane concentration of 1 g/100 ml. Further increases in silane concentration did not increase the surface coverage. To ensure the maximum coverage of magnetic particles by silane molecules and to study the effects of solvents on silanation, a high concentration (10%) of APTES in water and toluene was used in our experiments. The magnetic particles were well dispersed in the solvents before the addition of APTES to create an environment for enhancing the condensation of silanols with surface hydroxyls.

4.3 MATERIALS AND EXPERIMENTS

4.3.1 Materials

The magnetic particles (γ-Fe_2O_3) used as before were dried in an oven at 120 °C in order to remove any physisorbed water from the surface. Dried samples were stored in a desicator before use. The 3-aminopropyl triethoxysilane (APTES) purchased from

Petrarch® System (Bristol, PA) with a purity of 98% was used as received. Glass distilled toluene with a purity of 99.9% from OmniSolv and in-house distilled absolute ethanol were used. Water used was prepared with a Milipore water treatment system. All glass ware was cleaned by the procedure described in chapter 3.

4.3.2 Silanation

A 3 gram sample of γ-Fe_2O_3 was mixed by vigorous stirring with 90 ml of solvent (water or toluene) in a 500 ml three neck flask equipped with a condensing tube. After the particles were well dispersed, 10 ml of APTES was added slowly to the flask, and the suspension was heated to refluxing temperature, then refluxed for 3 hours, while maintaining nitrogen bubbling and mechanical stirring. The suspension was then cooled and centrifuged at 9000 rpm (Dynac™ centrifuge) for 20 mins. After washing twice with the solvent, and once with ethanol, the particles were dried in the oven at 80 °C for three hours. The dried samples were stored in a vacuum desicator prior to surface characterization. (Note: when water was used as a solvent, the pH of the suspension was ca. 10.5.)

4.3.3 Film Characterization

As mentioned in section 4.2, either silanols or amino groups of silane coupling agents can react with the surface hydroxyls, leaving the other exposed to the environment. To examine the orientation of silane molecules, several techniques as described in chapter two can be used. Among the techniques described, the most informative are FTIR and XPS. In the FTIR, the -O-CH_2-CH_3 stretching band provides the information on the hydrolysis of silanes, while the Si-O-Si and N-H stretching/deformation bands yield valuable structural information about APTES on the surface. In the XPS, the N(1s) binding energy region furnishes an insight into the interaction between the surface hydroxyls and the silane amino groups. In this chapter, these two techniques are used to determine the orientation and interaction of molecules on the surfaces. Other techniques such as zeta-potential

measurements and elemental analysis are also used as the complementary methods to complete the picture of silane molecules on the surface.

Silanized particles were characterized by XPS and DRIFTS using the procedures described in the previous chapter. As reference, the transmission IR spectrum of APTES was obtained using a liquid cell with KBr windows at the same wavenumber resolution as DRIFTS. The zeta-potential of the magnetic particles with and without silanation were measured in 5 mM of KCl background electrolyte solution using a Lazer-zee meter (Model 501, USA). About 5 mg of particles was conditioned for 10 minutes in 100 mL of test solution. The slurry pH was adjusted by NaOH and HCl stock solutions. The suspension was then taken for zeta potential measurement. The results presented here are the average of three independent measurements with a typical variation of ±3 mV.

The magnetic properties of silanized particles were characterized by home-made VSM. Elemental analysis was performed using the Model 240 XA elemental analyzer (Control Equipment Corporation, Lowell, MA, U.S.A.), in which acetanilide was used as an internal standard.

4.3.4 Stability of Surface Films

To examine the stability of surface films, leaching tests were conducted. Twenty milligrams of γ-Fe_2O_3 with and without silanation was mixed separately with 25 mL of acid (0.01 N HCl) or base (0.01 N NaOH) solutions for 20 hrs. The suspension was then centrifuged using a Sorvall® RC-5B refrigerated superspeed centrifuge (Du Pond Instruments) at 12000 rpm for 30 minutes. The supernatant was collected and analyzed for iron concentration by atomic absorption spectroscopy (Perkin Elmer 310, USA). The settled solids were washed and centrifuged three times with Millipore water, then dried in a vacuum oven at 60 °C. Finally, the samples were stored in a desicator. Changes in zeta-potential before and after contact with acid or base were used as an indication of the detachment of silane molecules from the surface.

4.4 RESULTS AND DISCUSSION

4.4.1 Orientation of Silane Molecules on the Surface

The molecular orientation of silane coupling agents on the surface bears a significant impact on the applications of silanized particles. In most applications, a desirable organofunctional group reactive on the surface is required for coupling with other materials. An understanding of molecular orientation and the reactivity of the functional group on the surface is needed for exploring the applications of the silanized materials.

XPS Analysis: XPS spectra of relevant elements on γ-Fe_2O_3 silanized using APTES from water and toluene solutions (cured at 80 °C) are shown in Figure 4.6. As reference, the corresponding XPS spectra of untreated magnetic particles are also included in this figure. The appearance of nitrogen (N_{1s}) and silicon (Si_{2p}) bands (at 399.4 and 101.8 eV, respectively) after silanation in both water and toluene solutions indicates that silanes are deposited on the surface. A close examination of the spectra shows that the nitrogen bands are broad and asymmetric. Deconvolution of the nitrogen band resulted in two distinct bands centered at ca. 399.4 and 401.3 eV, indicating nitrogen in two different environments: one free and the other from the protonated amino groups, respectively (Horner, et al., 1992). Two oxygen bands at binding energies of 531.8 and 529.6 eV were observed. The band at higher binding energy (531.8 eV) is assigned to the oxygen connected to the silicon, while the one at lower binding energy (529.6 eV) is attributed to the oxygen in γ-Fe_2O_3 (Moulder, et al., 1992).

Based on the best fitted, deconvoluted band areas, the ratios between the two nitrogen and the two oxygen bands were calculated, from which the proportion of the protonated to free amino groups and the relative percentage of the two oxygen components on APTES silanized magnetic particles are obtained, and the results are given in Table 4.1.

The proportion of the oxygen in Si-O environment (531.8 eV) was found to be higher in the film silanized from water than that from toluene (Table 4.1), suggesting that more silanes are deposited on the surface from a water solution. This observation is consistent with the elemental analysis which indicated a nitrogen content of 0.36 and 0.42% for the particles silanized in toluene and water, respectively. The higher ratios of other elements such as silicon, nitrogen and oxygen to iron for APTES films silanized from water than the ones from toluene further confirmed that more APTES molecules were deposited on magnetic particles from water.

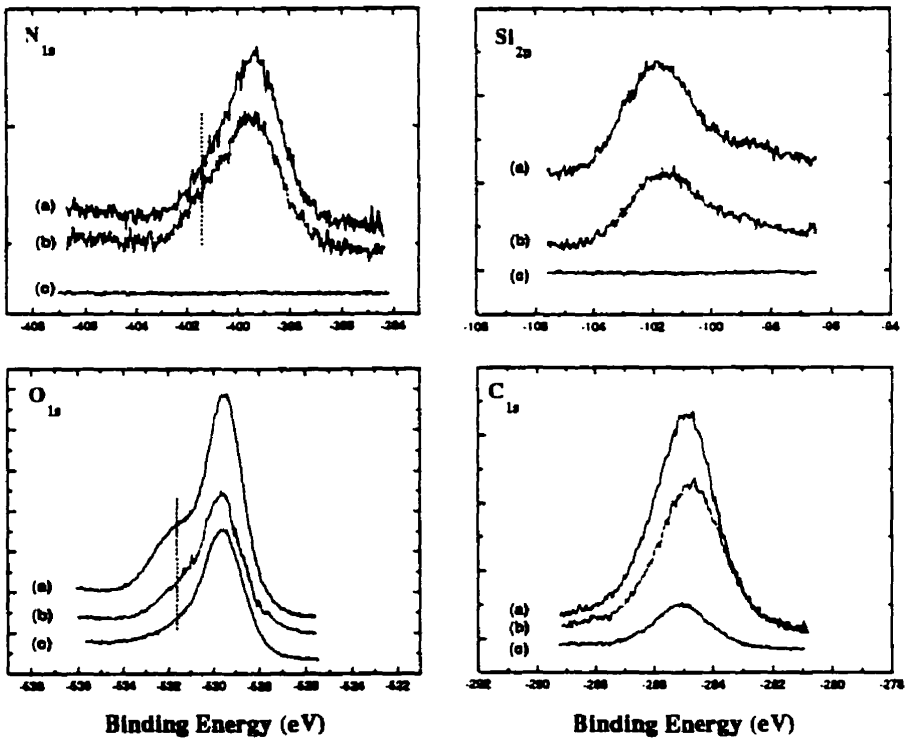

Figure 4.6 The XPS spectra of elements on the surface of γ-Fe_2O_3 with and without deposition of APTES (a) from water; (b) from toluene; (c). γ-Fe_2O_3 only.

Table 4.1 The proportion of amine protonation and the two oxygen components and assay of surface atom ratios of APTES films formed from water and toluene on γ-Fe_2O_3[a]

Solvent	$-NH_2$ (%) (399.4 eV)	$-NH_3^+$ (%) (401.3 eV)	O_{1s} (%) (531.8 eV)	O_{1s} (%) (529.6 eV)	Si_{2p} /$Fe2p_{3/2}$	N_{1s} /$Fe2p_{3/2}$	O_{1s}[b] /$Fe2p_{3/2}$
water	73.6	26.4	24.3	75.7	3.1	0.4	2.8
toluene	83.4	16.6	13.7	86.3	2.1	0.3	1.3

a: reaction is conducted at refluxing temperature, and samples are cured at 80 °C in air; b: oxygen band at 531.8 eV.

Table 4.1 also shows that the film deposited from aqueous solution contains a higher proportion of protonated amine (26.4%) compared to that from toluene solution (16.6%). It should be noted that the pH of suspension increased from ca. 5.0 to 10.5 upon the addition of APTES, indicating that approximately $10^{-3.5}$ M hydroxide ions were released probably due to the protonation of amine groups. Compared to toluene, therefore, more protonated amines were anticipated to be present in aqueous solutions and hence in the film silanized from these solutions. Further calculations, based on the amount of OH^- released, suggest that no more than 0.07% of the amino groups were protonated in aqueous solution, while a much higher fraction of amines was protonated on the surface. This simple calculation indicates that the protonated (and hence positively charged) amines adsorb preferentially on the surface, probably by long range electrostatic attractions, since magnetic particles carry negative surface charges at this pH (pH 10.5 is well above the isoelectric point, IEP, of magnetic particles ca. pH 5). It has been reported from angle-resolved XPS studies that most protonated amines were indeed located near the acidic glass surfaces (Fowkes, et al., 1990).

In dry toluene, on the other hand, the protonation of the amino groups was less significant compared to that in water. A lower fraction of protonated amine in the silanized film was therefore expected. The electrostatic interaction in organic solvent is unlikely to be significant. These factors contribute to the observed low degree of protonation of amino groups in the silanized film from toluene. Hydrogen bonding between the amino groups and surface hydroxyls or surface water is considered to be responsible for the protonation of amino groups (Fig. 4.7).

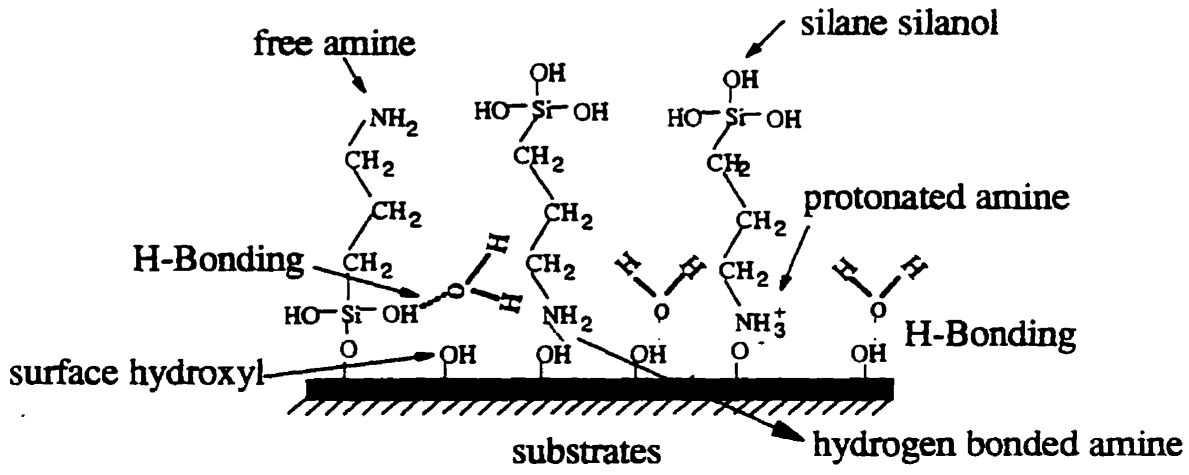

Figure 4.7 Schematic representation of possible orientations of APTES on the surface. The hydrogen bonded water may prevent the lateral polymerization of silanol on the surface, but may promote the adsorption of amino groups toward the surface.

We also noticed that the degree of amine protonation (26.4%) on magnetic particles is less than that on silica (43%), both silanized in aqueous solutions (Horner, et al., 1992). One reason may be due to a stronger electrostatic attraction between positively charged amine and the more negatively charged silica (iep at ca. pH 2.1) as compared to γ-Fe_2O_3 (pH iep = 4.5) which requires less protonated amine to neutralize its surface charge. The acid-base interaction between silane and substrates may also play a role in this regard. Horner, et al. (1992) found that the amino groups of APTES were protonated by interaction with hydroxyl groups on the surface of silicon, iron, titanium, and magnesium. The extent of protonation was greatest on silicon and titanium; followed by iron; and least on magnesium, which correlates well with the predicted IEP's of these metal oxides as listed in Table 4.2. According to the theory developed by Parks (1965), magnesium oxide, having an IEP near 12.0, is basic. Silicon and titanium oxides, with IEP's near 2.1 and 4.1, respectively, are relatively acidic. Iron oxide with an IEP near 8.5 lies in between. The reduced fraction of protonated amines present on the surface of a substrate of increasing basicity (43, 32, 21 and 9% protonation for APTES on silicon, titanium, iron and magnesium, respectively) indicates a significant acid-base interaction effect on both the degree of silanation and the orientation of silane molecules on the surface.

The above XPS analysis confirmed that the magnetic particles can be silanized with APTES from either water or toluene solutions. The coverage of APTES from water on magnetic particles is higher than that from toluene, and a higher fraction of the amines were protonated in the films silanized in water than in toluene. However, XPS analysis is unable to determine the degree of hydrolyzation of ethoxy groups and subsequent cross-linking, which has a significant impact on the density and stability of the film.

Table 4.2 Degree of amine protonation of APTES on various acid-base substrates[a]

Substrate	Protonated amine (%) NH_3^+ (401.3 eV)	Primary amine (%) NH_2 (399.2 eV)	IEP
Silicon	43	57	2.1
Titanium	32	68	4.2
Iron	21	79	8.5
Magnesium	9	91	12.0

a: XPS is taken at 75° take-off angle (after Horner, et al., 1992).

DRIFTS Characterization: The DRIFTS spectra of magnetic particles silanized with APTES in water and toluene, and cured at 80 °C in air, are shown in Figure 4.8. For the reference, the IR spectrum of bulk APTES is also shown in this figure (spectrum c). In the high wavenumber region, the spectrum of APTES contains the characteristic bands of -NH_2, -CH_3, -CH_2, and Si-O-C vibration modes. The bands at 3380 and 3292 cm^{-1} are assigned to -NH_2 asymmetric and symmetric stretchings (Culler, et al., 1984; Battjes, et al., 1992), respectively , while the weak band at 3187 cm^{-1} may be due to intermolecularly hydrogen bonded amino groups. The bands at 2974 and 2887 cm^{-1} are characteristic of -CH_3 asymmetric and symmetric stretchings in the ethoxy group of APTES, and the bands at 2927 and 2865 cm^{-1} are assigned to asymmetric and symmetric stretching modes of -CH_2 in alkyl chains. In the low wavenumber region, the broad band at 1606 cm^{-1} is assigned to the bending mode of free amino groups, which are characteristic of APTES. The bands at 1167, 1105, 1083. 959 cm^{-1} are characteristic of Si-O-C vibrations. The detailed band assignments are summarized in Table 4.3.

As shown in Figure 4.8, a broad band at 3360 cm^{-1}, assigned to free amino asymmetric stretching, appeared on the spectra of magnetic particles silanized in either water or toluene solutions (spectra a and b). The broad bands at 3245 and 3124 cm^{-1} due to stretching vibrations of protonated and hydrogen bounded amine groups, respectively, were also observed. In addition, the bands at 2927 and 2865 cm^{-1} assigned to the asymmetric and symmetric stretching of CH_2 in alkyl chains were present. These observations confirm the silanation of APTES on γ-Fe_2O_3 as suggested in the XPS analysis.

Table 4.3 Mode Assignments and Band Positions for APTES.

wavenumber (cm^{-1})	Assignment
3380	-NH_2, asym str
3292	-NH_2, sym str
2974	CH_3, asym str (-OCH_2CH_3)
2890-2855	-CH_2, sym str ($CH_2CH_2CH_2$), CH_3, sym str(OCH_2CH_3)
1606	NH_2, def (bending)
1483	CH_2 propyl, sym def
1442	CH_3 sym def
1410	CH_2 adjacent to Si (scissors)
1167, 1105, 1083, 959	Si-O-C

In the low wavenumber region, the characteristic bands of Si-O-C at 1167, 1105, 1083 and 959 cm^{-1} (spectrum c) disappeared for APTES silanized on magnetic particles in both water and toluene (spectrum a and b). Instead, two broad new bands at 1115 and 1010 cm^{-1} characteristic of siloxane bonds appeared, suggesting that most ethoxy groups were hydrolyzed, and a siloxane bond was formed on the surface by condensation and/or lateral polymerization of APTES. Note that the bands at 1580 and 1477 cm^{-1} are due to the deformation bendings of free amine groups on the surface (it appears at 1606 cm^{-1} in liquid) and hydrogen bonded or protonated amine groups, respectively.

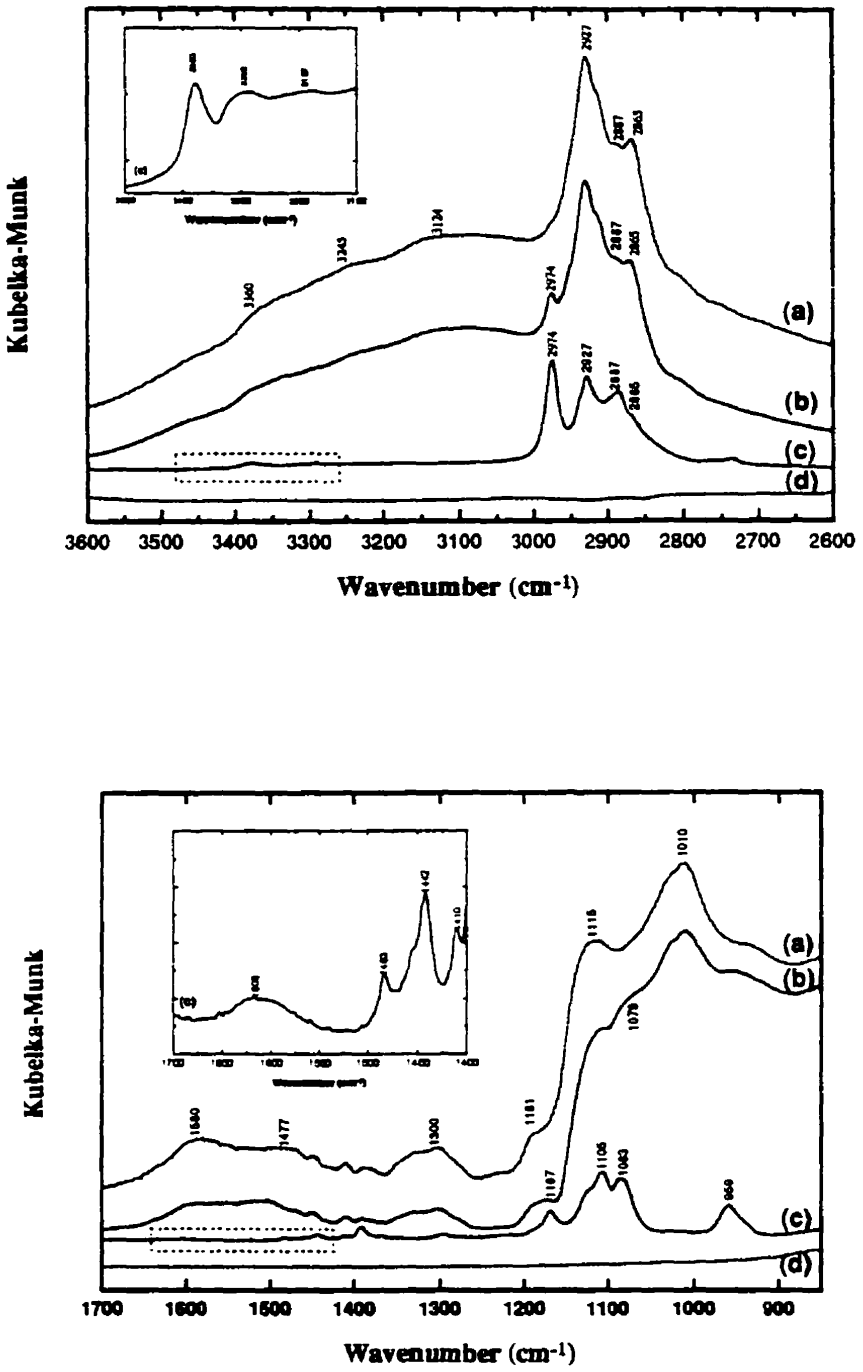

Figure 4.8 Infrared spectra for (a) magnetic particles silanized by APTES from water; (b) magnetic particles silanized by APTES from toluene; (c) APTES only; (d) γ-Fe_2O_3. Insets show IR bands of amino groups in APTES.

It is interesting to note that when silanation was conducted in toluene, small bands at 2974, 2887, and 1079 cm^{-1} were observed, indicating that small fraction of APTES silanized from toluene remained unhydrolyzed. The unhydrolyzed ethoxy groups on the surface may inhibit the lateral polymerization of APTES, thus resulting in a poorer packing density and lower surface coverage as compared to the film silanized from water in which the hydrolysis is more effective. This observation is consistent with the findings from XPS and elemental analysis.

Zeta-Potential Measurement: Zeta-potentials of silanized magnetic particles were found to be significantly higher than unsilanized ones as shown in Figure 4.9. The IEP's of the particles silanized from water and toluene were at ca. pH 8.5 and 9.2, respectively, which were higher than the IEP (pH = 4.5) of unsilanized particles. These findings confirm the deposition of APTES on magnetic particles by silanation, with most amino groups being exposed to the environment. The difference in the measured zeta potentials of the particles silanized from water and toluene indicates the different coverage and orientation of APTES on the magnetic particles. Since XPS and elemental analysis have shown higher surface coverage of APTES on magnetic particles silanized from water, the slightly lower zeta-potential values observed for these particles suggests that more amino groups were hidden inside the films, as compared to the case for toluene. As a result, the contribution from amino groups to the number of positive surface sites decreases, while that from silanol groups to the number of negative sites increases. It is anticipated that these two counter effects result in a lower IEP values for the particles silanized from water. This is consistent with XPS analysis, which showed a higher degree of protonation of amino groups near the surface (i.e., a lower degree of the free amino groups in the surface films) (Fowkes, et al., 1990).

It is interesting to note that the electrokinetics of magnetic particles silanized with APTES from toluene were seen to resemble those of air bubbles in dodecylamine (a cationic surfactant) solutions, in which case the amino groups were exposed to water (Figure 2.9). The similarity between the two systems further suggests that the majority of

amino groups in APTES silanized on the surface were exposed to the environment and remained reactive.

The above experimental results showed that the silane coupling reagents can be silanized on magnetic particles to obtain desirable magnetic carriers. It has also demonstrated that the coating density and molecular orientation of APTES on the surface are controlled by the competing interactions shown in Figure 4.2. From the application point of view, it is important to know whether the silanized film fully covers the particles and how stable the film is, in addition to concerns about the density of the desired functional groups. For this purpose, the stability of silanized APTES films is studied as given below.

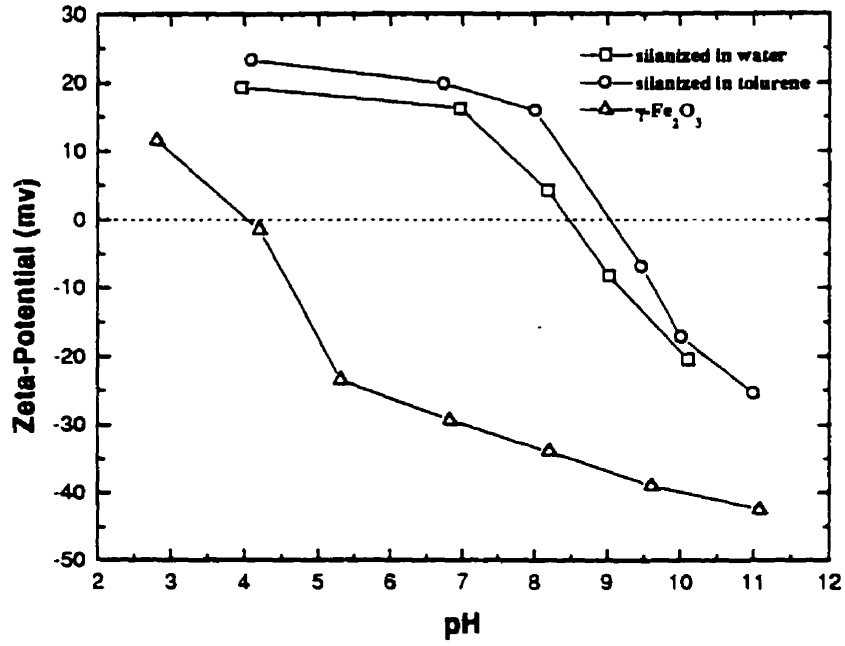

Figure 4. 9 Zeta-potential of magnetic particles with and without silanation by APTES in different solvents.

4.4.2 Stability of Silanized Films

Leaching Test: As shown in Table 4.4, the amount of iron leached out in 0.01 N HCl solutions decreased from 60 mg/g for unsilanized to 34 mg/g for silanized γ-Fe_2O_3 particles (either from water or from toluene). Clearly, the amount of iron leached remained significant for silanized particles, suggesting that the original particles were not fully covered, which may have been compounded with some degree of detachment of the APTES in acidic solutions. The formation of disordered, loosely packed films on oxidized silicon wafers using APTES has been reported by Bierbaum, et al. (1995). It is believed that weak van der Waals interactions between short alkyl chains are not sufficient to induce chain ordering. The loosely packed films will result in an exposure of some magnetic particles to environment, thus providing a channel for acid or base solution to reach the surface and to attack the APTES-surface bonds. To improve the stability of silanized films, a silane coupling agent with a long hydrocarbon chain may be required. It is anticipated that van der Waals interactions between long alkyl chains (e.g. $-(CH_2)_{18}$) will be sufficient to improve the packing density of silane molecules on the surface. A complete coverage will prevent the surface from being exposed to the environment, thus avoiding the breakage of Si-O or Fe-O bonds on the surface.

Table 4.4 The Fe ions leached from magnetic particles with and without silanation.

	Fe ions (mg/g particles)
γ-Fe_2O_3	60.3
γ-Fe_2O_3 coated by APTES from water	34.0
γ-Fe_2O_3 coated by APTES from Toluene	34.1

Zeta-Potential Measurements: Detachment of silanized APTES in acidic and basic solutions was confirmed by zeta-potential measurements as shown in Figure 4.10. After acid leaching, the zeta potentials of magnetic particles silanized with APTES from water shifted back towards the original zeta potential values of unsilanized particles. Figure 4.10 also shows a much larger shift in IEP values after base leaching (from pH 8.5 to 4.3), suggesting that the APTES coating is less stable in basic than in acidic environments. IR

spectra of silanized films after acid or base leaching showed a significant decrease in the intensity of APTES characteristic bands, confirming a significant degree of detachment of silanes from the surface. Whether the detachment of APTES is due to the breakage of Si-O or Fe-O bonds remains uncertain. It is well documented that the Si-O bond is relatively stable in acidic solutions compared to that in basic solutions (Iler, 1979). It appears that the breakge of Fe-O bonds on the surfaces accounts for the above observations. (Should the breakage be at Si-O bonds, the destructed surfaces should resemble a silica surface with an IEP around pH 2.)

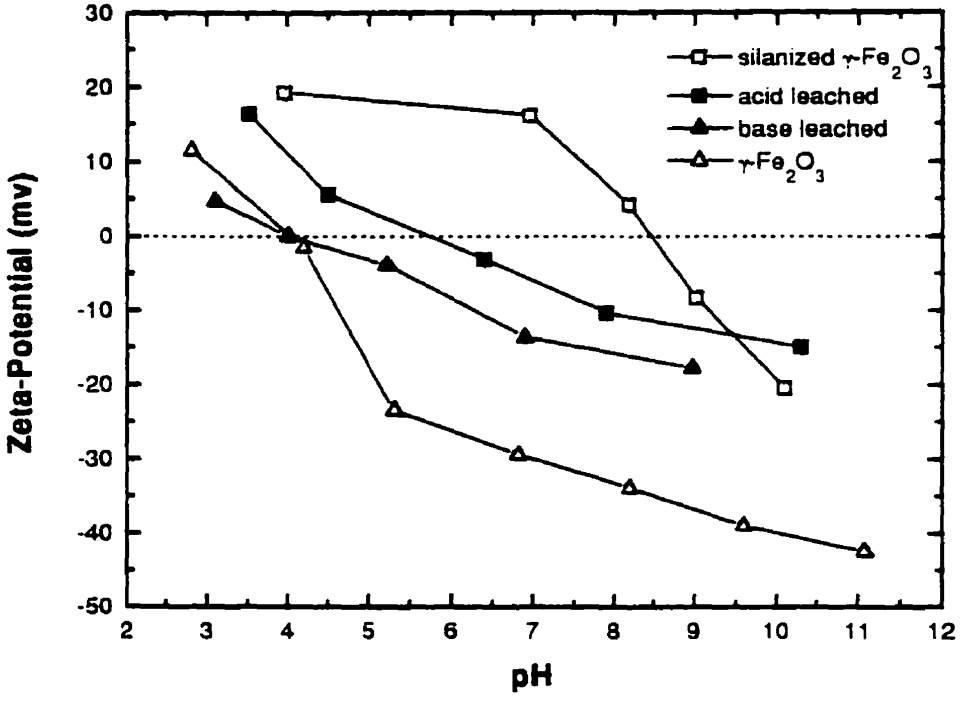

Figure 4.10 The changes of the zeta-potentials of APTES silanized magnetic particles from water before and after acid or base leaching.

Similar trends in electrokinetics were observed for the particles silanized with APTES from toluene (Fig. 4.11). After base leaching, the IEP values of the silanized particles were shifted from pH 9 to 4.3, indicating that the films formed from toluene were unstable in a basic environment. However, after acid leaching, the IEP values were only shifted from pH 9.0 to 8.5, suggesting that the films formed from toluene were relatively stable in a acidic environment, as compared to the ones silanized from water (Figure 4.10). These findings may be attributed to a higher degree of free amino groups in the films silanized from toluene, as shown in XPS analysis.

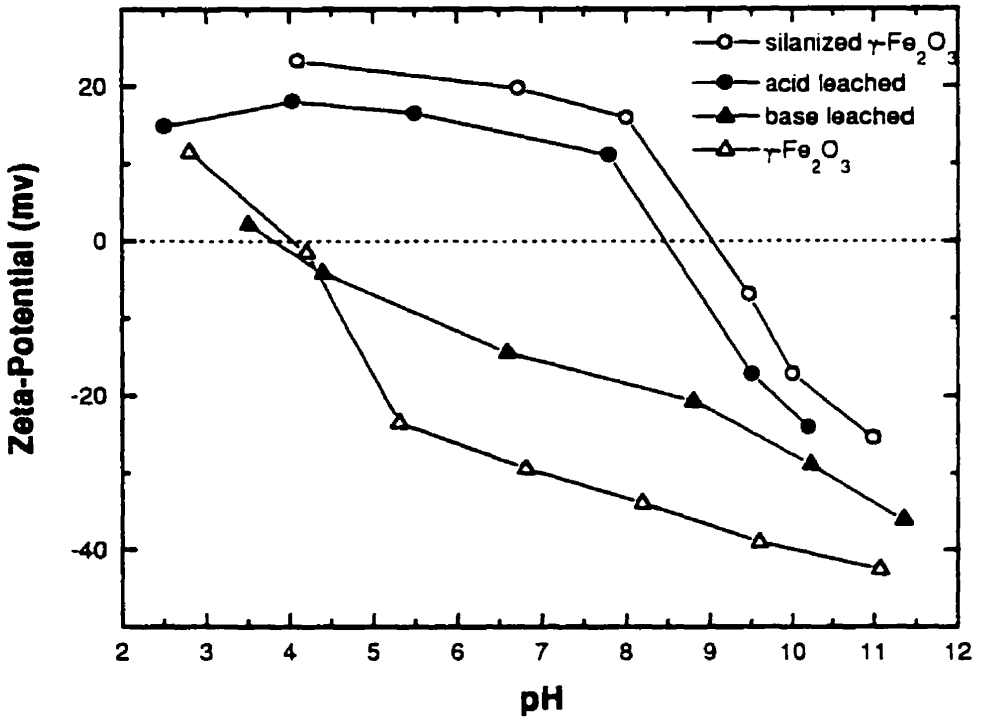

Figure 4.11 The changes of zeta-potential of APTES silanized magnetic particles from toluene before and after acid or base leaching.

4.4.3 Magnetic Properties of Silanized Magnetic Particles

Magnetization curves of magnetic particles, with and without silanation, are shown in Figure 4.12. It can be seen that the magnetization of magnetic particles reduced only marginally after silanation. The saturated magnetization of silanized magnetic particles from toluene is higher than that from water, indicating less silane being loaded onto the surface from the toluene. This is consistent with XPS and elemental analysis results. The very small coercivity and hysteresis in the magnetization curves for silanized magnetic particles indicates that the particles remain paramagnetic. These magnetic features permit the application of silanized magnetic particles in magnetic carrier technology.

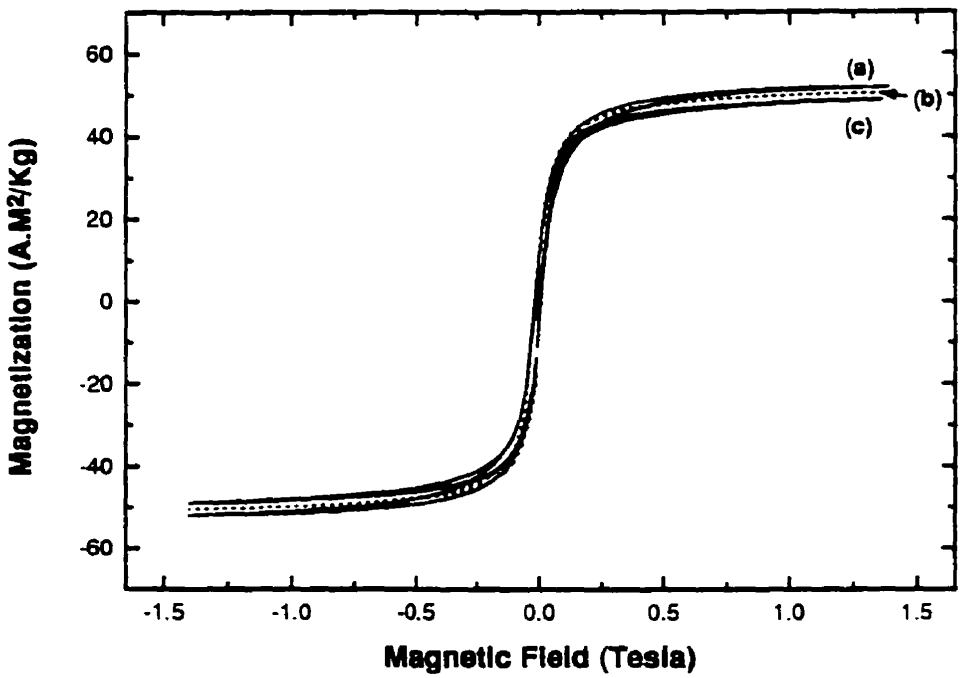

Figure 4.12 The magnetization of magnetic particles with and without silanation (a) γ-Fe_2O_3; (b) silanized from toluene; (c) silanized from water.

4.5 CONCLUSIONS

1. XPS, IR, and zeta-potential measurements indicate that silanation of magnetic particles using APTES was successful from solutions of water and toluene.
2. The degree of protonation of the amino groups in the films formed from water was higher than the ones from toluene, so was the silane coverage.
3. The IEP (9.2) of magnetic particles silanized from toluene was higher than the one (8.5) from water, probably due to the lower degree of protonation of the amino groups in the film.
4. The films formed from toluene were relatively stable in acidic solutions compared to those formed from water, but both films were unstable in alkaline solutions.
5. The saturated magnetization of magnetic particles reduced marginally after silanation.

CHAPTER 5 PREPARATION OF MAGNETIC CARRIERS (III): SILICA COATING

5.1 INTRODUCTION

In chapter 4, direct silanation on nanosized magnetic particles (γ-Fe_2O_3) using APTES in water and toluene was discussed. It was found that the silanized films on magnetic particles from toluene were relatively stable in acidic solution (0.01 N HCl) compared with the ones from water. In basic solution (0.01 N NaOH), however, silanized films both from water and toluene were unstable. It has been well documented that the silanized films on silica are relatively stable compared to those on iron oxides (Arkles, 1992). Therefore, the stability of silanized films is anticipated to be improved if a thin layer of silica can be coated on magnetic particles prior to silanation. The objective is to develop a method to deposit a thin, densely packed silica layer on magnetic particles, making the surface more amenable for subsequent silanation, while maintaining the maximum magnetization required for applications. To explore this idea, the silica coating on γ-Fe_2O_3 using the sol-gel process and/or dense liquid silica coating (DL process) is studied in this chapter. A schematic diagram for preparing the magnetic carriers by silica coating and subsequent silanation is shown in Figure 5.1.

5.2 SOL-GEL PROCESS AND DENSE LIQUID SILICA COATING

There are many methods available for silica coatings on different substrates (flat surfaces or powder samples). These include chemical vapor deposition (Tsugeki, et al., 1994; Hoffman, et al., 1995), electron beam evaporation (Vigil, et al., 1995), sol-gel process (Brinker and Scherer, 1990; Sando, et al., 1995; Shih, et al., 1995; Tada, 1995), and dense liquid silica coating (Iler, 1959; Furlong, et al., 1980; Firment, et al., 1989, Furlong, 1994). The sol-gel process and the dense liquid silica coating are more suitable

for powder samples. The present study will, therefore, focus on the sol-gel process and dense liquid silica coating.

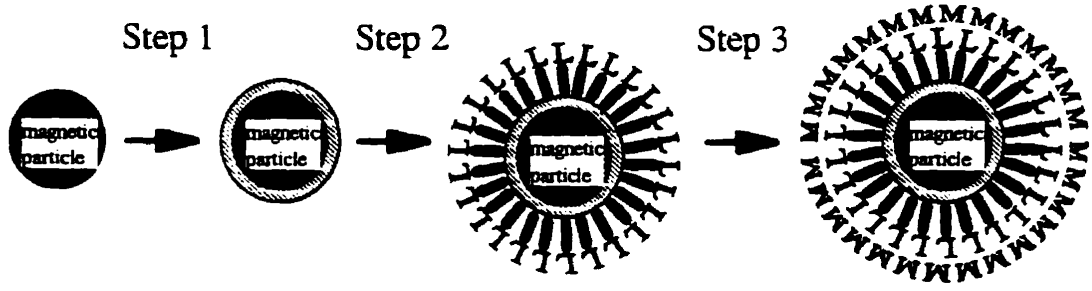

Figure 5.1 Schematic representation of the preparation of magnetic carriers by silica coating and silanation process. The magnetic particles were first coated by a thin silica layer (step 1), and then silanized by silane coupling agents (step 2). The targets, e.g. metal ions (M) in aqueous solution, are loaded on magnetic carriers through functional group L (step 3).

5.2.1 Sol-Gel Process

Silica coating by sol-gel process is based on the hydrolysis of the precursors such as tetraethoxy silane (TEOS) in the presence of water and catalyst, followed by the condensation with surface hydroxyls. The hydrolysis of TEOS in the presence of water and catalyst (acid or base) has been reported to form monosilicic acid and ethanol (Brinker and Scherer, 1990):

$$Si(O\text{-}CH_2CH_3)_4 + H_2O \xrightarrow[OH^-]{H^+} HO\text{-}Si(OH)_2\text{-}OH + CH_3CH_2\text{-}OH \qquad (5.1)$$

Under proper conditions, the monosilicic acid can be further condensed to form an oilgomer, and then polymerized to form a network structure of silica as shown below:

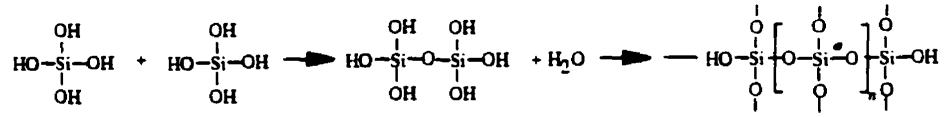

(5.2)

For a hydroxylated substrate, the silanol groups preferentially condense with surface hydroxyls to form chemical bonding (Si-O-Surface), building a two to three dimensional net work. In the sol-gel process, organic solvents such as ethanol are often used. Therefore, a silica film can be coated on the substrates slightly soluble in water by this method. In addition, uniform coatings can be obtained by controlling the hydrolysis rate of metal alkoxides (Bosch, et al., 1995; Tada, 1995). A low solubility of a silica in ethanol was found to contribute to a high coating efficiency. These features made the sol-gel process useful for fabricating inorganic thin films of unique properties, such as tailored porosity, refractive index, and compositional homogeneity (Brinker and Scherer, 1990).

5.2.2 Dense Liquid Silica Coating

Dense liquid silica coating is a process in which the aqueous silica, such as sodium silicate, is used as a precursor for the formation of the silica layer on substrates under the controlled supersaturation conditions (Iler, 1979). In essence, dense liquid silica coating involves the heterogeneous surface nucleation from supersaturated aqueous solutions. To better understand the process and to obtain optimal surface coatings, a brief discussion on the nucleation and crystal growth theory is given below.

A) Homogeneous Nucleation

Nucleation is termed as the formation of new crystals or new phases. It is a common phenomenon in nature; as we all experienced the appearance of liquid drops on grass or leaves in the morning and the formation of air bubbles in boiling water. It is also a common observation that organisms deposit highly oriented, flaw-free ceramics from aqueous solutions under ambient conditions onto the substrates as delicate as living tissues such as teeth (Bunker, et al., 1994). Nucleation and crystal growth can occur either in solution (homogenous) or on the surface of other solids (heterogeneous). According to nucleation and crystallization theories (Evans and Wennerstrom, 1994), the free energy for the formation of stable nuclei (ΔG) in aqueous systems (homogenous nucleation) depends

on the degree of supersaturation (S), temperature (T), solid-liquid interfacial energy (σ), and interfacial area (A), and is given by:

$$\Delta G = -nkT \ln S + \sigma A \tag{5.3}$$

where k is the Boltzman constant. For the formation of spherical particles in aqueous solution, the supersaturation level S is defined as the concentration in excess of the solubility limit, and A is equal to $4\pi r^2$. Equation (5.3) thus becomes:

$$\Delta G = -\frac{4}{3}\pi \frac{r^3}{V_m} kT \ln \frac{C}{C_s} + 4\pi r^2 \sigma \tag{5.4}$$

where C is the standing concentration: C_s is the equilibrium concentration: and V_m represents molecular volume.

When $C > C_s$ the first term on the right-hand side will make $\Delta G < 0$ for sufficiently large r, but for sufficiently small r, the positive second term will dominate. Consequently, a maximum in ΔG occurs at some intermediate value of r. At the maximum of ΔG, the equation (5.4) becomes

$$kT \ln(\frac{C}{C_s}) = \frac{2\sigma V_m}{r_c} \tag{5.5}$$

which is known as the Kelvin equation. Here C represents minimum standing concentration required for the formation of tiny nuclei with radius of r_c. It can be seen that the high supersaturation level is needed for homogeneous nucleation. If we introduce a seed particle of radius r_1 into the solution, the particle will grow if r_1 is larger than r_c. Otherwise, it will vanish (Ostwald ripening). In the presence of seed particles, nucleation rate will be increased dramatically at a given supersaturation level. Since the r_c is often in the range of a few angstroms to a few nanometers for homogeneous nucleation, even impurity particles such as dust can be larger than r_c and thus act as foreign particles for nucleation, which becomes the case for heterogeneous nucleation.

B) Heterogeneous Nucleation

Heterogeneous nucleation refers to the new crystals or new phases formed on foreign particles or substrates. Dense liquid silica coating is a typical example of heterogeneous nucleation. The surface free energy for heterogeneous nucleation is described by three terms as shown in equation (5.6):

$$\Delta G = -nkT \ln S + \sigma_{cl} A_{cl} + (\sigma_{cs} - \sigma_{sl}) A_{cs} \qquad (5.6)$$

where subscripts c, s, and l represent interfaces involving the coated film, the substrate, and the liquid phase, respectively. Comparing equation (5.6) with equation (5.3), it is clear that due to the presence of foreign particles, heterogeneous nucleation usually occurs at lower supersaturation levels than those required for homogenous nucleation. The coating on a seed particle with the same chemical composition and crystal structure as the films to be coated represents a special case, called homogenous coating, where σ_{cs} becomes negligible and the solid-solution interfacial energy of the substrate is similar to that of the cluster. As a result, the free energy change associated with homogenous coating becomes:

$$\Delta G = -nkT \ln S \leq 0 \qquad (5.7)$$

One example satisfying this condition is the silica coating on a silica substrate, which is illustrated in our two-step silica coatings on nanosized magnetic particles.

An important aspect of the heterogeneous nucleation is to control the interfacial energy between the substrate and the film to be coated (σ_{cs}) (Bunker, et al., 1994; Mann, 1988). The surface with desired functional groups such as carboxylic, amine, sulfate, may lower the interfacial energy between the substrate and the film to be coated, i.e., σ_{cs}. For example, carboxylic groups on the surface are favored for calcite deposition (Mann, et al., 1993), amine for silica deposition (Stumm and Morgan, 1995), and sulfonic acid for iron oxyhydroxide formation (Rieke, et al., 1995). The functionalization of surfaces with these groups can be achieved by molecular self-assembly, silanation, and chemical (e.g. etching) or physical (e.g. plasma) treatment. In recent years, several investigators have shown that

by manipulating surface energies through chemical modifications and solution additives, the film composition, morphology, growth pattern, orientation, and even chirality of growth in aqueous media can be modified and controlled (Mann, 1993; Heywood and Mann, 1994). A typical example is the ceramic thin-film formation on functionalized surfaces through biomimetic processing (Bunker, et al., 1994). The study on the nucleation and crystal growth of inorganic materials on functionalized surfaces has improved our understanding of the formation of teeth and kidney stones in the human body (Mann, 1993).

The supersaturation level (S) for film coatings can be controlled in many ways to achieve heterogeneous nucleation, including: (a) inducing a chemical reaction to produce a species in excess to its solubility; (b) lowering the solubility by either drowning out aqueous solutions with organic solvents or adjusting the pH of the solutions; (c) constant addition of precursors to the system to maintain the supersaturation level. For coatings of inorganic materials on a desired surface from aqueous solutions, nucleation and crystal growth are generally induced when solution conditions (pH, concentration, and temperature) are changed from a regime in which precursors are soluble to a regime in which solutions are supersaturated as shown schematically in Figure 5.2.

In dense liquid silica coating, the solubility of aqueous silica and/or monosilicic acid in aqueous solution can be readily changed by adjusting the solution pH as shown in Figure 5.3 (Furlong, et al., 1979). Sodium silicate is highly soluble at alkaline pH, ca. 11.5. As the pH decreases, the system moves from regime A in which sodium silicates is soluble to regime B where the supersaturation is reached and nucleation occurs. As coating proceeds, the consumption of sodium silicate will change the degree of the supersaturation level (moving to C) until reaching the solubility limit of precipitated silica (ca. 2.5×10^{-3} M). By controlling the supersaturation level (constant reactant addition), the silica layers will form on the substrate through heterogeneous nucleation.

Dense liquid silica coating (DL process) was first developed by Iler in 1959 (Iler, 1959). A silica layer was initially coated on titania from aqueous solutions to prevent the

photodegradation of organic resin in paint films. In its broad applications, silica coating on surfaces of carbon and steel materials was used to prevent their oxidation in harsh

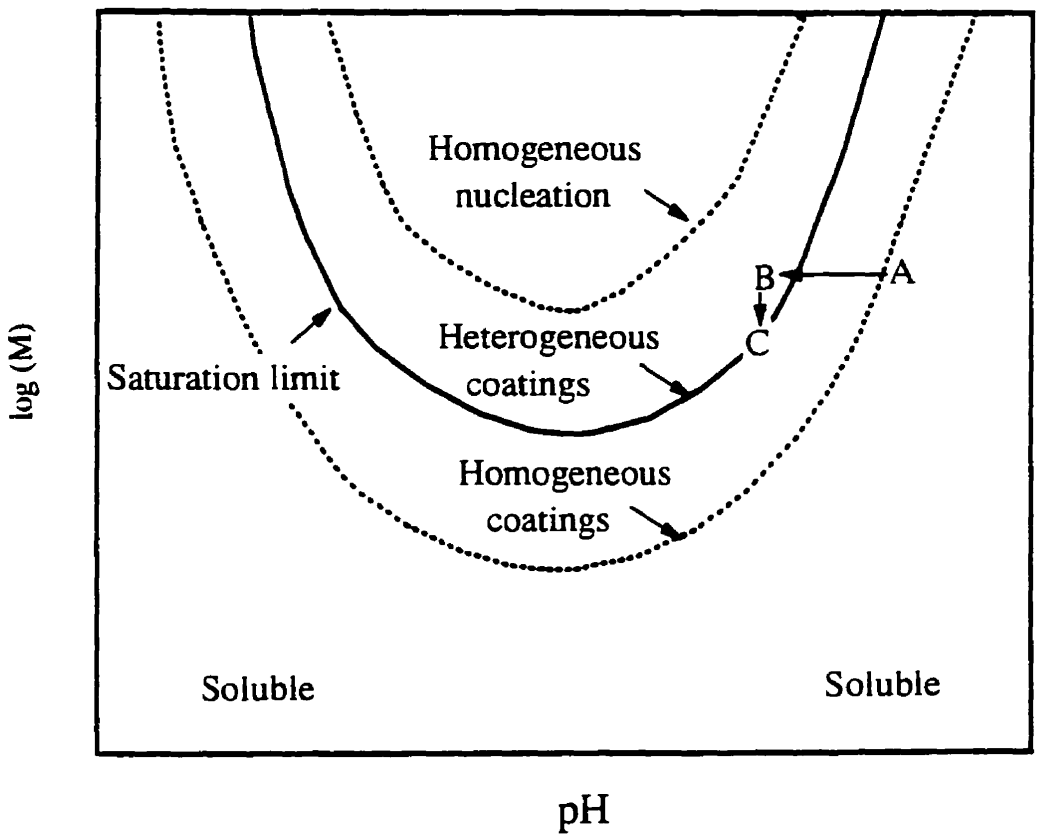

Figure 5.2 Schematic solubility diagram for understanding surface coatings. Solubility generally depends on temperature and pH. Heterogeneous coating occurs when solution conditions change from (A), a regime in which precursors are soluble, to (B), a condition of supersaturation. In general, homogeneous coating occurs at a lower supersaturation level than that for heterogeneous coating. Proper supersaturation promotes surface coating without bulk precipitation. In a batch process, the consumption of precursors in surface coating can change the degree of supersaturation (moving to C). In general, for optimum surface coatings the regime for homogeneous nucleation should be avoided.

environment. Silica coatings on substrates such as alumina were used to obtain a desirable surface wettability, adhesion, chemical reactivity, and acid-base properties. (Niwa, et al., 1990). As a low-temperature process in which water and sodium silicates are used, the DL process is environmentally benign and economic. However, for silica coating on substrates that are slightly soluble in water, the dissolved species may react with monosilicic acid, thus reducing the concentration of reactive species and lowering the supersaturation level for surface coatings. Extensive literature of silica coatings on various substrates using the DL process is available. However, there seems to be no report on silica coatings on nanosized magnetic particles (γ-Fe_2O_3), which is studied in this work.

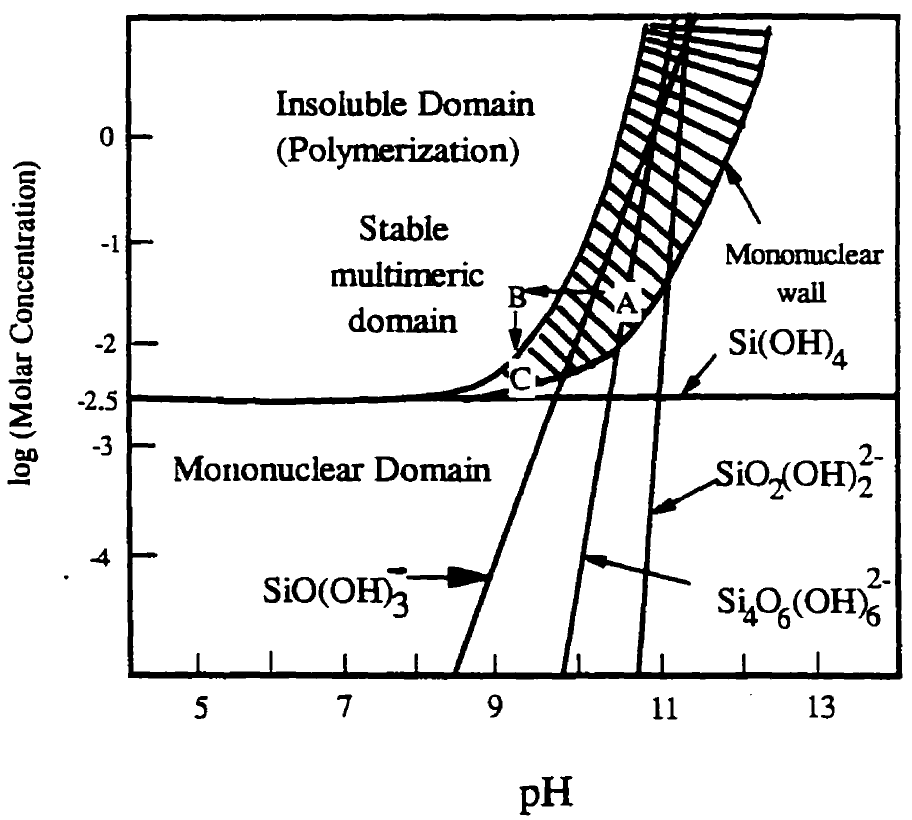

Figure 5.3 Schematic illustration of solubility domains for amorphous silica in aqueous solution. (A) represents the initial concentration of soluble sodium silicate at high pH value (ca 11.5). As the pH decreases, the system moves from regime (A) in which the sodium silicates are soluble to regime (B) where the supersatuation is reached, and the nucleation occurs.

Single step silica coating by either DL method or sol-gel process was conducted on nanosized magnetic particles (γ-Fe_2O_3). Based on the experimental results of single step coating, a two-step silica coating process, i.e., sol-gel followed by dense liquid silica coating, was developed. The concept behind this approach is to coat a silica layer on particles by the sol-gel process first. The objective of this step is to obtain a thin, uniform, most likely porous, silica layer on particles. Once the surface is covered by a thin silica layer, the DL coating is applied to fill the pores in the first layer and to grow the film uniformly. Because of the presence of the first silica layer prepared from the sol-gel process, although porous, the second step represents a homogeneous coating which can be achieved in a more controlled manner at lower supersaturation levels than those required for the direct DL coating. By using the two-step silica coating, a uniform, thin, and densely packed silica layer is anticipated to form onto magnetic particles for (i) preventing Fe from being leached into acidic solutions, and (ii) making the surface more amenable for silanation using silane coupling agents, while maintaining the maximum magnetic properties as required in magnetic carrier technology.

5.3 MATERIALS AND EXPERIMENTS

5.3.1 Materials

The same magnetic particles (γ-Fe_2O_3) as used before were dried in a vacuum oven at 12 psi and 120 ^{o}C for 24 hours prior to the coating experiments. The quartz distilled TEOS from Petrarch® System and the reagent grade ammonium hydroxides (30 wt%) from Caledon were used as supplied. Millipore water was used in all experiments. An aqueous silica solutions (27 wt% SiO_2) from Aldrich was used in dense liquid silica coating experiments. Amorphous fused silica particles with an average particle size of about 24 nm and specific surface area of 100 m^2/g were kindly provided by Cabot Corporation, Cab-O-Sil division (Tuscola, IL, U.S.A.). The silica particles were used as recieved.

5.3.2 Experiments

A) Sol-gel Process

In a typical coating experiment, 0.9 gram of magnetic particles was mixed with 40 mL of pure ethanol under ultrasonification for 30 minutes, followed by addition of 14 mL TEOS solution (0.2 mL TEOS in 13.8 mL pure ethanol). 6 mL of 30% NH_4OH solution (as catalyst) was then added dropwise into the suspension, and the reactions were allowed to continue for 5 hours to ensure the complete hydrolysis of TEOS and the formation of monosilicic acid necessary for the coatings. The treated particles were separated from solution by a hand magnet, rinsed twice with pure ethanol, and then dried in the oven at different temperatures for eight hours, which permits the study of post-reaction. In the experiment discribed above, the amount of added TEOS corresponds to 6 wt% silica level (on γ-Fe_2O_3 basis), provided that all TEOS are fully hydrolyzed and coated on magnetic particles. In other experiments, the silica levels were controlled by changing the amount of added magnetic particles when keeping the same concentration of TEOS. The less the added magnetic particles, the higher the silica levels (See appendix I for detailed calculation).

B) Dense Liquid Silica Coating

Iler's method (Iler, 1959) was used in dense liquid silica coating experiment. A given weight of γ-Fe_2O_3 (see Appendix II) was mixed with 90 mL of Millipore water in a 500 mL three neck flask under vigorous mechanical agitation. The pH of the suspension was raised to 9.5 ± 0.1 by adding 0.1 N NaOH, and the suspension was heated up to 90 ± 3 °C. Ten milliliter of 0.1 M aqueous silica solution was then added to the flask concurrently with 0.1 M H_2SO_4 within one hour while maintaining the solution pH at 9.5 ± 0.2. The reaction was continued for one hour, after which the suspension was cooled to room temperature and centrifuged. The solid product was then washed three times with Millipore water and finally dried in a vacuum oven at 110 °C for 24 hours.

C) Two-Step Silica Coating

Magnetic particles were first coated using the sol-gel process described above in a TEOS concentration corresponding to 6 wt% silica. One gram of the coated particle was then mixed with 90 mL of Millipore water in a 500 mL three neck flask under vigorous mechanical agitation. The slurry was heated up to 90 ± 3 °C, and the pH of the slurry was raised to 9.5 ± 0.1 by adding 0.1 N NaOH. Ten milliliters of 0.1 M aqueous silica solution was introduced, within one hour, into the flask, concurrently with 0.1 M H_2SO_4 to maintain the solution pH at 9.5 ± 0.2. The reaction was continued for another hour, after which the suspension was cooled to room temperature and centrifuged. The solid product was then washed three times with water and finally dried in a vacuum oven at 110 °C for 24 hrs. The total amount of added silica is about 11 wt% (on γ-Fe_2O_3 basis).

D) Characterization Techniques

The particles with and without silica coatings were characterized by DRIFTS, XPS, Zeta-potential measurements, VSM, and leaching tests. The experimental procedures and operating conditions are the same as described in chapters 3 and 4.

5.4 RESULTS AND DISCUSSION

5.4.1 Sol-Gel Process

A) Surface coatings

XPS: The XPS survey scan spectra for magnetic particles coated at various silica levels using the sol-gel process are shown in Figure 5.4. The XPS narrow scan spectra for the elements of interest are shown in Figure 5.5. The XPS band positions and their assignments are given in Table 5.1. Compared with the spectrum of bare magnetic particles, the appearance of Si_{2p} band at 103.4 eV (spectra a and b) in the spectra of TEOS treated magnetic particles indicates that the silica was deposited on the surface. The

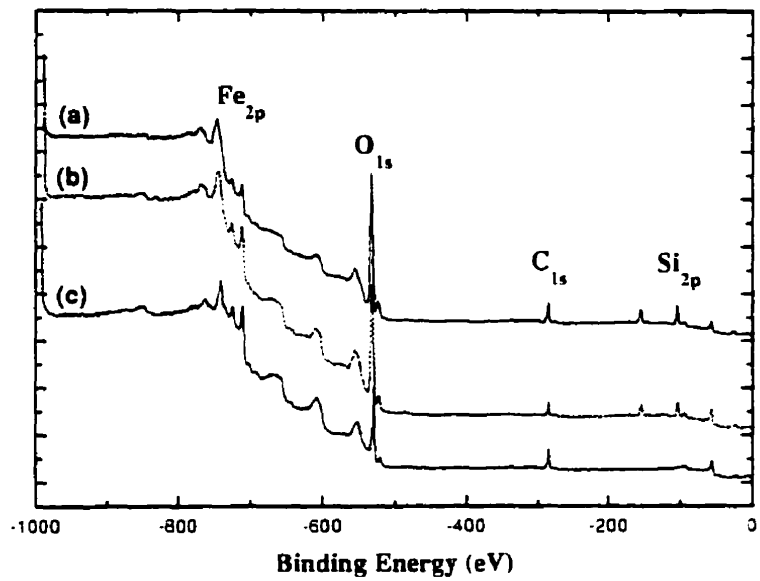

Figure 5.4 XPS survey scan spectra of magnetic particles treated at various silica levels (a) 11 wt% ; (b) 6 wt%; (c) γ-Fe_2O_3.

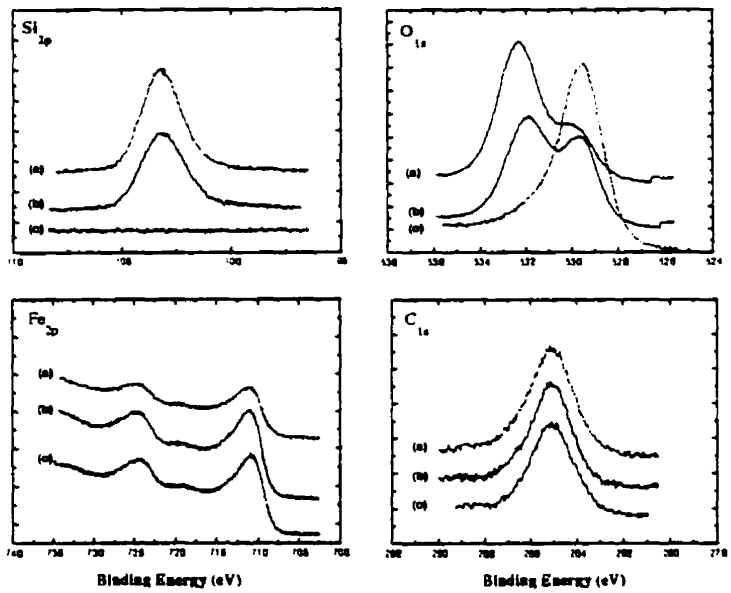

Figure 5.5 XPS narrow scan spectra of the elements of interest on the magnetic particles treated at various silica levels (a) 11-wt%; (b) 6-wt%; (c) γ-Fe_2O_3.

Table 5.1. Band Maxima (eV) Obtained from XPS Data[a]

	Binding Energy (eV)			
system	O_{1s}	Si_{2p}	Fe_{2p}	C_{1s}
γ-Fe_2O_3	529.8	nd[b]	724.3 710.7	284.6
silica coated γ-Fe_2O_3	529.8 532.8	103.4	724.3 710.7	284.6

a: Band positions are accurate to ±0.7 eV. b: not detected.

weak C_{1s} band at 284.6 eV might come from either the background carbon or unhydrolyzed ethoxy group. It appears that the carbon was mainly from environment since this band was also observed on spectra c for untreated γ-Fe_2O_3. Two distinct oxygen bands at 529.8 and 532.8 eV, respectively, were observed for the magnetic particles treated with TEOS. As discussed in the previous chapter, the band at 529.8 eV was attributed to oxygen in magnetic particles. Therefore, the band at 532.8 eV is assigned to the oxygen in coated silica. A similar binding energy (532.9 eV) for oxygen in silica has been reported (Moudler, et al., 1992). Table 5.2 summarizes the results of band fittings, i.e., the proportion of the two oxygen components and the ratio of normalized band areas of the oxygen (532.8 eV) and silicon to that of $Fe_{2p3/2}$ band (at 710.7 eV). As shown in Table 5.2, in parallel with an increase in silicon to iron ratio, the proportion of oxygen in silica (band at 532.8 eV) increased from 60 to 73 % as silica levels increased from 6 to 11 wt%, suggesting an increased deposition of silica on the surface at higher silica level. It should be noted that the oxygen (532.8 eV) to silicon ratio was found to be about 2 for both cases, indicating the films coated on magnetic particles are indeed silicon dioxide (i.e. silica).

DRIFTS: DRIFTS spectra of γ-Fe_2O_3 particles with and without silica coatings are shown in Figure 5.6. To identify the surface reaction between TEOS and magnetic particles, the infrared spectra of TEOS and silica (Cab-O-Sil) are also shown in this figure. The characteristic band positions and mode assignments are given in Table 5.3. As shown

Table 5.2 The proportion of the two oxygen components and the elemental ratio on magnetic particles treated by TEOS.

TEOS concentration (mole/dm^3)	Silica Level (wt%)	O_{1s} (%)		Si2p/ $Fe2p_{3/2}$	O1s[b] /$Fe2p_{3/2}$	O1s[b] /Si2p
		SiO_2 (532.8 eV)	γ-Fe_2O_3 (529.8 eV)			
0.015	6	60.2	39.8	1.8	3.8	2.1
0.015	11[a]	73.7	26.3	4.1	9.3	2.2

a: Silica level increased with decreasing the amount of γ-Fe_2O_3 used in coating experiment when keeping the same concentration of TEOS. See appendix I for detailed calculation. b: Oxygen band at 532.8 eV.

before, γ-Fe_2O_3 does not have any characteristic band in the spectral region above 800 cm^{-1} (Figure 5.6: spectrum d). When magnetic particles were coated with TEOS from ethanol solutions, two characteristic bands at 1204 and 1085 cm^{-1} on spectrum b were observed. The presence of these two bands, assigned to asymmetric stretching of the siloxane bond (Si-O-Si) (Shafei and Mokhtar, 1995), confirms the deposition and polymerization of hydrolyzed TEOS on magnetic particles. A weak band at 3745 cm^{-1}, characteristic of silanol groups originating from the hydrolysis of TEOS (Bergna, 1994), was observed (spectrum b), indicating the presence of free silanol groups on the surface. A similar band at 3745 cm^{-1} was also present in the IR spectrum of Cab-O-Sil fused silica. These findings indicate that silica was deposited on γ-Fe_2O_3, further supporting the XPS results.

It is interesting to note that a weak band at 928 cm^{-1} appears on spectrum b, which is absent in the spectra for silica (spectrum a) and TEOS chemicals (spectrum c). This band is, therefore, probably associated with Si-O-Fe vibrations, suggesting the formation of Si-O-Fe bonds on the magnetic particles. Seyedmonir, et al. (1982) observed a similar band at 925 cm^{-1} for a silica gel support impregnated with an aqueous solution of $(NH_4)_2Mo_2O_7$ (6% Mo on SiO_2) and calcined at 500 °C. They assigned this band to Si-O-Mo vibrations, an analogy to Si-O-Fe vibrations as in our case. IR bands at 950, 963 and 965 cm^{-1}

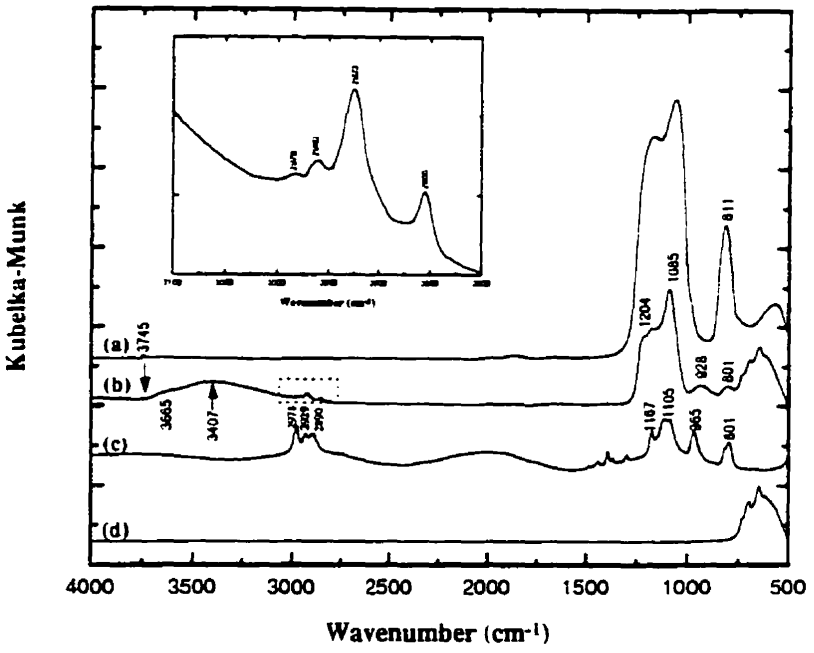

Figure 5.6 DRIFTS spectra of (a) Cab-O-Sil fused silica; (b) TEOS coated on γ-Fe_2O_3; (c) TEOS chemicals; (d) γ-Fe_2O_3. The coatings are performed at 0.01M TEOS and 1.76 M NH_4OH ethanol solution. Inset shows unhydrolyzed ethoxy group in spectrum b.

Table 5.3 Mode Assignments and Band Positions of Infrared Spectra in Fig.5.6.

wavenumber (cm^{-1})	Assignment
3745	single (isolated) silanols (Si-OH) or germinal
3665	vicinals
3407	hydrogen bonded OH with H_2O
2978	CH_3 asym str (-OCH_2CH_3)
2924	ν_{as} (-CH_2)
2890-2855	-CH_2 sym str, CH_3 sym str in -OCH_2CH_3
1481	CH_2 sym def
1441	CH_3 sym def
1204, 1085	ν_{as}(Si-O-Si)
1167, 1105, 965	Si-O-C
928	Si-O-Fe
811	ν_s(Si-O-Si)

observed previously have been attributed to the formation of Si-O-Ti, Si-O-Al (Kinney and Staley, 1983) and Si-O-Pb bonds (Miller and Ishida, 1986) on the surface of corresponding metal oxides. These spectral findings suggest that nanosized magnetic particles in our coating experiment acted as foreign nuclei, and silanol groups of hydrolyzed TEOS condensed with hydroxyl group on the surface to form Si-O-Fe covalent bonds. It is believed that the hydrolyzed TEOS bound on the surface was further polymerized to form a thin layer silica coating.

From the IR spectra, it is not clear what would be the state of silanol groups on the surface. The possible forms of silanols on silica coated magnetic particles are schematically shown in Figure 5.7. The band at 3745 cm^{-1} on the IR spectrum of silica could be attributed to either isolated silanol or silanediol (germinal) (Vranchen, et al., 1995). It is well known that the hydrogen bonding causes a reduction in the O-H stretching frequency, and the magnitude of band shift depends on the strength of hydrogen bond, and thus on the O-H to O distance. The small shoulder at 3655 cm^{-1} in spectrum b is probably from vicinal (H-bonded) silanol, that is the Si-OH groups located on neighboring Q^3 sites in which the OH to O distance is sufficiently small so that hydrogen bonding occurs (Hair, 1980; Brinker and Scherer, 1990). A broad band at 3407 cm^{-1} is characteristic of hydrogen bonded water on the surface.

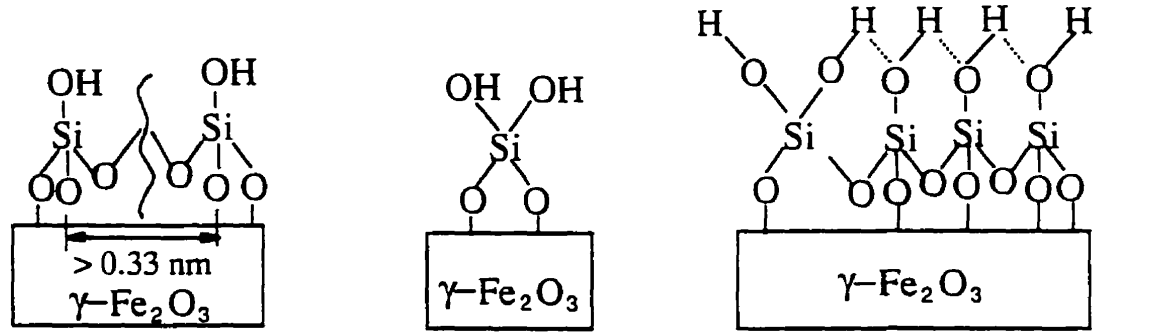

single (isolated) silanol Q^3 silanediol(germinal) Q^2 Silanediol vicinal Vicinal

Figure 5.7 Possible forms of silanols on silica coated γ-Fe_2O_3

It is important to note that TEOS coated on magnetic particles as such is not completely hydrolyzed as indicated by the presence of a characteristic band of ethoxy groups at about 2978 cm^{-1}. The unhydrolyzed ethoxy groups may have two different impacts on the preparation of magnetic carriers. If they are exposed to the environment, the subsequent silanation will be hindered. If they exist in the films, they will prevent cross-linking and hence reduce the packing density and stability of the coatings. It is therefore essential to eliminate these residual ethoxy groups.

B) Effect of Curing Temperature on Silica Coatings

The unhydrolyzed ethoxy groups on the surface, although small in amount, are a major concern in the sol-gel coating process because they may occupy the sites available for subsequent dense silica coating and silanation. To completely remove these unhydrolyzed ethoxy groups and to enhance the cross linking of TEOS (i.e. polymerization) on the surface, a post-treatment is needed. A convenient approach to remove the unhydrolyzed ethoxy groups is to cure the films at elevated temperatures. The DRIFTS spectra of magnetic particles coated using the sol-gel process and cured at different temperatures are shown in Figure 5.8. It can be seen that the broad band at 3440-3540 cm^{-1} in spectrum b disappeared at or above a curing temperature of 150°C, indicating the removal of physisorbed water from the surface. At the curing temperatures above 400°C, the characteristic bands of alkyl chains at 2978 to 2855 cm^{-1} disappeared, suggesting the removal of unhydrolyzed ethoxy groups from the surface. An increase in the intensity of the Si-O-Si band at 1204 cm^{-1} with curing temperature indicates the enhanced crosslinking of siloxane bonds on the surface.

The above results demonstrate that silica coating on iron oxide surfaces is feasible by the sol-gel process. For subsequent silanation using silane coupling agents, the dehydroxylation of silica coated on magnetic particles at high curing temperatures raises some concerns because the reactive silanol groups are necessary for silanation. The

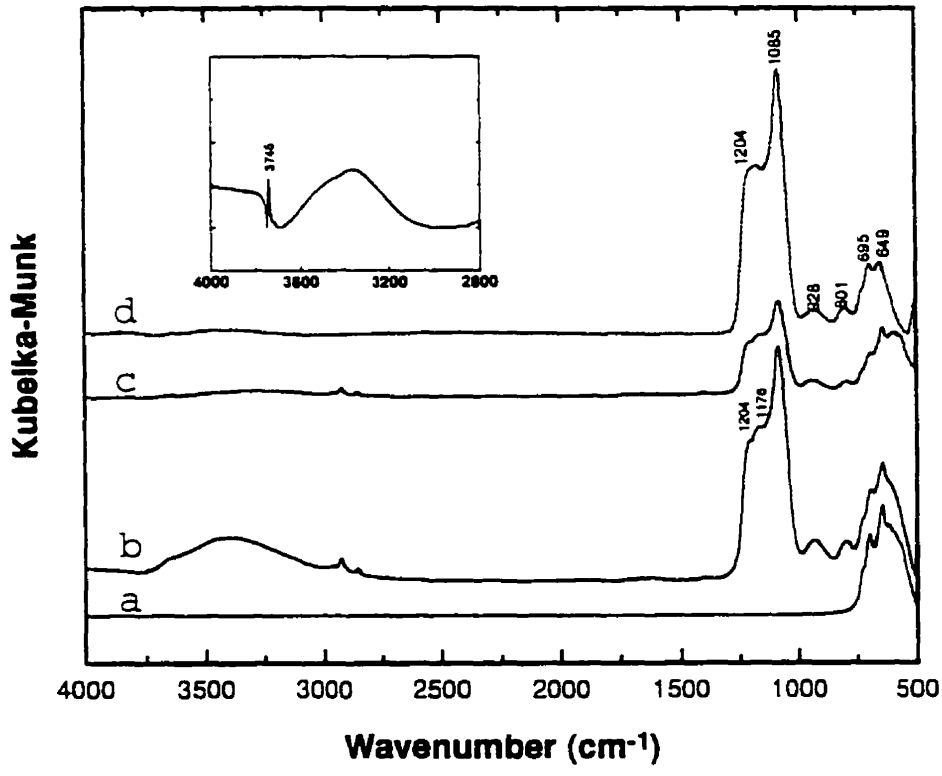

Figure 5.8 Infrared spectra of magnetic particles with and without TEOS coatings at various curing temperatures (a) γ-Fe_2O_3; (b) **90** °C; (c) **150** °C; (d) **400** °C. Inset shows the rehydroxylation of TEOS coated magnetic particles upon exposure to water steam.

disappearance of the band at 3745 cm^{-1} for the coated particles, cured at temperatures above 400 °C, indicates that most of silanols have been removed from the surface. This observation is consistent with that reported in literature, i.e., silanols on silica surface are dehydroxylated at temperatures above 400 °C, forming siloxane bridges (Zhuravlev, 1993). Strained siloxane bridges are reported to form on the silica thermally dehydroxylated at temperatures about 500 °C (Vansant, et al., 1995). At higher temperatures, the strained siloxane groups are relaxed to form stable siloxane groups, as schematically shown below (Bergna, 1994):

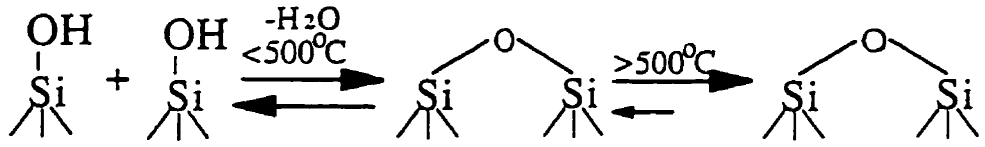

Silanols Strained Siloxane groups Stable Siloxane groups

The strained siloxane bridge can be readily rehydroxylated upon exposure to water. The appearance of an IR band at 3745 cm^{-1} as shown in inset Figure 5.8 indicated the rehydroxylation of strained surface siloxane groups upon exposing the dehydoxylated silica films (at 400 °C) to water steams for two minutes. At curing temperatures higher than 500 °C, the siloxane bridge generated can only be rehydroxylated at a limited rate. For example, it has been reported that it took 5 years of contact with water at room temperature to rehydroxylate completely a porous silica sample calcined in air at 900 °C (Zhuravlev, 1993). The above observations suggest that curing temperature has to be controlled in silica coatings using the sol-gel process. It appears that a curing temperature of 400-500 °C would be optimal for removing unhydrolyzed ethoxy groups while siloxane bonds formed are readily rehydroxylated to recover the surface silanols upon exposure to water vapor.

C) Structure of Coated Silica Layer

Zeta-potential: The zeta-potentials of magnetic particles with and without silica coating are shown in Figure 5.9. The IEP of the particles coated with TEOS at about 6 wt% silica level shifted toward that of amorphous silica, indicating that silica was indeed deposited on the surface. As the silica level increased to about 11 wt%, the IEP of coated particles was found to be identical to that of amorphous silica, indicating a complete coverage of the surface by silica. Based on theoretical calculations, only 5.5 wt% of silica coating is needed to completely cover the magnetic particles with a SiO_2 layer, provided that one SiO_2 molecule occupies 0.1 nm^2 on the surface (Bergna, et al., 1994). The IEP value (2.9) of γ-Fe_2O_3, coated at silica level about 6-wt%, is higher than that of silica particles (2.1), suggesting that the surface may not be fully covered with silica. This is further confirmed by leaching tests.

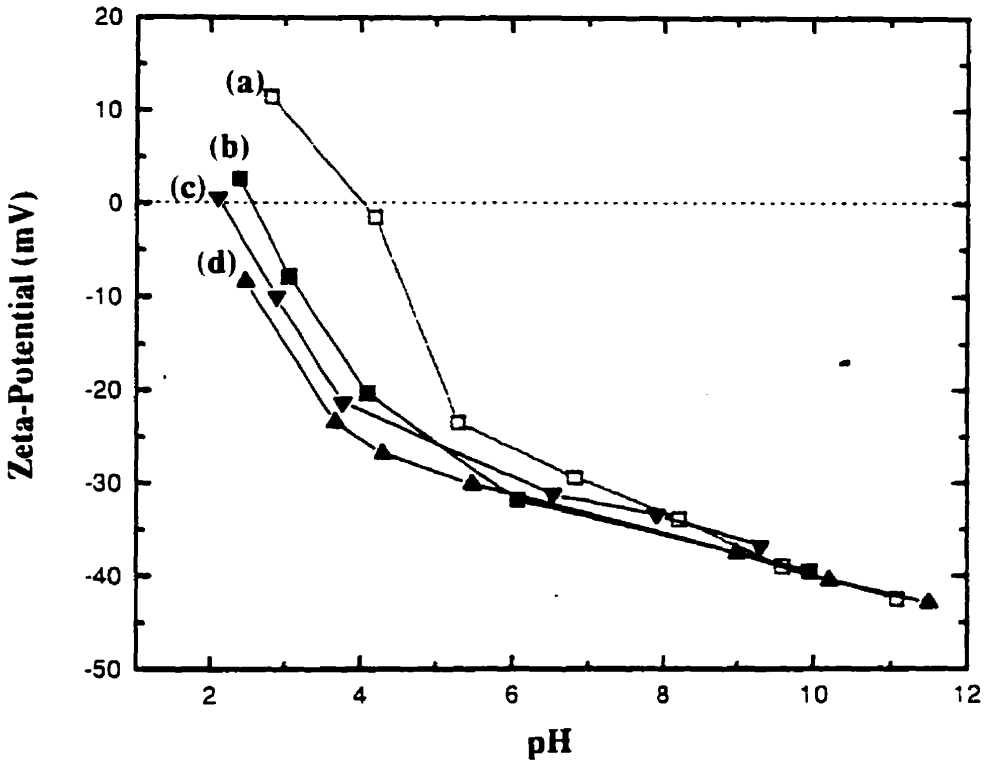

Figure 5.9 Zeta-potentials of magnetic particles as a function of pH: (a) uncoated magnetic particles; (b) coated at 6 wt% silica level; (c) coated at 11 wt% silica level; (d) Cab-O-Sil fused silica.

Leaching Test: As shown in the previous chapter, Fe was detected in leachate of bare magnetic particles in 0.01 N HCl solution. This finding suggests that the leaching test is a convenient and valuable approach to examine the structure and the stability of the coated silica layer on the surface. Ideally, if the surface were completely covered by a densely packed, stable silica layer, no Fe should be leached out in acid. Our experimental results indicated that, even when the surface is coated at a silica level about 11 wt %, Fe was still detected in leachate as shown in Table 5.4. Considering that the surface was fully covered by silica as indicated by zeta-potential measurement, it is evident that the silica layer on the surface contains significant amount of pores, through which Fe was leached out.

Table 5.4 Data of silica coatings on nanosized magnetic particles by the sol-gel process.

sample and methods	TEOS concentration ($mole/dm^3$)	Ammonium concentration ($mole/dm^3$)	Silica level (wt%)	Fe leached in 0.01 N HCL (mg/g)	IEP (pH)	Ms (emu/g)
γ-Fe_2O_3	--	--	--	60.25	4.5	52.0
Sol-Gel	0.015	1.47	6	4.30	2.9	46.8
Sol-Gel	0.015	1.47	11	1.10	2.1	43.2
Sol-Gel	0.015	1.47	27	1.10	2.2	35.1
Sol-Gel	0.015	1.47	54	nil	2.1	30.8
SiO_2	--	--	--	0.00	2.1	--

At higher silica levels (54 wt% SiO_2), no Fe was detected in acid leachates, indicating the formation of a densely packed silica layer on the surface. However, magnetization measurements as shown in Figure 5.10 indicated that the saturated magnetization of coated magnetic particles was reduced more than 40 % at such high silica levels (54 wt% SiO_2). These results indicated that to maintain the maximum bulk magnetic properties of coated particles while having a thin dense layer of silica, a different approach is needed.

5.4.2 Dense Liquid Silica Coating

XPS: XPS survey scan spectra of magnetic particles coated at various silica levels using DL process are shown in Figure 5.11. The XPS narrow scan spectra of the elements of interest are shown in Figure 5.12. Comparing to the spectrum of bare magnetic particles, the appearance of Si_{2p} band at 102.3 eV after dense liquid silica coatings indicates that the silica was deposited on the surface. As in the sol-gel process, two distinct oxygen bands at 529.8 and 532.8 eV, one from magnetic particles and the other from coated silica, were observed. Table 5.5 summarizes the results of band fittings, i.e., the proportion of the two oxygen components and the ratio of normalized band areas of

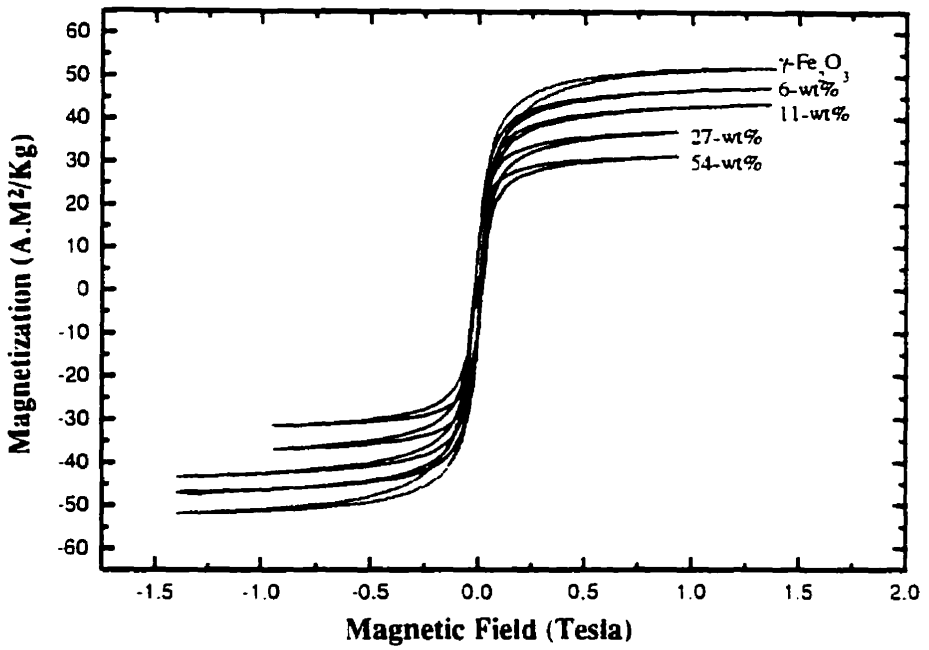

Figure 5.10 Magnetization curves of magnetic particles coated at various silica levels using sol-gel process.

the oxygen (532.8 eV) and silicon to that of $Fe2p_{3/2}$ band (at 710.7 eV). It is interesting to note that as silica levels increased from 11 to 27 wt%, the proportion of the oxygen band at 532.8 eV increased from 34 to 41 %. Also noted is the increase in the silicon to iron ratio with increasing SiO_2 level, indicating that an increased amount of silica was deposited on the surface. These two consistent observations suggest an increased SiO_2 coating with increasing SiO_2 level in DL process.

The ratio of oxygen to silicon (ca. 1.3 and 1.5) on mganetic particles coated at low silica levels (11 and 15 wt% SiO_2) is less than the stoichiometric value of silica (2.0). Only at higher silica level (27 wt% SiO_2) is the ratio (2.2) close to the stoichiometric value of

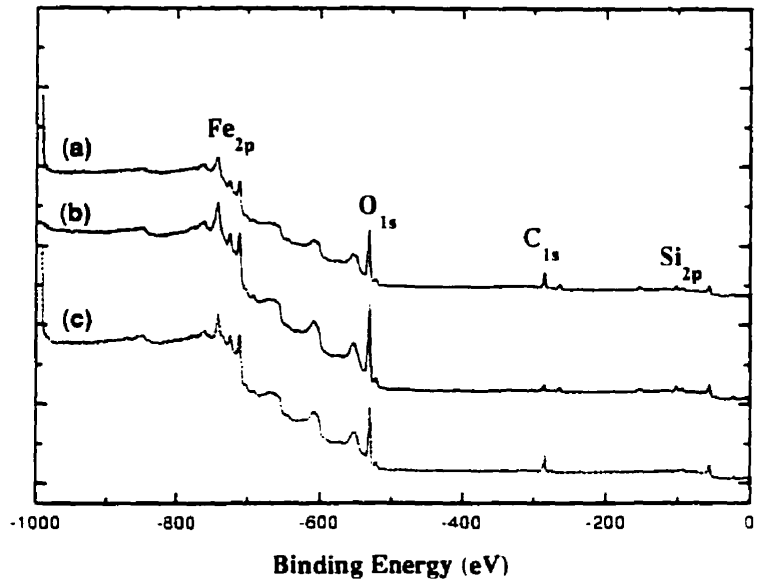

Figure 5.11 XPS survey scan spectra of magnetic particles coated at various silica levels using DL process (a) 11 wt%; (b) 27 wt%; (c) γ-Fe_2O_3.

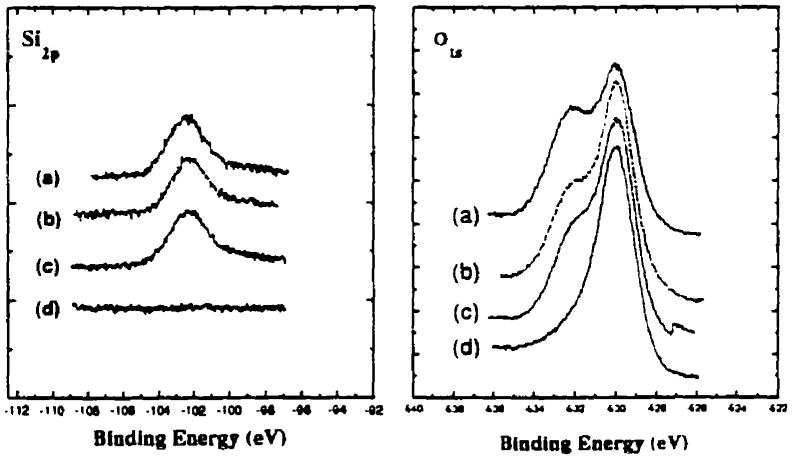

Figure 5.12 XPS narrow scan spectra of the elements of interest on magnetic particles coated at various silica levels using DL process (a) 11 wt% silica; (b) 15 wt% silica; (c) 27 wt% silica; (d) γ-Fe_2O_3.

Table 5.5 The proportion of two oxygen components and elemental ratio on magnetic particles coated at various silica levels using DL process.

sample	Silica level (wt%)	O1s (%)		Si2p/ $Fe2p_{3/2}$	O1s[a] /$Fe2p_{3/2}$	O1s[a] /Si2p
		SiO_2 (532.8 eV)	γ-Fe_2O_3 (529.8 eV)			
DL 11	11	34.4	65.6	0.7	1.6	1.3
DL 15	15	31.6	68.4	0.7	1.7	1.5
DL 27	27	41.3	58.7	0.8	1.8	2.2

a: Oxygen band at 532.8 eV.

silica (2.0). This is different from the sol-gel process where the ratio of oxygen to silicon is close to 2 even at low silica level (6 wt% SiO_2). This observation is probably attributed to the non-uniform silica coatings on magnetic particles at low silica levels using the DL process. Following DRIFTS and zeta-potential measurements, the structure of the coated silica films was further elucidated.

DRIFTS: DRIFTS spectra of silica and γ-Fe_2O_3 particles with and without dense liquid silica coatings are shown in Figure 5.13. Two new bands at 1053 and 1155 cm^{-1} in spectrum a and b were observed on the magnetic particles processed by dense liquid silica coating. These two bands were assigned to asymmetric stretching of the siloxane bond (Si-O-Si). Also shown in this figure is the apperance of a new band at 3742 cm^{-1}, charateristic of silanol groups of coated silica. These observations confirm the silica coatings on magnetic particles. In contrast to the sol-gel process, there is no residual hydrocarbon bands on the spectra of silica coated particles. Therefore, post treatment and rehydroxylation are not needed.

Zeta-potential: The zeta-potential of magnetic particles with and without a silica coating is shown in Fig. 5.14. The IEP of the magnetic particles coated with 11 wt% silica was shifted toward that of amorphous silica, indicating the silica coatings on the surface. As the silica level increased to about 27 wt%, the IEP of coated particles approached to

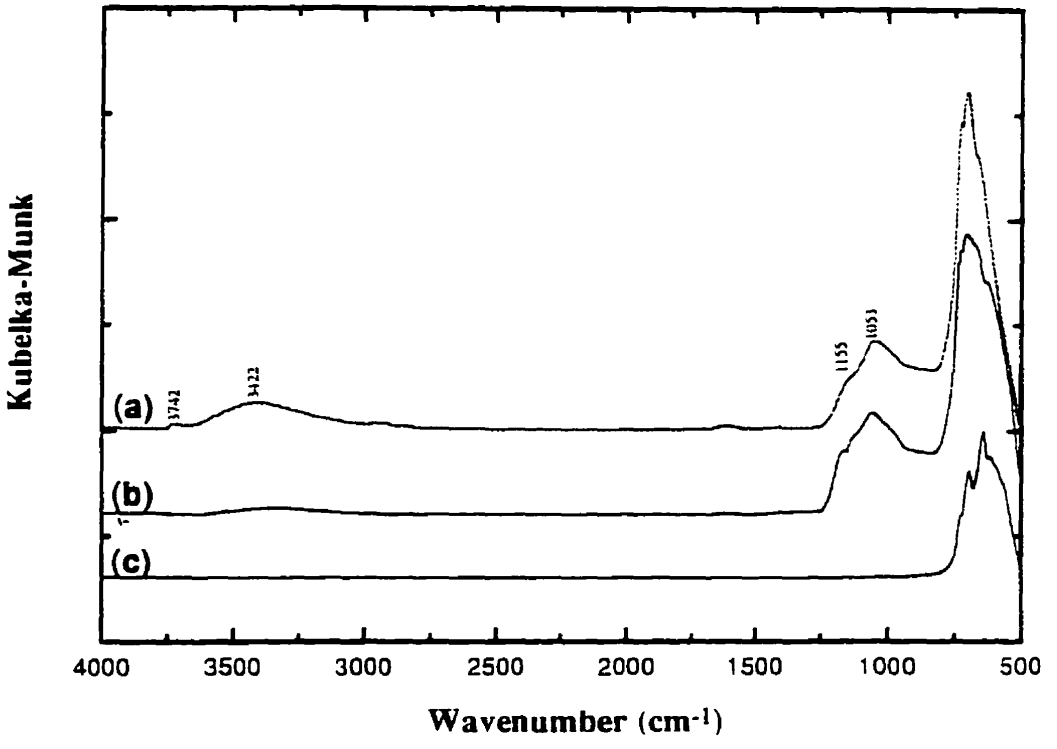

Figure 5.13 DRIFTS spectra of dense liquid silica coatings for (a) 15 wt% silica; (b) 11 wt% silica; (c) γ-Fe_2O_3.

that of amorphous silica. As mentioned earlier, theoretical calculation indicated that only 5.5 wt% silica coatings should be enough to completely cover the surface of magnetic particles. The IEP value (3.1) of the magnetic particles coated at 11 wt% silica level is still higher than that of silica (2.1), suggesting that the surfaces are not completely covered with silica. In comparison, the sol-gel process is more effective where the IEP of the magnetic particles coated at 11 wt% silica level is close to that of silica.

The following leaching test provides more information on the coated silica layer and further supports the findings obtained from the XPS, DRIFTS, and zeta-potential measurements.

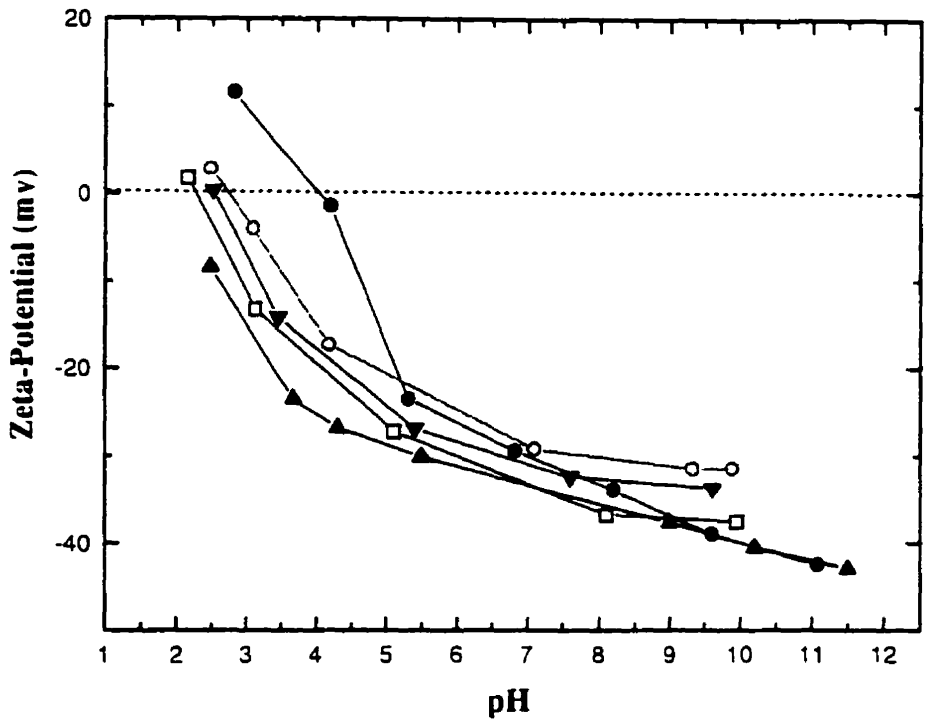

Figure 5.14 Zeta-potentials of the magnetic particles coated at various silica levels using DL process: uncoated particles (solid circle); 11 wt% (open circle); 15 wt% (downtriangle); 27 wt% (open square); Cab-O-Sil fused silica (up triangle).

Leaching Test: The results of leaching tests and magnetization measurements are listed in Table 5.6. It can be seen that, even when the surface is coated at a silica level of 11 wt %, Fe was still detected in the leachate as shown in Table 5.6. As the silica level increased, the Fe leached was reduced, indicating the increase of surface coverage at high silica level. However, even at higher silica level (27 wt%), Fe was found in the acid leachate, suggesting an incomplete coverage of the surface by the silica. Compared to the sol-gel process, at the same silica level, more Fe was leached out from γ-Fe_2O_3 coated by DL process, indicating that the DL process is less effective than the sol-gel process. Magnetization measurments indicated that DL coated particles remained superparamagnetic. However, at a given silica level, the saturation magnetization is lower for the particles coated by sol-gel process than by DL process. This finding again suggests

that DL coating is less effective than the sol-gel process. The detailed reasons for the differences between the two processes will be discussed in section 5.5.

The above results indicated that the sol-gel process is more effective than DL coating. At low silica levels, the sol-gel process forms a porous silica layer, while DL process forms non-uniform coatings. Both processes did not form a thin, densely packed silica coating as required by magnetic carrier technology. Therefore, a search for an alternative method is needed.

Table 5.6 The silica coatings on nanosized magnetic particles by DL coating.

sample and methods	concentration of aqueous silica (mole/dm^3)	Silica level (wt%)	Fe leached in 0.01 N HCL (mg/g)	IEP (pH)	Ms (emu/g)
γ-Fe_2O_3	--	--	60.25	4.5	52.0
DL 11	0.01	11	2.75	2.9	48.5
DL 15	0.01	15	1.65	2.5	48.7
DL 27	0.01	27	1.50	2.3	48.1

5.4.3 Two-Step Silica Coating

The underlying idea of two-step silica coating is based on homogeneous coating. Once the magnetic particles are coated by silica, the next coating is on silica itself. Two-step silica coating on magnetite particles was reported by Philipse et al. (1994) who prepared stable magnetic fluids. Silica was first coated onto the magnetite particles by the DL process, then followed by the sol-gel method. The resultant thick silica layer (a few times larger than the diameter of the magnetite particles) was used to reduce anisotropic magnetic dipolar attractions of magnetite. Clearly, this coating method is not suitable for our purpose. A reverse coating order was, therefore, tested in our two-step coating process. A thin silica layer was first coated on the magnetic particles by the sol-gel process in an organic solvent, by which a thin uniform silica layer on the surface (although porous) was obtained. In the second step, the dense liquid silica coatings were applied mainly to fill the pores in the first layer.

XPS: To compare the two-step silica coating with each single step, XPS spectra of narrow scans for the elements of interest in each coating step are shown in Figure 5.15. Table 5.7 summarizes the results of band fittings, i.e., the proportion of the two oxygen components and the ratio of normalized band areas of the oxygen (532.8 eV) and silicon to that of $Fe_{2p3/2}$ band (at 710.7 eV). It can be seen that, at the same silica level, the silicon to iron ratio in the coatings by a two-step process is close to that by the sol-gel process alone, but significantly higher than that by dense liquid silica coating. This semiquantative XPS analysis suggests that more silica was coated on the particle surface from the sol-gel or two-step process than from the DL method. (The weak carbon bands at 284.8 eV are probably from the environment.)

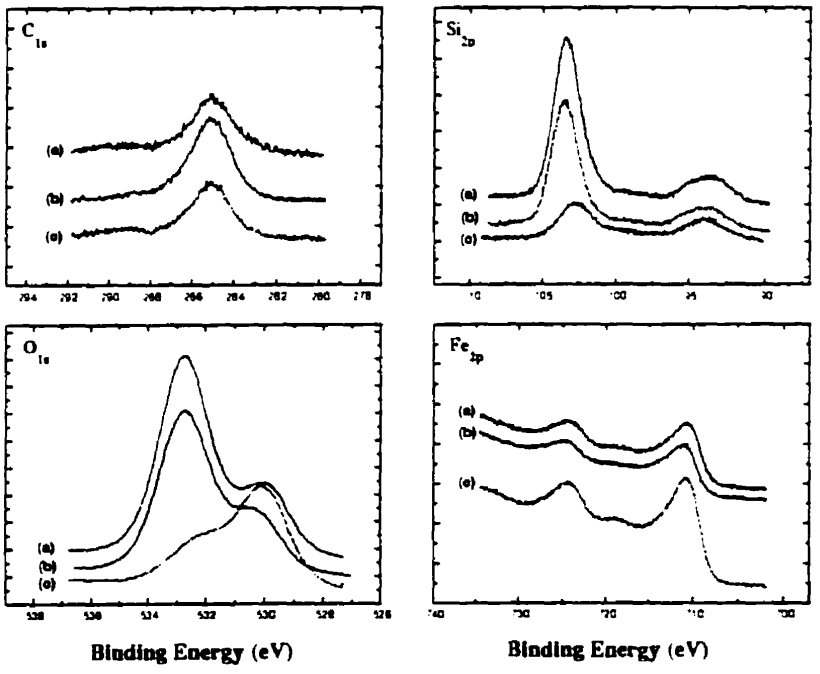

Figure 5.15 XPS narrow scan spectra of the elements of interest (a) two-step process; (b) sol-gel process; (c) DL process.

Table 5.7 The proportion of the two oxygen components and the elemental ratio on magnetic particles coated at the same silica level using different processes

system	Silica level (wt%)	O_{1s} (%)		Si_{2p}/ $Fe_{2p3/2}$	O_{1s}^a /$Fe_{2p3/2}$	O_{1s}^a /Si_{2p}
		SiO_2 (532.8 eV)	γ-Fe_2O_3 (529.8 eV)			
sol-gel	11	73.7	26.3	4.11	9.3	2.2
two-step	11	73.6	26.4	4.12	8.9	2.2
DL process	11	34.4	65.6	0.71	1.6	1.3

a: Oxygen band at 532.8 eV.

DRIFTS: The DRIFTS spectra of silica coated magnetic particles using different coating methods are shown in Figure 5.16. The appearance of siloxane bands at 1204 and 1085 cm^{-1} indicate that silica was coated on the surface by all of these methods. The inset of Figure 5.16 shows the characteristic band of surface silanols (3743 cm^{-1}). It is evident that surface silanols were well generated in the films formed by two-step silica coatings. Compared with the sol-gel process, a unique feature for dense liquid silica coating and two-step coating is that no curing step is needed because sodium silicates are used as precursors which do not contain any hydrocarbons. It is the combination of this advantage of the sol-gel process and the dense liquid silica coating that makes the two-step process successful in the fabrication of densely packed, thin silica films on magnetic particles, which were further confirmed by zeta-potential measurments and leaching tests.

Zeta-Potential Measurements: The zeta-potentials of magnetic particles with and without silica coatings are shown in Figure 5.17. The IEP (3.0) of silica-coated magnetic particles by dense liquid silica coating alone was higher than that of Cab-O-Sil fused silica (2.1), indicating that the surface was not fully covered by silica. In contrast, the sol-gel process alone provided a better coverage as the IEP of the coated particles was closer to that of fused silica. However, the best coating was achieved by the two-step process, where almost identical electrokinetics to natural silica was observed.

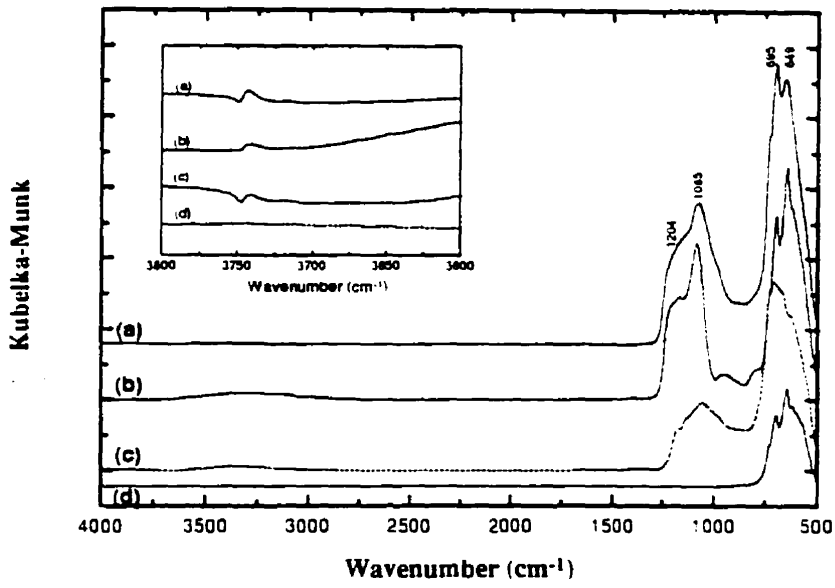

Figure 5.16 DRIFTS spectra of magnetic particles coated at 11 wt% silica level using various coating methods (a) two-step process; (b) sol-gel process; (c) dense liquid silica coating; (d) γ-Fe_2O_3. Inset shows the characteristic bands of silanol group at 3743 cm^{-1}.

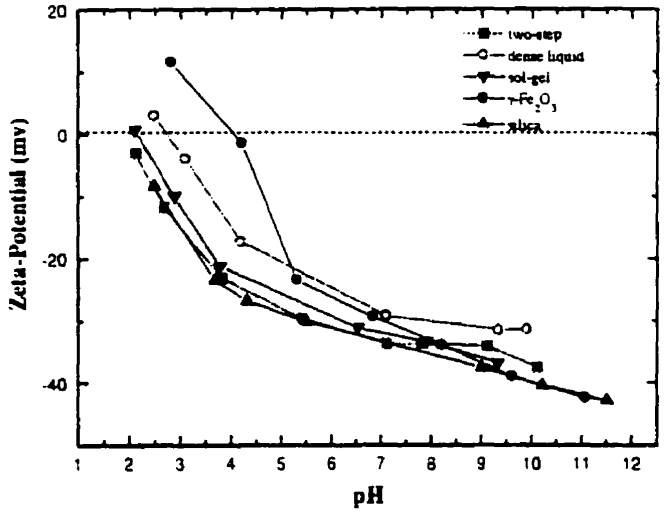

Figure 5.17 The zeta-potentials of silica coated magnetic particles using different processes at 11 wt% silica level.

Leaching Test: The results of the leaching tests, IEP, and saturation magnetization values are given in Table 5.8. As shown, no iron was detected in the leachate when the particles were coated using the two-step process, indicating the densely packed silica layer on the surface. It is believed that when a porous silica layer formed in the first step by sol-gel process reacted with liquid silica solution, the pores in the coated layer were filled by dense liquid silica through homogeneous surface coatings, thus forming a densely packed, uniform thin silica layer on the surface. A schematic diagram for different coatings is shown in Figure 5.18.

Table 5.8 The results of silica coatings on magnetic particles by the sol-gel, DL and two-step processes at 11 wt% silica level.

sample and methods	TEOS concentration ($mole/dm^3$)	Fe leached in 0.01 N HCl (mg/g)	IEP (pH)	Ms (emu/g)
γ-Fe_2O_3	--	60.25	4.5	52.0
DL coating	0.010[a]	2.75	3.0	48.5
sol-gel	0.015	1.10	2.4	43.2
two-step	0.015+0.01[a]	nil	2.2	42.5

a: concentration of liquid silica: To keep the same silica and supersaturation level, the amount of magnetic particles used is different in each step (see appendix I and II for details).

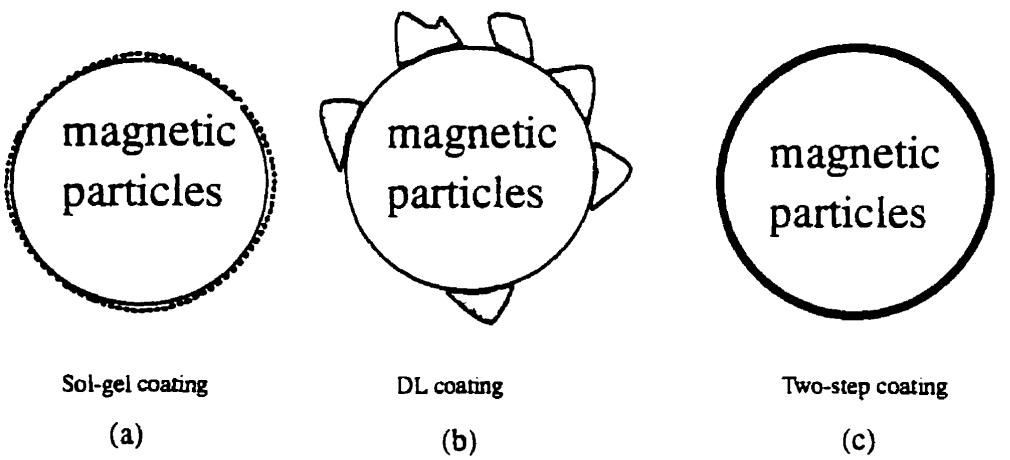

Figure 5.18 Schematic illustration for the films prepared using different silica coating methods. At low silica levels, the sol-gel process forms a porous thin silica layer (dashed circle); the DL process forms a non-uniform coating; the two-step process forms a densly packed, thin silica layer (solid circle).

Magnetic Properties: The magnetization curves of silica coated magnetic particles by different processes are given in Figure 5.19. The magnetic particles coated using DL process showed the highest saturation magnetization, further confirming that less silica is deposited on the surface. The magnetic particles coated using sol-gel or two-step processes showed a similar magnetization characteristics. The remained saturation magnetization (ca. 43.2 emu/g) after two-step process permits the applications of silica coated particles in magnetic carrier technology.

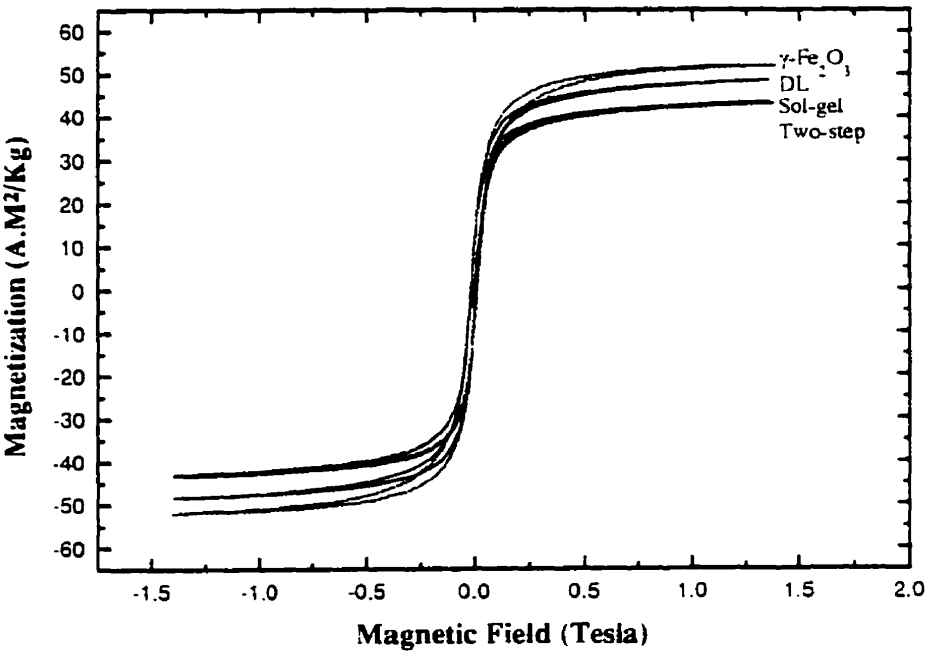

Figure 5.19 Magnetization of magnetic particles coated at 11 wt% silica using different coating processes.

5.5 GENERAL OBSERVATIONS

The proportion of oxygen in the Si-O-Si environment (532.8 eV) and the ratio of silicon to iron as a function of silica levels for different coating processes are shown in

Figure 5.20. It can be seen that at the same silica level, the proportion of oxygen from coated silica and the silicon to iron ratio for the particles coated using sol-gel and two-step processes are higher than that using dense liquid silica coating.

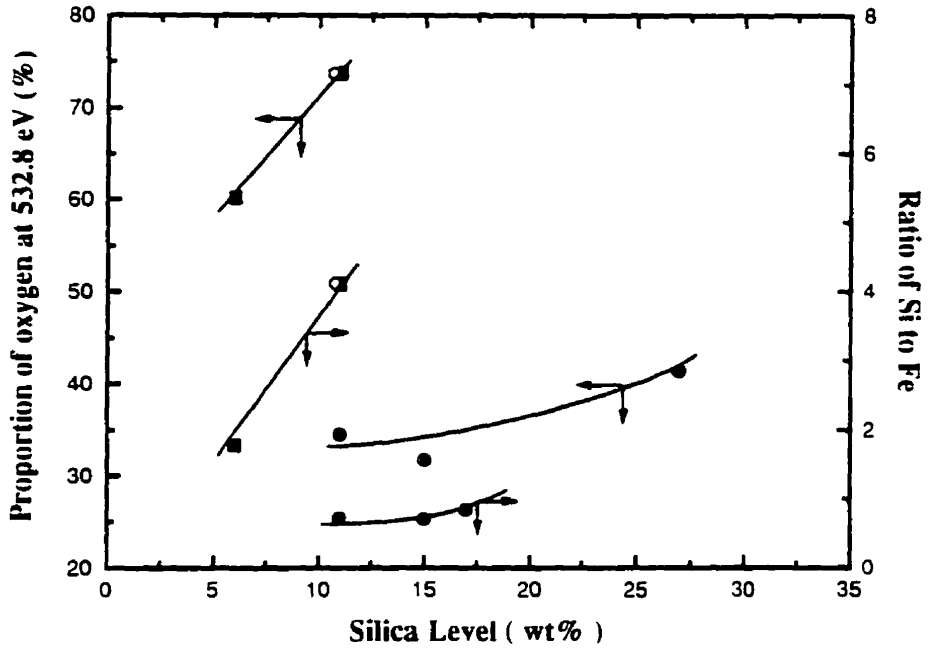

Figure 5.20 The proportion of the oxygen component in coated silica (532.8 eV) and the ratio of silicon to iron as a function of silica levels for DL process (sollid circle); Sol-gel process (solid square); and Two-step process (open circle).

Based on the solubility limit of precipitated silica (ca. 2.5×10^{-3} M) and initial concentration of aqueous silica used in DL coating experiment (ca. 1×10^{-2} M equivalent to silica level of 27 wt %; see appendix II for detailed calculation), the maximum silica coating on the surface are about 20 wt%, i.e. four layers of silica, since only 5.5 wt% coated silica is required for a monolayer coverage as calculated previously. This calculation indicates that if the coatings were uniform, the magnetic particles would be fully covered by up to four layers of silica (about 1.3 nm in thickness) and be protected, i.e., no Fe would be leached out from the coated magnetic particles in acidic solutions. Leaching tests, however, showed that even when magnetic particles were coated at 27

wt% silica level by DL process, a substantial amount of Fe was detected in the leachate (Table 5.6), indicating the incomplete surface coverage by silica. In the study of silica coatings on alumina (d =150 nm), Bergna, et al. (1994) found, based on similar calculations, that only 1 wt% SiO_2 coatings should be sufficient to cover entire surface if it were deposited in a uniform monolayer (0.35 nm thick). However, 5 wt% of silica coatings was actually needed to fully cover the surface, indicating that the actual amount of silica needed for a full coverage of the surface by DL process was much higher than that for a theoretical monolayer coverage. A similar observation was also obtained by Furlong (1994) and Howard and Parfitt (1977) where the adsorption of sodium silicate on titania at pH 9.5 did not proceed to complete surface coverage and the uniform coatings at low silica levels were not achieved. Similar incomplete coverage by sodium silicates was also noted on geothite (Yokoyama, et al., 1980) and on some fluoride minerals (Marinakis and Shergold, 1985).

Non-uniform coatings in the DL process appear to be related to the difference of the surface energy in homogeneous and heterogeneous surface coatings. As discussed before, dense liquid silica coating is a surface heterogeneous nucleation process. It involves the adsorption of reactive species on the surface, possibly as clusters, and the subsequent growth on the surface. Since the formation of a uniform layer of silica on γ-Fe_2O_3 creates a new interface as compared to the growth of SiO_2 on nucleation centers, unfavorable energy condition drives SiO_2 onto SiO_2 islands on which silica grows nonuniformly as shown in Figure 5.18 b. This hypothesis agrees with the nucleation and crystal growth phase diagram shown in Figure 5.2 and 5.3. As a result, only at high silica coating levels will the surface be fully covered through island growth and cross-linking. Detailed assessment of a wide range of silica coatings on various substrates such as TiO_2, α-Al_3O_2, and γ-Fe_2O_3 showed that complete surface coverage indeed requires a silica concentration to be increased to a level sufficiently high to induce a lateral polymerization of adsorbed species on the surface.

In the sol-gel process, the hydrolysis of TEOS produces the monosilicic acid that can condense with surface hydroxyls to form a chemical bond. As hydrolysis proceeds with reaction time, the chemically bonded monosilicic acid can polymerize laterally to form two to three dimensional networks on the surface. The in-situ generation of monosilicic acid by controlling the hydrolysis of TEOS in ethanol followed by condensation with the surface hydroxyls seems responsible for the uniform coating on the surface. The reduced electrostatic force between the surface and reactive species in ethanol (often used as a solvent in the sol-gel process) may also be a contributing factor. As a result, if monosilicic acid instead of sodium silicate is used as precursor, the dense, uniform silica coatings are anticipated by the DL process.

In our two-step coating process, since the surface has already been covered by a thin layer silica formed in the sol-gel process, further silica coating using the DL process is on the silica surface. This is equivalent to the seeded nucleation (or homogenous surface coating) where σ_{cs} in equation (5.6) is zero and σ_{sl} equals to σ_{cl}. The free energy change associated with the coating is, therefore, negative, favoring the surface coatings at lower supersaturation levels. Our results obtained with the two-step process demonstrated that the porous silica layer formed by the sol-gel process is further densified by DL coatings, forming a densely packed, thin silica layer on magnetic particles.

5.6 CONCLUSIONS

1. Silica coatings on magnetic particles were achieved by both sol-gel process and dense liquid silica coating.

2. In the sol-gel process, curing temperatures of 400-500 °C were needed to remove unhydrolyzed ethoxy groups on the surface while ensuring siloxane bonds formed to be rehydroxylated readily upon exposure to water vapor to recover the surface silanols.

3. A uniform but porous silica layer was coated on magnetic particles by the sol-gel process, while a non-uniform silica coating formed using the dense liquid silica coating at low silica levels.

4. Densely packed, thin silica layers were coated on magnetic particles by an innovative two-step process, i.e., sol-gel process followed by dense liquid silica coating.

CHAPTER 6 PREPARATION OF MAGNETIC CARRIERS (IV): SILANATION ON SILICA COATED MAGNETIC PARTICLES

6.1 INTRODUCTION

In chapter 4, it was shown that APTES films directly silanized onto γ-Fe_2O_3 were unstable in alkaline solutions, although the films silanized from toluene were relatively stable in acidic solutions. An idea to coat γ-Fe_2O_3 with a thin silica layer before silanation was proposed in order to obtain a stable silanized film. In chapter 5, it was shown that densely packed, thin silica films were successfully coated onto γ-Fe_2O_3 using the sol-gel process followed by dense liquid silica coating. The purpose of silica coating is to make the surface more amenable for silanation. It has been well documented that silanized films on silica are relatively stable compared to those on other metal oxides (Arkels, 1992).

In this chapter, the silanation of silica coated magnetic particles using APTES in toluene is studied. Toluene is used as a solvent simply due to the fact that the films formed on the magnetic particles are relatively stable compared to those formed from water as shown in chapter 4. The silanized films on silica coated magnetic particles are characterized using XPS, DRIFTS and zeta-potential measurements. The leaching tests are conducted in acidic or basic solutions in order to examine the stability of the silanized films. The thermal stability of the films is also examined by thermal gravimetric analysis (TGA).

6.2 MATERIALS AND EXPERIMENTS

All the materials used and experimental procedures were the same as before. A thin silica layer was coated on magnetic particles using the two-step process: sol-gel followed

by DL process, as described in chapter 5. The silica coated magnetic particles were dried at 120 °C to remove physisorbed water before silanation. The silanation was conducted by refluxing in toluene. After washing twice with toluene, the samples were cured in a vacuum oven at 80 °C for three hours. Thermal gravimetric analysis (TGA) of the magnetic particles with and without silanation was conducted using a Seiko 220 TGA instrument at a heating rate of 3 °C/min in N_2 (160 mL/min). The temperature was kept at 110°C before scanning until a constant mass was achieved to ensure that trace amounts of water were completely eliminated. The experimental procedures for XPS, DRIFTS, and zeta-potential measurement were the same as those used in the previous chapters.

6.3 RESULTS AND DISCUSSION

6.3.1 XPS analysis

XPS spectra of γ-Fe_2O_3 with various treatments are shown in Figures 6.1 (survey scans) and 6.2 (narrow scans). A nitrogen band centered at 399.2 eV was observed on the spectrum of silica coated magnetic particles silanized with APTES, indicating the deposition of APTES on the surface. The deconvolution of the nitrogen band showed that two distinct components centered at 399.4 and 401.3 eV, respectively, were present, suggesting the two different nitrogen environments: one for free and the other for protonated amino groups. This finding is consistent with the results discussed in chapter 4 where two nitrogen components were also found for the APTES films silanized on bare magnetic particles. From the integrated area of these two components, the proportion of protonated to free amines was calculated and the results are given in Table 6.1. For comparison, the results obtained in chapter 4 for the APTES films directly silanized on bare magnetic particles are also presented in this Table. It is interesting to note that the degree of protonation of the amine groups in the films formed on silica coated surfaces is only slightly higher than the one on bare γ-Fe_2O_3 (Table 6.1). It has been reported that the hydroxyls on silica surfaces are more acidic than those on magnetic particles, and the

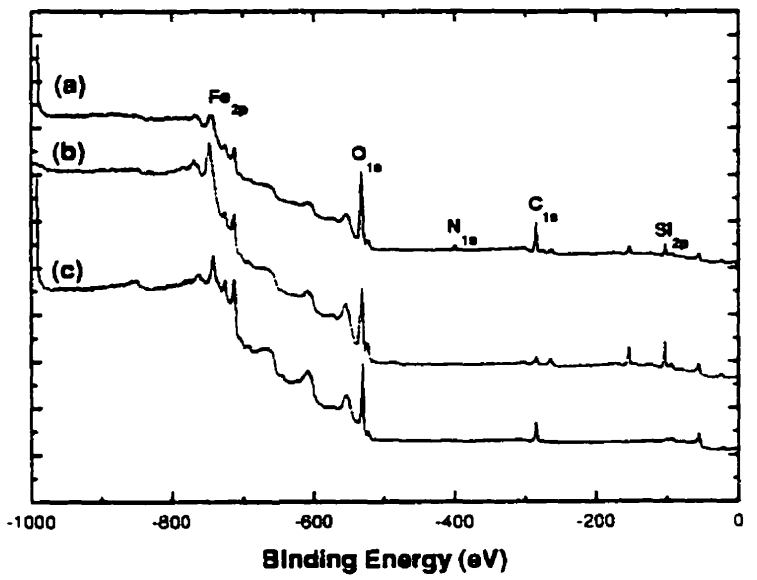

Figure 6.1 XPS survey scan spectra (a) silica coated γ-Fe_2O_3 silanized with APTES; (b) silica coated γ-Fe_2O_3; (c) γ-Fe_2O_3 only.

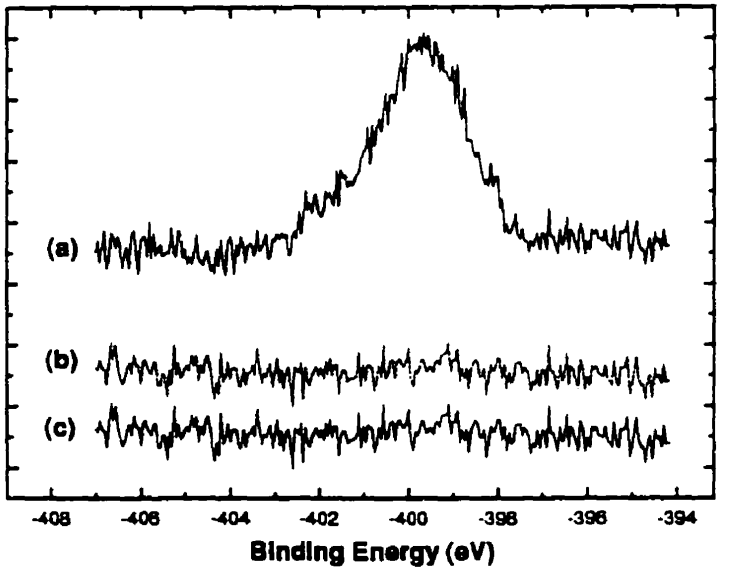

Figure 6.2 XPS narrow scan spectra of nitrogen (a) APTES on silica coated γ-Fe_2O_3; (b) Silica coated γ-Fe_2O_3; (c) γ-Fe_2O_3 only.

density of these hydroxyl groups on silica surface, ca. 4.7 OH/nm^2 (Zhuravlev,1993; Lloyd, et al., 1992), is higher than on magnetic particles, ca. 2.6 OH/nm^2 (Simmons and Beard, 1987; Fowkes, et al., 1988). The more acidic hydroxyl groups on silica coated magnetic particles may provide more favorable conditions for basic amino groups of APTES to react with the surface. As a result, more protonated amino groups would be expected to form on the surface. However, more surface silanol groups on silica coated magnetic particles may provide favorable conditions for coupling reactions with silane silanols. These two competitive interactions may account for our observation that the fraction of protonated amines on silica coated magnetic particles is only slightly higher than on bare magnetic particles. However, from the XPS analysis, it seems unlikely to compare the relative surface coverage of APTES on silica coated magnetic particles with that on bare magnetic particles due to the presence of a thin silica layer on the former.

Table 6.1 The degree of amine protonation of APTES films on γ-Fe_2O_3 with and without silica coatings[a]

	-NH_2 (%) (399.4 eV)	-NH_3^+ (%) (401.3 eV)
APTES on bare γ-Fe_2O_3	83.4	16.6
APTES on silica coated γ-Fe_2O_3	81.6	18.4

a: reaction was conducted at refluxing toluene and samples were cured at 80 °C.

6.3.2 DRIFTS

The infrared spectra of silica coated magnetic particles with and without silanation are shown in Figure 6.3. It is interesting to note that the peak at 3743 cm^{-1}, assigned to surface silanols, on the spectrum of silica coated magnetic particles (spectrum b) disappeared after silanation by APTES (spectra a), indicating the coupling of surface silanol groups with silane coupling agents. In contrast, a band at 3360 cm^{-1} on spectrum a (inset of Figure 6.2), assigned to the free amino asymmetric stretching, was observed. The two weak bands at 3274 and 3160 cm^{-1} on spectrum a are probably due to stretching

vibrations of protonated and hydrogen bonded amino groups. The bands at 2927 and 2860 cm^{-1} are assigned to the asymmetric and symmetric stretching of $-CH_2$ in alkyl chains, respectively. The band at 1580 cm^{-1} is assigned to deformation bending of free amino group on the surface. These IR spectral features confirm the deposition of APTES on γ-Fe_2O_3 and the presence of two types of amine groups, consistent with XPS results.

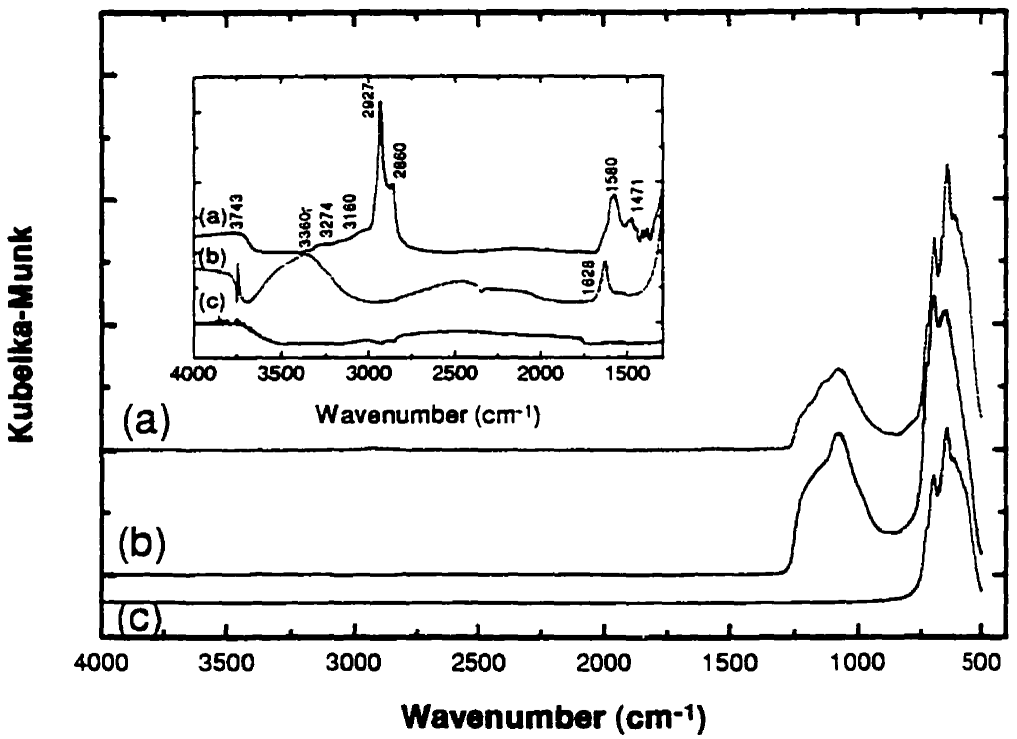

Figure 6.3 DRIFTS spectra for (a) APTES on silica coated γ-Fe_2O_3; (b) silica coated γ-Fe_2O_3; (c) γ-Fe_2O_3. Inset shows the enlarged spectra from 4000 to 1300 cm^{-1}.

The absence of the characteristic band of $-CH_3$ asymmetric stretching (at 2974 cm^{-1}) in ethoxy groups on spectrum a (APTES silanized on silica coated magnetic particles) indicates that silanes are fully hydrolyzed on the surface. This observation is different from the results obtained from APTES films silanized on bare magnetic particles where residual ethoxy groups were found on the surface. The more acidic feature of surface silanols on silica coated magnetic particles may enhance the hydrolysis of silane coupling agents upon

condensation which releases water for further hydrolysis of silanes. In addition, the higher density of silanols may provide more favorable conditions for coupling with silanes. These two factors may account for our observations that silanes are fully hydrolyzed and well deposited on silica coated magnetic particles.

6.3.3 Thermal Gravimetric Analysis (TGA)

The weight loss of magnetic particles with different treatments as a function of temperature is shown in Figure 6.4. It can be seen that both silica coated and uncoated magnetic particles reached a constant weight loss of ca. 1 % at a temperature about 400 °C (curve a and b). These two curves are, therefore, used as the baseline for comparison with the weight loss of silanized magnetic particles. The magnetic particles silanized directly with APTES from water (curve e) showed the most significant weight loss (ca. 2.5 %) at 500 °C, while the ones silanized from toluene (curve c) showed the least weight loss (ca. 2.0 %). The silica coated magnetic particles silanized with APTES from toluene showed an intermediate weight loss (ca. 2.2 %). Since the weight loss of silica coated and bare magnetic particles is the same and constant (1%) at this temperature, the observed increase in weight loss is attributed to the decomposition of silanized films on the surface. The more weight loss at the final temperature (about 550 °C) indicates that more silane coupling agents have decomposed from the surface, which, in turn, can be considered as more silanes were present on the surface. From this point of view, it is evident that more APTES were deposited on bare magnetic particles from water than from toluene. This is consistent with previous XPS and elemental analysis results. For the silanation in toluene, relatively large amounts of silanes were deposited on silica coated than on bare magnetic particles due to the higher reactivity and surface density of silanols on silica coated magnetic particles.

Detailed analysis of these TGA curves shows that the silanized films on silica coated magnetic particles decompose much slower than those on bare magnetic particles, indicating the high thermal stability of the surface films. On bare magnetic particles, the thermal stability of APTES films silanized in toluene is slightly higher than in water.

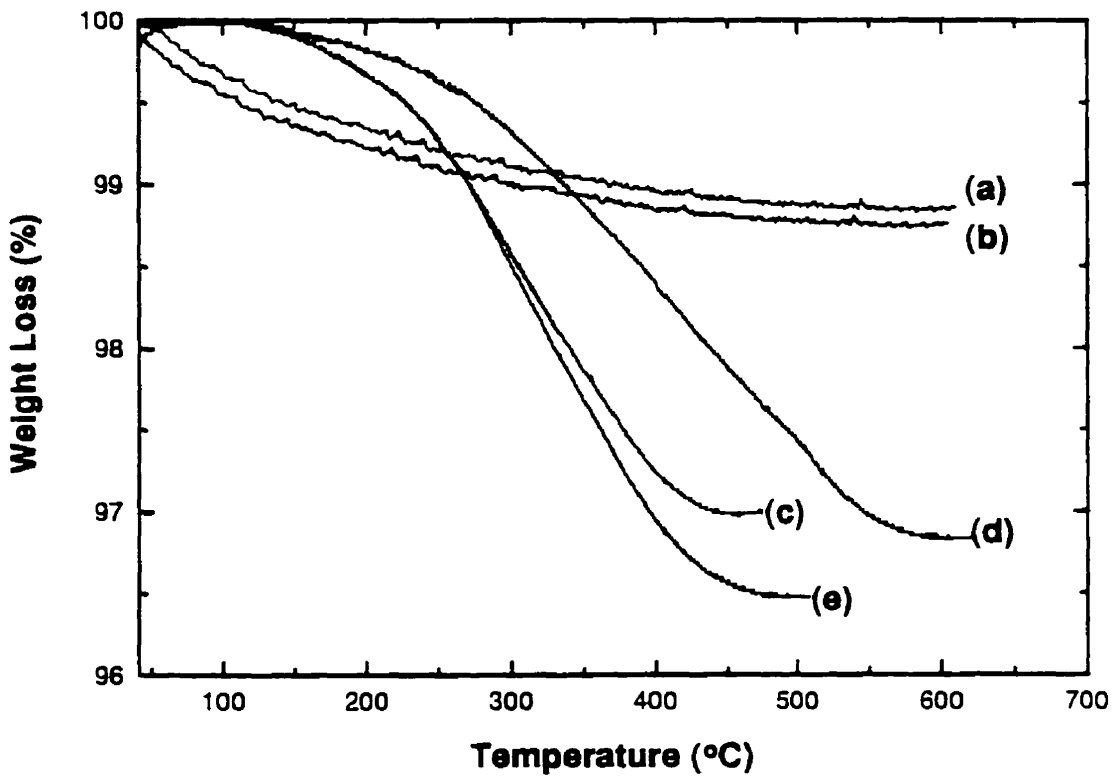

Figure 6.4 Thermogravimetric analysis for (a) silica coated magnetic particles; (b) bare magnetic particles; (c) APTES on bare magnetic particles from toluene; (d) APTES on silica coated magnetic particles from toluene; (e) APTES on bare magnetic particles from water.

6.3.4 Zeta-potential Measurement

Over the pH range studied, silanation of APTES on silica coated magnetic particles increased zeta-potentials significantly as shown in Figure 6.5, further confirming the deposition of APTES on the surface. The electrokinetics of silica coated magnetic particles silanized by APTES is almost identical to APTES deposited on the bare magnetic particles. This observation is consistent with our XPS results that the proportion of

protonated amino groups in APTES films silanized on silica coated magnetic particles was only marginally higher than that on bare magnetic particles.

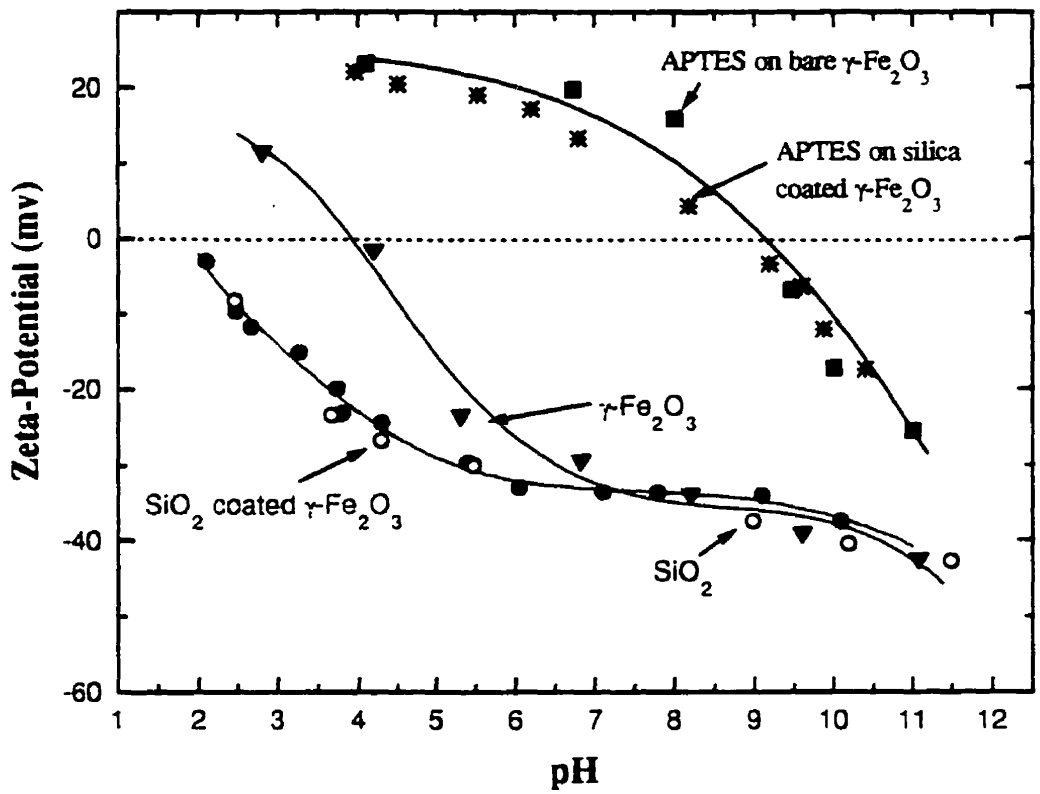

Figure 6.5 The zeta-potential of magnetic particles with and without APTES silanation.

6.3.5 Stability of silanized film

Leaching tests to detect Fe in leachates are not suitable for studying the stability of APTES films on silica coated magnetic particles because the magnetic particles are protected by silica coatings even if APTES films were detached. However, a significant reduction in zeta-potential was observed upon the detachment of silanized APTES films as

shown in previous chapters (Figure 4.10 and Figure 4.11). If APTES is completely detached from the surface, the zeta-potential would return to that for the original surface, in this case, silica coated magnetic particles. Therefore, zeta-potential measurement can be a useful alternative for studying the stability of silanized films on the surface.

The zeta-potentials of APTES films silanized on silica coated magnetic particles as a function of leaching time were shown in Figure 6.6. In acidic solutions (pH<5.0) the zeta-potentials remained the same with leaching time, indicating a stable APTES film on silica coated magnetic particles in an acidic environment. However, in alkaline solutions (pH 10.1), the zeta-potential becomes progressively more negative with leaching time. After 20 hours, the zeta-potential reached the value of silica (also see Figure 6.7). This finding indicates that the silanized films were unstable in alkaline solution.

It is interesting to note that at neutral pH (6.7) the zeta-potentials of silanized APTES films on silica coated magnetic particles became more negative with leaching time but leveled off, after ca. 25 hrs, at a value (-10 mV) significantly higher than that (-33mV) of silica coated magnetic particles (Figure 6.6). This finding suggests that the silane molecule may not be completely detached from the surface at this pH instead a dynamic equilibrium seems to be established.

To further illustrate the relative stability of APTES films silanized on magnetic particles with and without silica coatings, the zeta-potentials were measured as a function of pH after particles were soaked in solutions for 20 hours, and the results are shown in Figure 6.7. It is evident that in acidic solution, the silanized films on silica coated magnetic particles are more stable as compared to those on bare magnetic particles. This may be related to the difference in chemical bonding and the packing of silane molecules on the surface. On silica coated magnetic particles, more siloxane bonds (Si-O-Si) may be formed through the coupling between surface silanols and silanols of APTES due to a high density of Si-OH on the surface. On bare magnetic particles, the lower density of surface

hydroxyls (Fe-OH) may only form a small number of Fe-O-Si bonds on the surface by the coupling reaction. As discussed in chapter 4, The strength of Si-O bond is higher than Fe-O bond in acidic solutions (a well known example is that acid can dissolve iron oxide but not silica). The difference in the strength and density between these two types of bonds may have contributed to the observed difference in the stability of these two silanized films. Both films were found to be unstable in alkaline solution, simply due to the fact that even silica can be dissolved in alkaline solution.

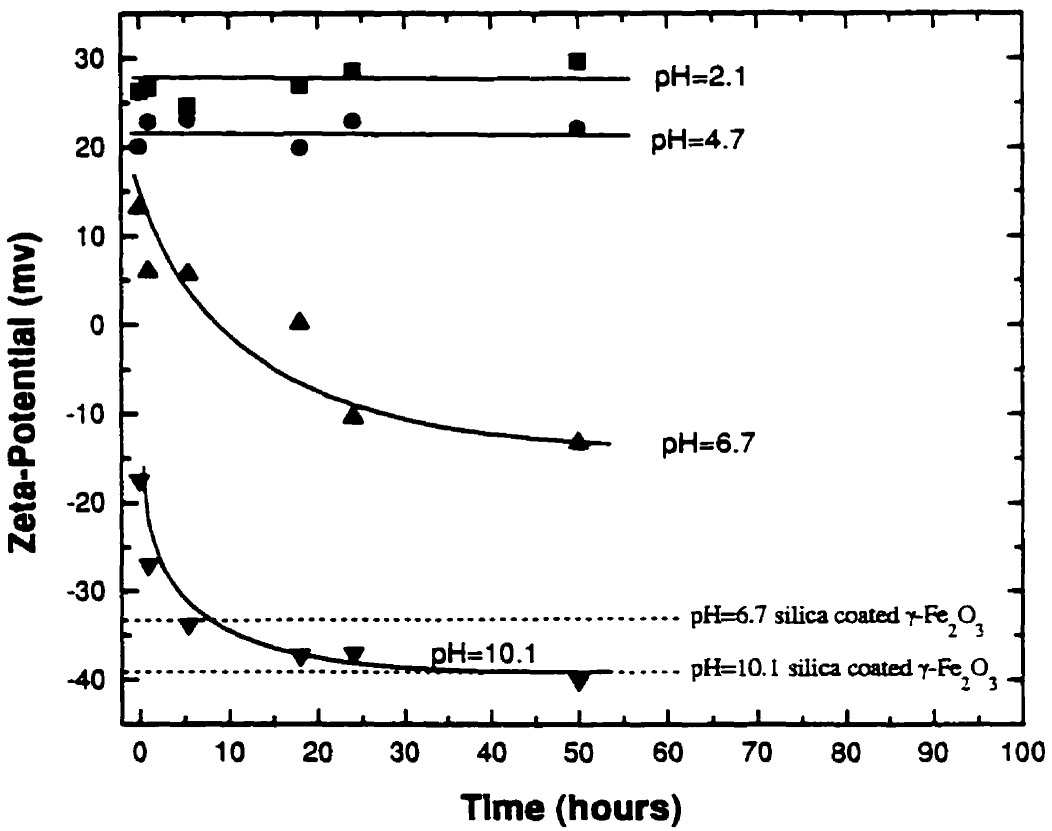

Figure 6.6 The zeta-potential of APTES silanized particles as a function of leaching time.

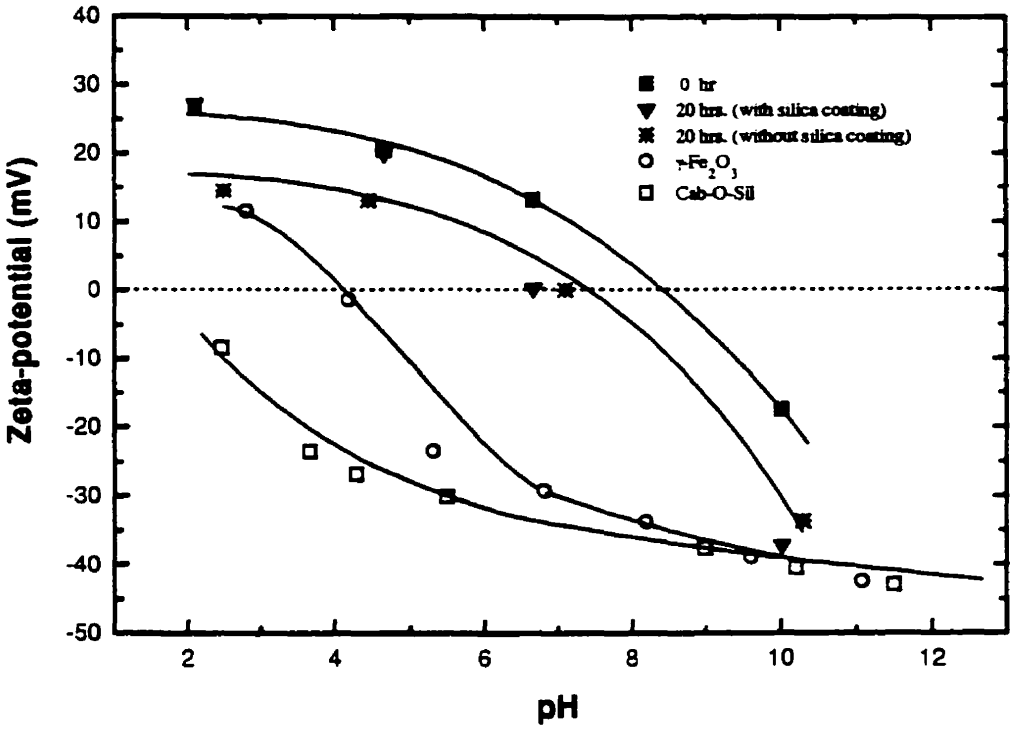

Figure 6.7 The zeta-potentials of APTES silanized particles after soaking 20 hours in solutions of various pHs.

6.3.6 Magnetic properties

The room temperature magnetization curve for γ-Fe_2O_3 particles with various treatments, is shown in Figure 6.8. Little change in saturated magnetization is observed after silanation using APTES on silica coated magnetic particles. The particles remained superparamagnetic at room temperature, allowing the reuse and/or recycling of magnetic carriers.

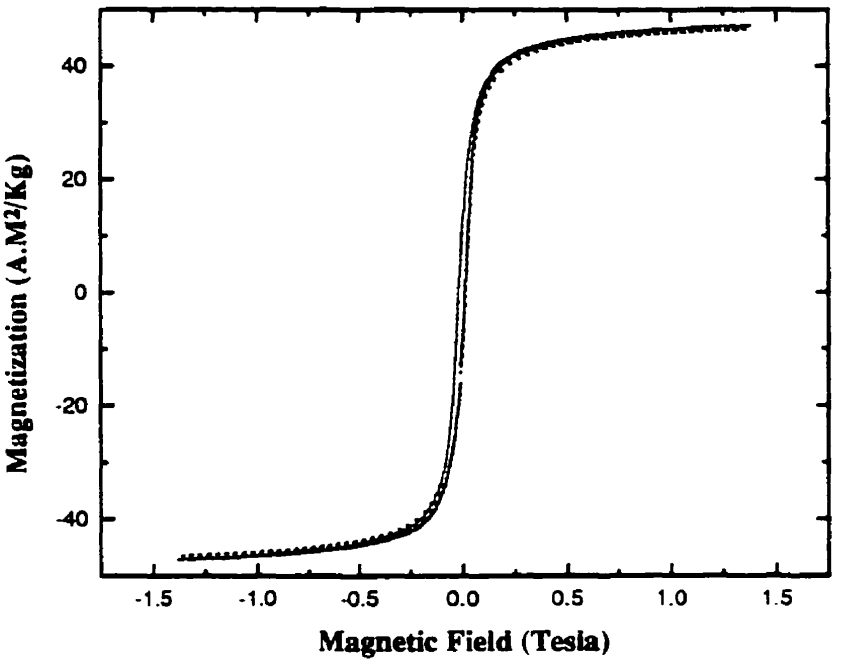

Figure 6.8 Room temperature magnetization curves of silica coated γ-Fe_2O_3 before (solid line) and after (dot line) silanation using APTES.

6.4 CONCLUSIONS

1. Magnetic carriers with amino groups were prepared by silanation of silica coated magnetic particles using APTES in toluene.

2. The proportion of protonated amino groups in silanized films was slightly higher on silica coated than on bare magnetic particles.

3. Stability tests indicated that in acid and neutral solutions, the silanized films were more stable on silica coated than on bare magnetic particles, but both were unstable in

alkaline solutions. An improvement in film stability is needed for the uses of the prepared magnetic carriers in alkaline solutions.

4. The magnetic property of the prepared magnetic carriers permits their applications in magnetic carrier technology.

CHAPTER 7 APPLICATIONS OF PREPARED MAGNETIC CARRIERS

7.1 INTRODUCTION

Magnetic carrier technology has found wide applications in biological cell separation (Molday and Mackenzie, 1982), raw material recovery (Liu and Friedlaender, 1994), waste remediation (Nunez, et al., 1995), and drug delivery (Rozenfeld, et al., 1994). The distinct features of magnetic carriers prepared in this work: specific functional groups on the surface, high saturation magnetization and superparamagnetism, allow their applications in these areas. The present work focuses on the removal or recovery of heavy metals from aqueous solutions. The potential applications in biological cell separation, magnetic fluid, and magnetic catalysis are also discussed.

7.2 APPLICATIONS IN HEAVY METAL RECOVERY OR REMOVAL

Amino groups can react with most of transition metals to form complexes (Davis, et al. 1984), while thiol and disulfide groups have strong affinity to precious metals such as gold and silver (Zhong and Porter, 1994). Using amine-type collectors is a common practice in oxides flotation (Klassen and Mokrousov, 1963; Finch, 1973). Recently, diethylenetriamine (NH_2-CH_2-CH_2-NH-CH_2-CH_2-NH_2) has been used in sulfide mineral flotation to minimize the inadvertent activation of gangue minerals by metal ions (Rao, et al., 1995; Kelebek, et al., 1995; and Yoon, et al., 1995). The silanized silica by silane coupling agents with reactive functional groups such as primary amine, diamine and triamine has been used to preconcentrate trace heavy metal ions from aqueous solutions (Leyden and Luttrell, 1975; Plueddemann, 1985).

A unique feature of using magnetic carriers is that the metal loaded magnetic carriers can be separated from the streams by magnetic separation, in which the interference of

non-magnetic particles can be minimized. Two types of magnetic carriers prepared in this work: one with thiol or disulfide groups and the other with reactive amino groups, can therefore be used to capture heavy metals often present in industrial effluents. Presented in this chapter are the studies on the uptake of metal ions by magnetic carriers and the loading capacity. The stripping of metal ions from loaded magnetic carriers by acids, required for recovering metals and recycling magnetic carriers, is also examined. A preliminary study on possible recycling of magnetic carriers is presented.

7.2.1 Materials and Experiments

Materials: Amine-type and thiol-type magnetic carriers were prepared by silanation of APTES on silica coated magnetic particles and molecular self-assembly on bare magnetic particles as described in chapters 6 and 3, respectively. The standard copper sulphate (0.198 mg/mL) and zinc sulphate (49.9 mM) stock solutions from Aldrich were used in loading test. Water was treated with a Millipore system. Glasswares was cleaned by a mixture of sodium hydroxide and ethanol (1:10), and rinsed thoroughly with distilled water. All other chemicals were reagent grade.

Capacity Test: The capacity is defined as the maximum amount of metal ions that can be loaded on magnetic carriers. To examine the loading capacity of magnetic carriers, the adsorption of metal ions (e.g. copper) with different concentrations on the magnetic carriers was conducted at the solution pH about 5.3. 50 mg of magnetic carriers was mixed with 25 mL metal ion solutions for about 30 minutes. The slurry was then centrifuged using a Sorvall® RC-5B superspeed centrifuge (Du Pond Instruments) at 12000 rpm for 30 minutes. The supernatant was then collected and analyzed for metal ion concentration by atomic absorption spectroscopy (Perkin Elmer 310, USA). The amount of metal ions loaded on magnetic carriers was determined from the difference of the initial and equilibrium metal ion concentration in supernatant. The adsorption of metal ions on magnetic carrier as a function of pH was studied in a similar way. The solution pH was adjusted by HCl and NaOH solutions.

Stripping and the Recycling: In the stripping test, the magnetic carriers with loaded metal ions were mixed with 25 mL of 0.01 N HNO_3 (or 0.01 N HCl) for about 30 minutes. The suspension was then centrifuged and the supernatant was analyzed using the procedures described above. The stripping efficiency was calculated as the percentage of the loaded metal ions that detached. After removal of the supernatant, the magnetic carriers collected in the centrifuge tube, referred to recycled magnetic carriers, were mixed with 25 mL of copper solutions. The loading capacity of recycled magnetic carriers was determined using the same procedures as in initial loading capacity test.

7.2.2 Results and Discussion

A) Adsorption of Metal Ions on Magnetic Carriers

The adsorption of copper ions on amine-type magnetic carriers as a function of metal ion concentration is shown in Figure 7.1. For comparison the adsorption of copper ions on silica coated magnetic particles is also included in this Figure. It can be seen that at pH 5.3 copper ions were effectively adsorbed on magnetic carriers, while only marginal adsorption on silica coated magnetic particles, possibly as counterions, was observed. Figure 7.1 also shows that the adsorption of copper ions on magnetic carriers increased with copper concentrations, reaching a limiting value of 0.18 mM/g, which is considered as the loading capacity of magnetic carriers. This value is equivalent to 11.4 mg copper per gram of magnetic carriers. With this carrying capacity value, it is estimated that 10 gram of magnetic particles is needed to remove 100 ppm of copper ions from one liter solution, equevalent to one percent solids, which appears to be suitable for magnetic separation. It is also interesting to note that at low copper concentration (ca. 12 ppm), the loading of copper ions on amine-type magnetic carriers was very effective, reaching a 100% of removal efficiency. Even at maximum adsorption, about 75% of copper ions were removed from a copper solution of 32 ppm initial concentration. The trade-off between the removal efficiency and capacity should be considered in practical applications.

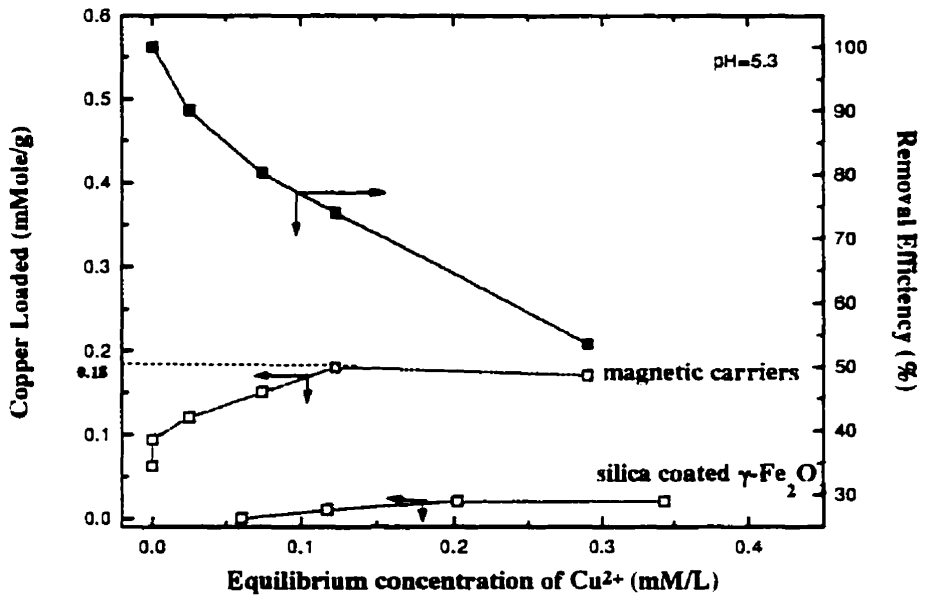

Figure 7.1 Uptake of copper ions on magnetic carriers as a function of copper concentration.

The effect of pH on the uptake of copper and zinc by magnetic carriers is shown in Figure 7.2. The initial copper concentration in these experiments was fixed at 0.185 mM/L (e.g. 11.8 ppm). It is evident that below pH 3, the loading of metal ions on magnetic carriers was not effective. This is probably related to the state of amino groups on magnetic carriers. At low pH, the amino groups are most likely protonated so that the magnetic carriers are positively charged. This will result in a strong electrostatic repulsive force between the magnetic carriers and positively charged metal ions. The competitive adsorption of hydrogen ions with metal ions onto amino groups at lower pH may also contribute to the observed low loading efficiency. As expected, the loading efficiency increased with pH, reaching the maxium, i.e., the complete removal of metal ions from solutions at pH about 5.2 for copper and 7.4 for zinc. At high pH, the uptake of metal ions on magnetic carriers reduced, probably due to the detachment of silane coupling agents from magnetic carriers. A similar observation was reported by Leyden and Luttrell (1975)

in the preconcentration of trace metals using amine-type silanes immobilized on silica. It is well documented that siloxane bonds break up at pH above ca. 10 (Iler, 1979; Plueddemann, 1982). A well known example is the dissolution of silica in an alkaline solution and the cleaning of glass ware with concentrated NaOH. The important implication here is the selective loading of metal ions onto magnetic carriers. At pH 4, for example, about 70 % of copper ions, as opposed to only 10 % of zinc ions, were removed. These findings indicate that the selective removal or recovery of metal ions can be achieved by controlling the solution pH.

The maximum loading at different pHs for different metals appears to be related to the distribution of metal species and their complexing nature with amines (Stumm and Morgan, 1995). The stronger catalytic effect of copper than zinc may have resulted in the detachment of APTES films from the surface at lower pH (6.0) as compared to zinc (8.0) (Yang, et al., 1995). To study why the maximum removal was achieved at these pH values is beyond the scope of this thesis.

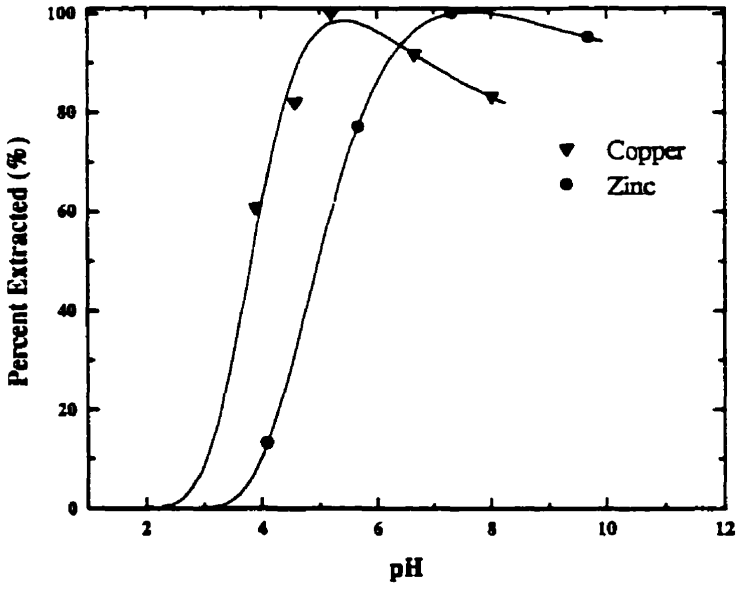

Figure 7.2 Effect of pH on uptake of metal ions on amine-type magnetic carriers.

In order to determine the loading efficiency of surface functional groups, i.e. the ratio of copper to amino group on magnetic carriers, the sample with maximum metal loadings (0.18 mMole/g) was analyzed by XPS. The survey scan spectra of magnetic carriers with and without copper loading are shown in Figure 7.3, and the narrow scans of the interested elements are shown in Figure 7.4. The new bands centered at 934 and 945 eV, characteristic of copper ions, were observed for copper loaded magnetic carriers (spectrum a in Figure 7.4: Cu_{2p}), indicating the uptake of copper ions by the magnetic carriers. The nitrogen band of loaded magnetic carriers (spectrum a in Fig.7.4: N_{1s}) was shifted to higher binding energy upon copper loading. The band fitting showed only one nitrogen band centered at 401.3 eV, unlike the unloaded magnetic carriers which showed two distinct nitrogen bands centered at 399.4 and 401.3, respectively. These XPS resutls suggest that most nitrogen atoms (more specifically amino groups) reacted with copper ions. A nitrogen to copper ratio, calculated using the corresponding band areas and sensitive factors, was found to be ca. 1.1, indicating that one amino group reacted with one copper ion, which is different from solution complexation of four to six cordinations. This is probably due to the two dimentional geometric constraint of primary amino groups on the surface.

To examine the application of the thiol-type magnetic carriers in precious and heavy metals removal or recovery, a "proof of concept experiment" was conducted as follows: 20 mg of magnetic carriers was brought in contact with about 20 ml of 10 mM $AgNO_3$ and $CuSO_4$ solutions for 30 minutes. The particles were separated from solution by hand magnet and washed three times with Millipore water to remove unbounded metals. The samples were then dried in a vacuum oven at 60 °C for overnight. The metal loaded magnetic carriers were characterized using XPS spectroscopy. The survey scan spectra are given in Figure 7.5, and the narrow scans are shown in Figure 7.6. As shown above, the bands centered at 934 and 954 eV on spectrum c (Figure 7.6: Cu_{2p}) are characteristic of copper ions, indicating the adsorption of copper from the solutions. The presence of

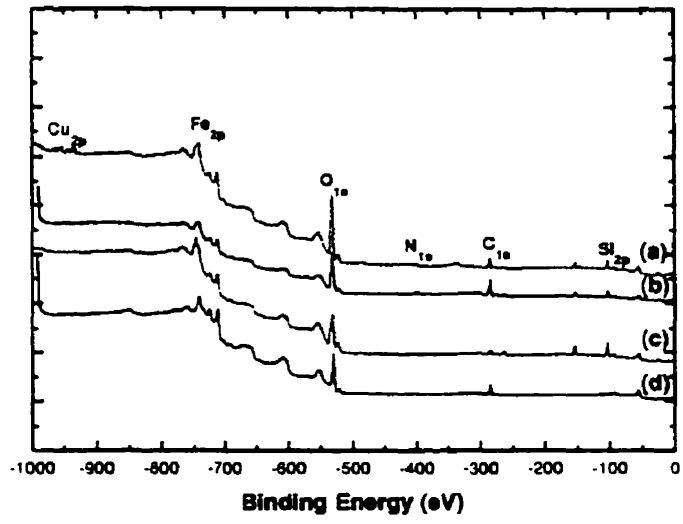

Figure 7.3 XPS survey scan spectra: (a) copper loaded on magnetic carriers; (b) magnetic carriers; (c) silica coated γ-Fe_2O_3; and (d) γ-Fe_2O_3.

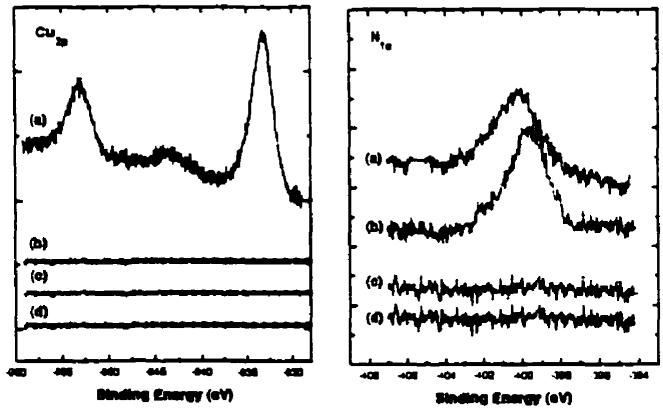

Figure 7.4 XPS narrow scan spectra of interested elements: (a) copper loaded magnetic carriers; (b) magnetic carriers; (c) silica coated γ-Fe_2O_3; and (d) γ-Fe_2O_3.

satellite band at 943 eV suggests that the majority of copper ions were in cupric form (Cu^{2+}) on thiol-type magnetic carriers. However, the area ratio of cupric satellite band to its $2p_{3/2}$ band was lower than expected for pure cupric ions, suggesting that some of the copper ions were in cuprous state. It appears that some of cupric ions were reduced as a result of thiol oxidation to disulfide, sulphonate or sulphate, which accounts for the presence of an additional weak sulfur band at higher binding energy (Figure 7.6: S_{2p}). In the case of silver-loaded magnetic carriers, two bands at 368 and 374 eV were observed (Figure 7.5: spectrum d; Figure 7.6: Ag_{3d}), suggesting the uptake of silver thiol-type magnetic carriers.

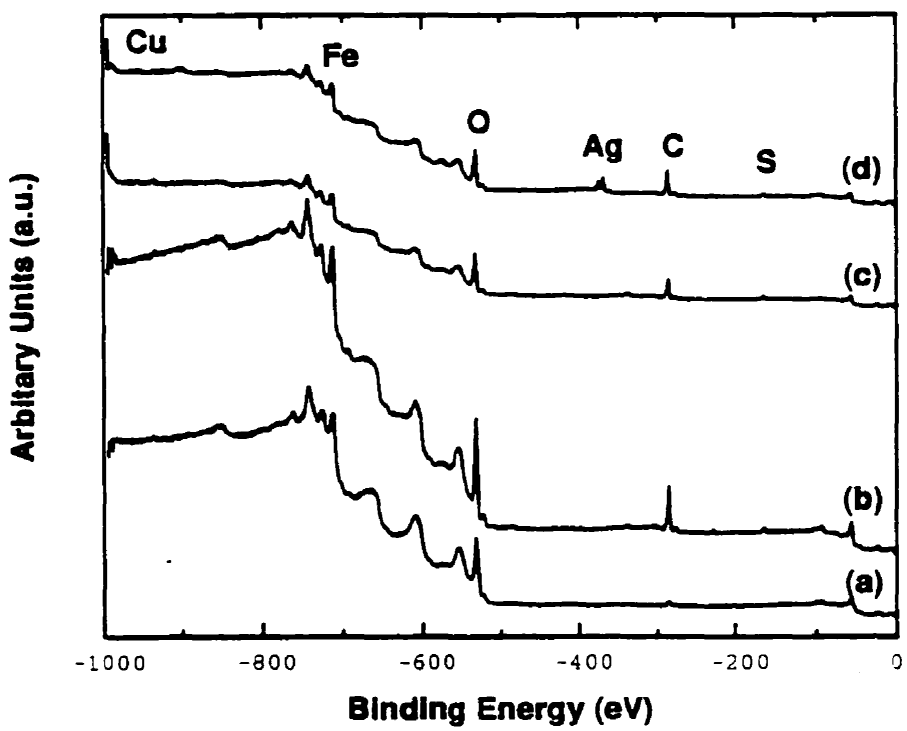

Figure 7.5 XPS survey scan spectra: (a) γ-Fe_2O_3; (b) thiol-type magnetic carriers; (c) after copper loading; and (d) after silver loading.

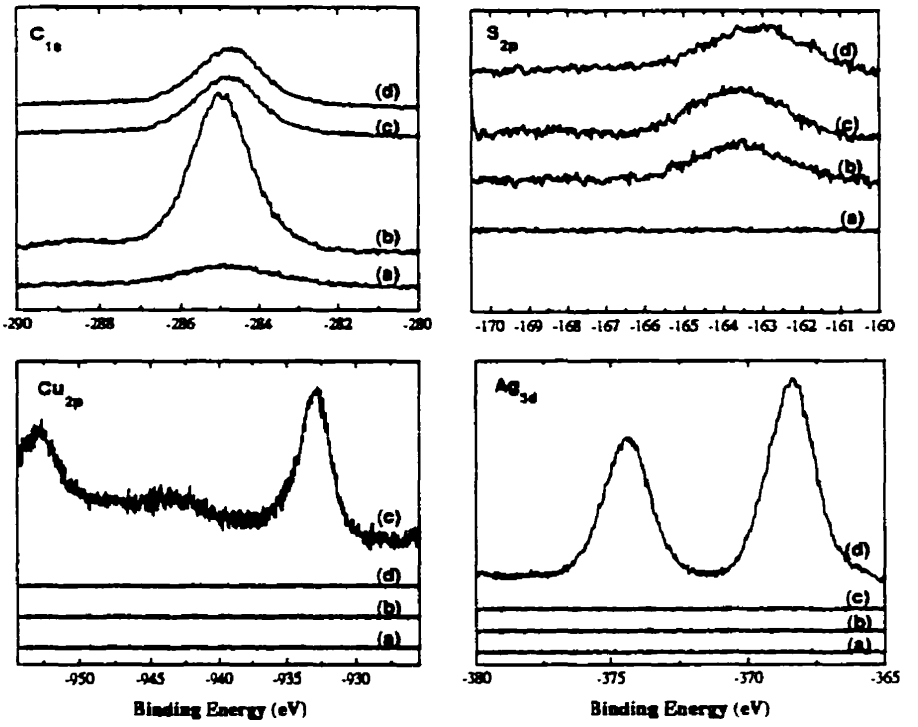

Figure 7.6 XPS spectra of narrow scans for the interested elements (a) γ-Fe_2O_3; (b) thiol-type magnetic carriers; (c) after copper loading; and (d) after silver loading.

The loading efficiency was evaluated by calculating the sulfur to metal molar ratio, based on the band area normalized by the element sensitivity factors. The calculation shows a 60% coverage of surface sulfur by copper ions and 80% by silver ions, demonstrating a high loading efficiency. These values suggest that each silver ion binds with one sulfur on magnetic carriers. Whether each copper ion binds with two surface sulfurs is, however, not clear. It appears that cuprous ions bind predominately with one while cupric ions with two sulfur atoms. This accounts for the low coverage of sulfur by copper ions (60%), yet higher than 50% as expected for a 2:1 S:Cu co-ordination. These preliminary results showed that thiol-type magnetic carriers prepared by molecular self-assembly can be used in recovery or removal of metal ions from solutions.

B) Stripping of Metal Ions and Recycling of Magnetic Carriers

Stripping of metal ions from loaded magnetic carriers is a major step for the subsequent recovery of metals by electrowining, while the recycling of magnetic carriers is a necessary step to offset the high price of magnetic carriers and lower the cost in industrial applications. Many methods such as acid washing (Plueddemann, 1985), EDTA (ethylenediamine tetraacetate) extraction, and electrowining can be used to strip off metal ions from loaded magnetic carriers. An ideal method would detach metal ions effectively while maintaining maximum reactivity of magnetic carriers. In this section, a preliminary study on the detachment of metal ions from loaded magnetic carriers by acid washing was conducted. The silanized films remained on the magnetic carriers were characterized by XPS, DRIFTS, zeta-potential measurement, and loading test.

The results of the stripping tests using nitric acid are given in Table 7.1. As reference, the results from initial copper loading tests are also included in this Table. The amount of copper detached vs. the amount of copper loaded is shown in Figure 7.7. The straight line through the origin represents the theoretical detaching curve, i.e., 100% detachment. It can be seen that within the experimental errors, loaded metal ions were detached completely from carriers by 0.01 N acid, suggesting that the recovery of copper by subsequent electrowinning processes is feasible. The mechanism of detachment of copper by acid washing seems similar to that in the regeneration of exhausted ion-exchange resin often used in wastewater management. The detachment is most likely accomplished by ion exchange due to the high chemical potential of hydrogen ions in acidic solutions, which compete with copper ions for amino groups on magnetic carriers.

After stripping off metal ions, the next step is to find out the density and reactivity of silanized films remained on magnetic carriers. For this purpose, the recycled magnetic carriers were characterized by XPS, DRIFTS, zeta-potential measurements and the copper loading test.

Table 7.1 Data of loading and stripping of copper ions [a].

Initial Cu^{2+} concentr. (ppm)	Cu^{2+} left in supernatant (ppm)	Uptake of Cu^{2+} (mg/g)	Cu^{2+} detached (mg/g)	Detaching efficiency (%)
7.92	0.02	3.96	3.97	100
11.88	0.01	5.94	6.11	103
15.84	1.56	7.13	7.18	101
23.76	4.68	9.54	9.95	104
39.6	14.24	10.61	10.74	101

a: loading test is conducted using 50 mg magnetic carrier and 25 mL copper solution; stripping test is conducted in 25 mL of 0.01 N HNO_3.

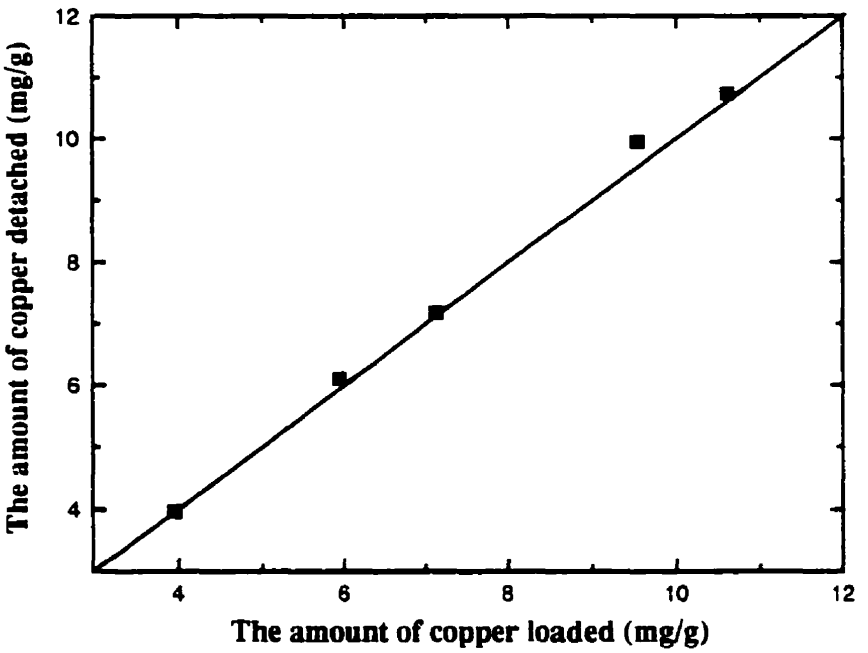

Figure 7.7 The amount of copper detached vs. the amount of copper loaded.

XPS survey scan spectra of magnetic carriers with various treatment are shown in Figure 7.8, and the narrow scans of the interested elements are given in Figure 7.9.

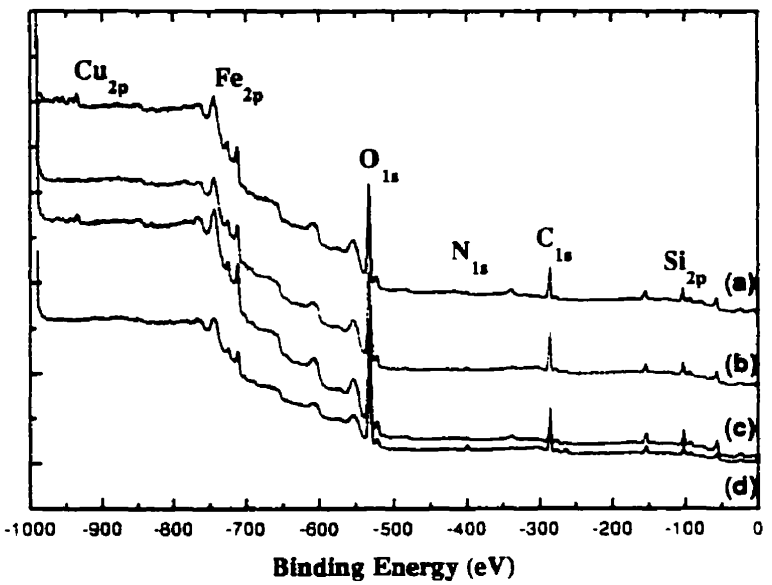

Figure 7.8 XPS survey scans of magnetic carriers (d); after copper loading (a); acid washing (b); and copper reloading (c).

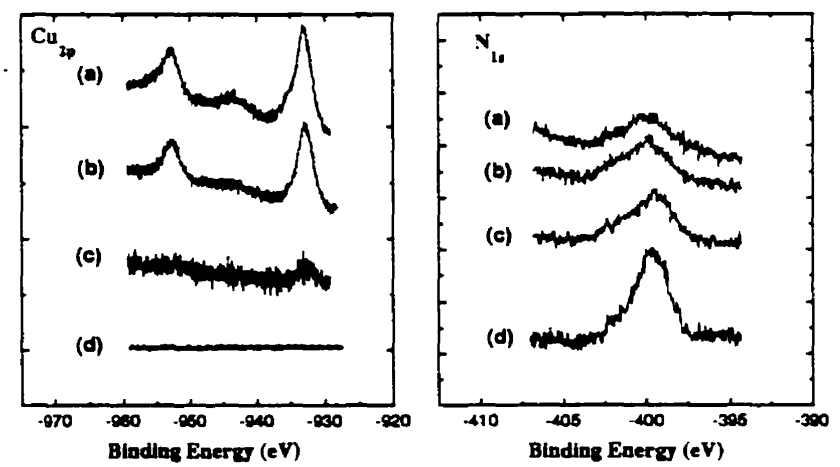

Figure 7.9 XPS spectra of narrow scan for the interested elements: (a) copper loaded magnetic carriers; (b) copper reloaded magnetic carriers; (c) acid washed magnetic carriers; (d) magnetic carriers.

The disappearance of copper band in spectrum c after acid washing confirmed the detachment of copper ions. The nitrogen band on spectrum c after copper detachment is characteristic of silanized APTES films, suggesting that the APTES films retained on the magnetic carriers. To have a semiquantitative analysis of the amount of surface films remained on the surface, the proportion of two-oxygen components and the molar ratio of interested elements to iron were calculated using corresponding areas and sensitive factors, and the results are given in Table 7.2.

Table 7.2 The proportion of two oxygen components and the ratio of interested element.

	O_{1s} (%) (532.8 eV)	O_{1s} (%) (529.6 eV)	Si_{2p} /$Fe_{2p3/2}$	O_{1s}[a] /$Fe_{2p3/2}$	N_{1s} /$Fe2p_{3/2}$	N_{1s} /Cu_{2p}
magnetic carriers	60.4	39.6	3.1	7.0	0.8	--
copper loaded	58.9	41.1	2.1	5.4	0.3	1.1
copper detached	55. 8	44.2	2.4	5.5	0.3	--
copper reloaded	55.6	44.4	2.3	5.3	0.4	1.3

a: Oxygen band at 532.8 eV.

The remained oxygen component at 531.8 eV after copper detachment suggests that the silica coatings are still on the surface. It can be seen that the nitrogen to iron ratio for copper detached magnetic carriers reduced from the original value of 0.8 for magnetic carriers to ca. 0.3, suggesting the detachment of immobilized silanes from the surface.

DRIFTS spectra of magnetic carriers with various treatments are shown in Figure 7.10. The band at 1580 cm^{-1} assigned to amino groups on magnetic carriers (spectrum c) was shifted to 1615 cm^{-1} after copper loading (spectrum b). This band shift to a higher wavenumber indicates that it was amino groups of magnetic carriers that reacted with copper, consistent with XPS results (Figure 7.4). The new band at 1711 cm^{-1} for detached magnetic carriers (spectrum a) is attributed to oxidized amines, possibly imides, which have little affinity to copper (Goelzhaeuser, et al. 1995), thus reducing the reactivity of magnetic carries with copper as shown in the following copper reloading test. Considering that amino groups are susceptible to oxidation (Lund and Baizer, 1991), using EDTA to extract loaded copper from magnetic carriers may be beneficial. The minimal breakage of siloxane bonds, and hence the detachment of APTES films from the magnetic carriers are

anticipated. Therefore, using EDTA or similar complexing reagent to detach metal ions from loaded magnetic carriers is worth exploring.

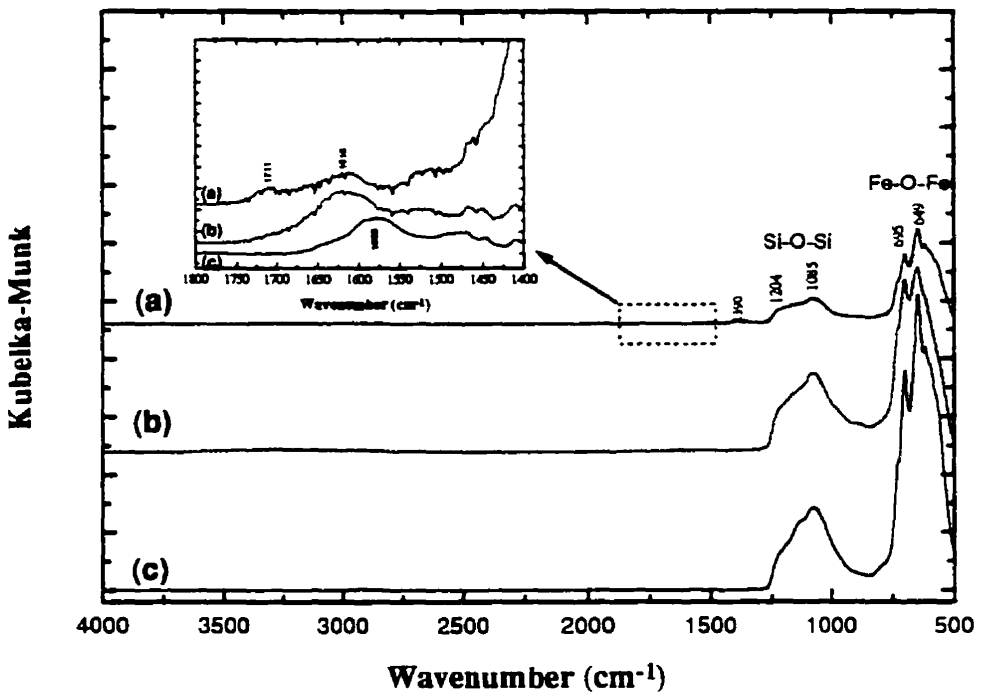

Figure 7.10 DRIFTS spectra for (a) copper detached magnetic carriers; (b) copper loaded magnetic carriers; (c) magnetic carriers. Inset shows characteristic bands of amino group.

The detachment of silanized films after detaching copper ions is further confirmed by zeta-potential measurement. The IEP value (at pH about 6.1) of magnetic carriers after detaching copper ions (Figure 7.11) is lower than that of original magnetic carriers (IEP at pH about 8.9), indicating the detachment of the films from the surface. However, the possible contribution of amino group oxidation to the shift of IEP to a lower pH value cannot be ruled out.

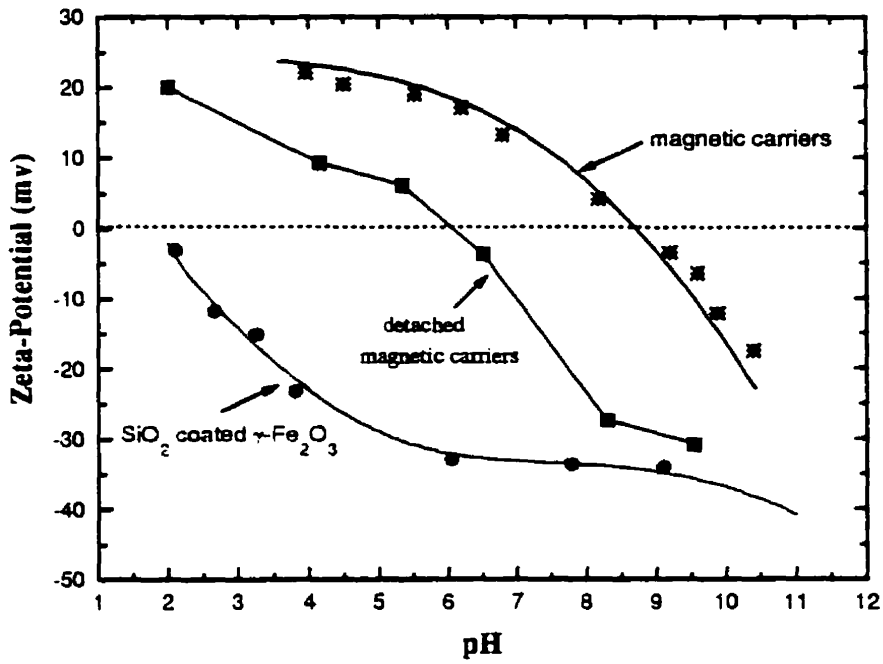

Figure 7.11 Zeta-potential of magnetic carrier before and after copper detachment.

Why surface films were detached after stripping off copper from magnetic carriers by acid remains to be resolved. In chapter 6, based on the zeta-potential measurement of magnetic carriers in acidic solution (Figure 6.6) it was concluded that the silanized films on silica coated magnetic particles is relative stable in acid solution (pH = 2.1). To further examine the stability of silanized APTES films and the effect of acid soaking on the reactivity of amino groups, the following experiment was conducted. First, 50 mg of magnetic carriers were soaked in 0.01 N hydrochloric acid for about 1 hour. The slurry was then centrifuged and the supernatant removed. After washing once with Millipore water, the magnetic carriers collected in centrifuge tube were mixed with 25 mL copper solution (31.3 ppm) of pH about 5.3 for 30 minutes and the amount of copper loaded was determined using the same method as described previously. The objective of this experiment is to examine whether the film detachment by acid soaking is the major cause for the reduced copper loading capacity. The results given in Table 7.3 show that copper

loading capacity for acid soaked magnetic carriers retained about 81% of original capacity (9.3 over 11.5). In other words, the copper capacity is reduced only by 19% after acid soaking. This reduced copper loading capacity suggests that some amino groups may have been protonated or oxidized after in contact with acid, thus becoming unreactive to copper.

Table 7.3 also shows that copper loading efficiency for recycled magnetic carriers retained only about 40 %, much lower than acid soaked one (81%). This finding suggests a catalytic effect of copper on detachment of silanized film by acid. A recent report showed that copper ions can indeed catalyze the hydrolysis of silane coupling agents (Yang, et al., 1995). XPS results given in Table 7.2 showed that the nitrogen to copper ratio for copper reloaded magnetic carriers (1.27) was higher than that for initial loaded the ones (1.1), indicating that some of the amino groups are indeed oxidized after acid washing, thus becoming unreactive to copper ions. This is in good agreement with the results obtained from DRIFTS spectra on which a new band at 1711 cm^{-1}, assigned to oxidized amines, for recycled magnetic carriers appeared. It is therefore evident that both the oxidation of amino groups and the detachment of silanized APTES films contribute to the reduced zeta-potential and copper reloading efficiency.

Table 7.3 Copper loading capacity of acid soaked magnetic carriers[a].

system	Initial Cu^{2+} concentr. (ppm)	Cu^{2+} left in supernatant (ppm)	Uptake of Cu^{2+} (mg/g)	Cu^{2+} detached (mg/g)	Detach efficiency (%)	Reloaded copper (mg/g)	Reload efficiency (%)
acid soaking	31.3	12.7	9.3	9.1	97.3	3.9	41.9
no acid soaking	31.3	8.2	11.5	11.8	102.8	5.0	43.5

a: copper detaching by 0.01 N HCl; all loading test is conducted at pH 5.5±0.1.

To avoid the catalytic effect of copper and to improve the stability of surface films, using long alkyl chain silane coupling agents may be necessary. It is anticipated that the strong van der Waals attractions between long alkyl chains, like the case in molecular self-assembly, will improve the packing density of silane molecules on the surface, thus preventing the siloxane bonds on the surface from the attack of acid or base. The isolation

of loaded copper ions from the surface by long alkyl chains may minimize the catalytic effects of copper ions on the breakage of the siloxane bonds on magnetic carriers. Therefore, it seems better to prepare magnetic carriers using long alkyl chain silanes through molecular self-assembly. Our preliminary study indeed showed an improved coating density and stability of silanized films even on bare magnetic particles using OTES (octadecyltrimethoxy silane) through molecular self-assembly.

These fundamental studies demonstrated that it is feasible to use magnetic carriers in metal recovery and/or removal. The loaded metal ions on magnetic carriers can be detached completely by acid washing. Although the loading efficiency of recylced magnetic carriers is reduced, the improvement of film stability on magnetic carrier will make recycling of magnetic carriers feasible. The concept of using MCT in recovery or selective removal of metal ions proposed in Figure 1.2 has thus been proved.

7.3 POTENTIAL APPLICATIONS

7.3.1 Toxic Species Removal

The removal of toxic species such as heavy metals from contaminated water to achieve the high quality living environment is of increasing importance. Since amines are known to complex with most of heavy metals, the magnetic carriers prepared in this work will find potential applications in these areas. It has been reported that APTES immobilized on silica was able to remove the toxic species such as arsenic anions and heavy metals (i.e., Hg, Pb, Cr, Ni) from aqueous solution (Leyden, 1975). Thus, the use of magnetic carriers with reactive amino groups to capture these toxic species from aqueous solutions, and then to separate them from the streams by magnetic separation are only a step away from practice.

7.3.2 Biological Cell Separation

Magnetic carrier with amino groups can also be used to immobilize enzyme, protein, etc. by following the routes as shown below (Bruning and Grobe, 1995):

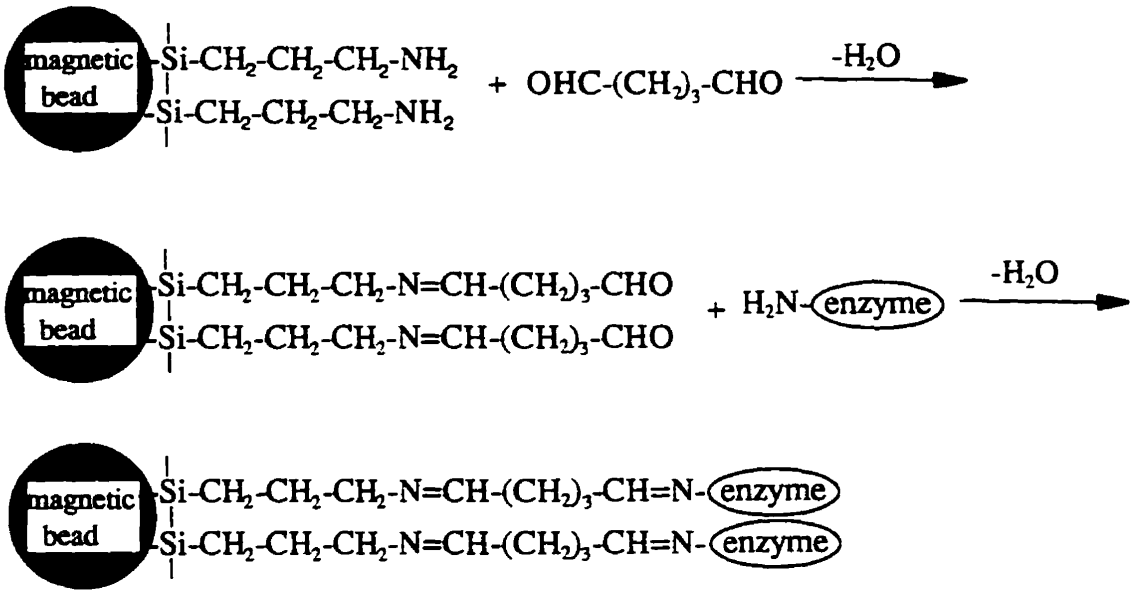

The magnetic carriers with thiol or disulfide groups also have potential applications in various areas. The special affinity of thiol with antibodies makes thiol-type magnetic carriers of special interest. It has been shown that monoclonal antibodies (mAb), usually containing disulfides in the basic unit, is readily cross-linked to another incubated antibody, forming tetrameric antibody complexes (Molday and Mackenzie, 1982). The thiol-type magnetic carriers as shown in Figure 7.12a can, therefore, be sensitized with a mAb of specific paratopes, such as anti-glycophorin, generating sensitized magnetic antibodies. These magnetic antibodies recognize glycophorin, one kind of protein (M and N blood group antigens) in red blood cell membranes. When the sensitized magnetic carriers are introduced into a biological system, the cells containing glycophorin will be captured by magnetically sensitized media (Figure 7.12b). These fractions may then be separated using magnetic separation methods. In the case where the thiol on magnetic carriers gets oxidized, the disulfide can be readily reduced nonenzymatically by glutathione to a thiol functionality, thus activating magnetic carriers for cell separation (Mathews and van Holds, 1990).

The potential application of magnetic carriers with reactive amine and thiol groups in biological system such as immobilization of cytochrome b_5 is also possible (Hong, et al., 1994), and prospective in these fields is wide open.

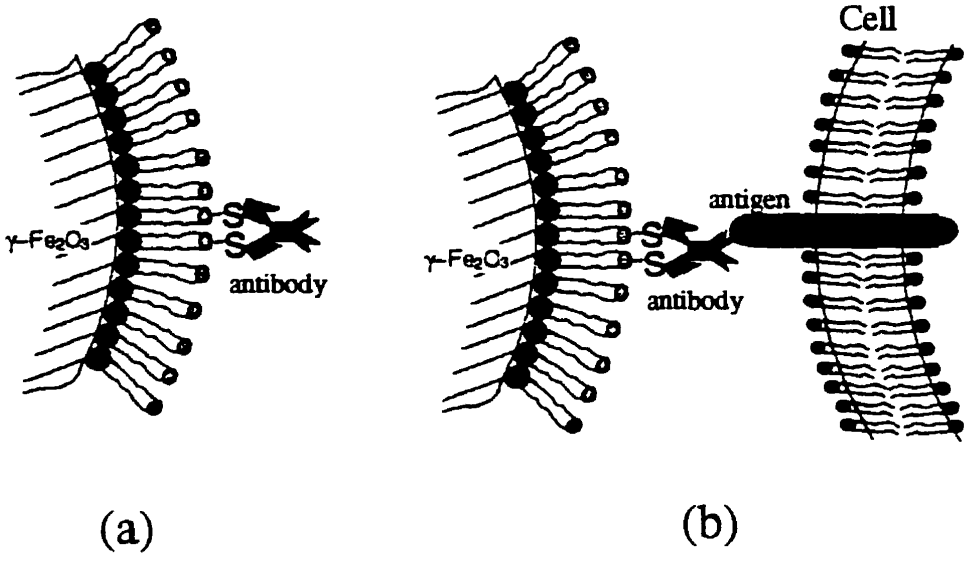

Figure 7.12 Schematic representation of magnetic carriers for biological cell separations (a) activated with an antibody; (b) attached to a targeted cell.

7.3.3 Others

The thiol or disulfide group on the magnetic carriers can also be oxidized to the functionality of sulphonate or sulfate (Collins and Sukenik, 1995). The calcium or barium thus can be loaded on these magnetic carriers, and then separated from streams by magnetic separation (Figure 7.13). This feature of magnetic carriers may open up new research area in controlling the hardness of water. The sulfate group on the surface of magnetic carriers can impose a negatively charged surface, which will be useful for stabilizing magnetic fluids.

The magnetic carriers with various functional groups may also be used as a template for improving a thin inorganic film coatings (Bunker, et al., 1994), which may result in a new route for making magnetic ceramics and catalyst (Whitesides, et al., 1976; Hill, et al., 1976).

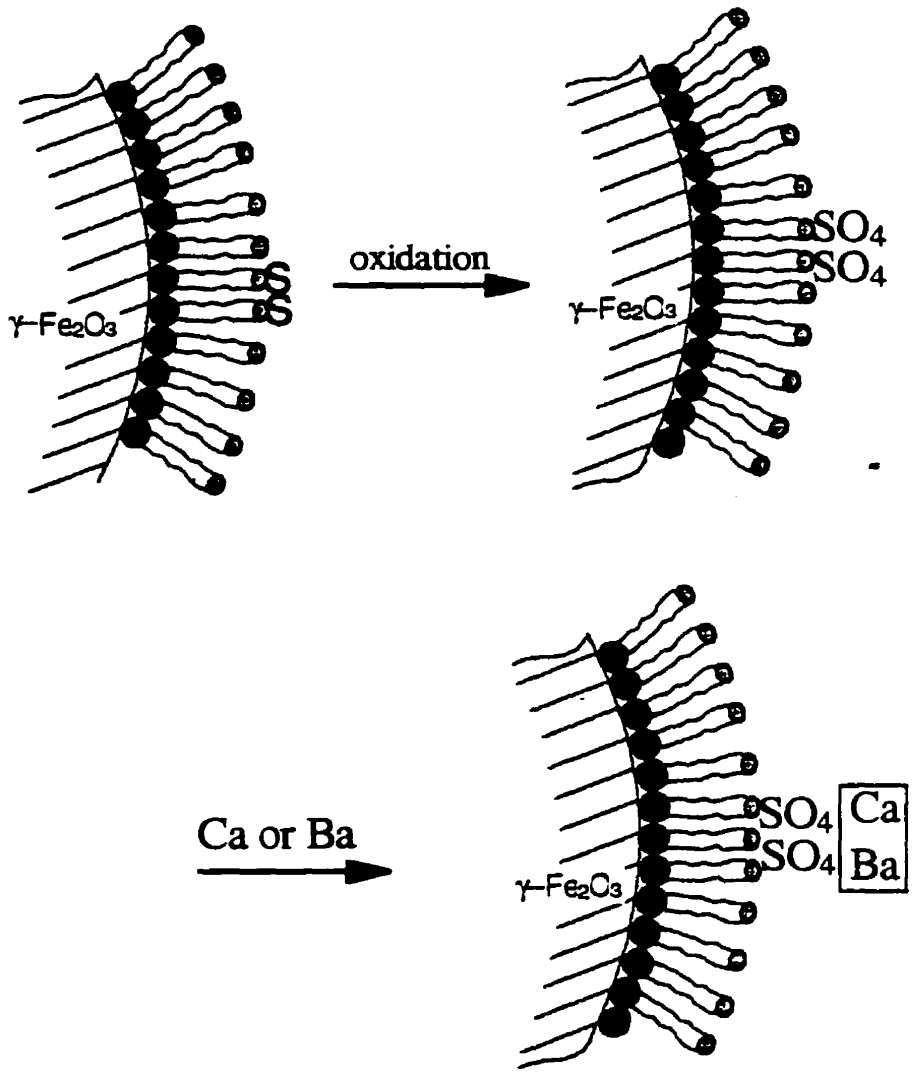

Figure 7.13 Schematic representation of the uptake of calcium and barium ions on thiol-type magnetic carriers.

7.4 CONCLUSIONS

1. Magnetic carriers with reactive amine groups were proved to be effective for removal or recovery of heavy metal ions such as Cu^{2+} and Zn^{2+} from aqueous solutions.

2. Selective separation of copper from zinc was achieved by controlling the solution pH.

3. Loaded metal ions on magnetic carriers were completely stripped off by 0.01 N nitric or hydrochloric acid.

4. The functionalized magnetic particles with reactive thio and/or disulfide groups were capable of capturing metal ions such as silver and copper from aqueous solution.

5. Magnetic carriers with reactive thiol or amine groups have potential applications in biological cell separation, immobilization of enzyme, and magnetic fluids.

6. The recycling of magnetic carriers is feasible.

CHAPTER 8 SUMMARY AND CONCLUSIONS

8.1 SUMMARY AND CONCLUSIONS

8.1.1 Preparation of Magnetic Carriers by Molecular Self-assembly

1. By controlling the reactivity of functional groups with surface, 16-mercaptohexadecanoic acid (MHA) was anchored onto γ-Fe_2O_3 surface through chemical bonding between the carboxylic head group of surfactant and iron on the surface, leaving the thiol or disulfide groups reactive.

2. The molecular orientation of MHA self-assembled on γ-Fe_2O_3 was inferred from XPS, DRIFTS and film flotation.

3. The self-assembled MHA film on γ-Fe_2O_3 is immobilized and resistant to acid and base attack.

4. Magnetic carriers with reactive thiol and/or disulfide groups are capable of capturing metal ions such as silver and copper from aqueous solution and have potential applications in biological cell separation, immobilization of enzyme, and magnetic fluids.

8.1.2 Preparation of Magnetic Carriers by Silanation Using 3-Aminopropyl Triethoxy Silane (APTES)

1. XPS, IR, and zeta-potential measurements indicated that APTES can be directly silanized on magnetic particles from water or toluene solutions. APTES films formed on bare magnetic particles from toluene are relatively stable in acid solution compared to the films formed from water. Both films are unstable in alkaline solution.

2. Silica coatings on magnetic particles were achieved by both sol-gel and dense liquid silica process. A uniform but porous silica layer was coated on magnetic particles by sol-gel process. At low supersaturation level, a non-uniform silica coatings were formed by dense liquid silica process. Densely packed, thin silica layer was coated on magnetic particles by a novel two-step process, i.e., sol-gel followed by dense liquid silica.

3. Magnetic carriers with amino groups were prepared by 3-amino-propyltriethoxyl silane (APTES) silanation in toluene on silica coated magnetic particles. Stability test indicated that the silanized films on silica coated magnetic particles in acid solution were more stable than on bare magnetic particles, but unstable in alkaline solutions. An improvement can be made by using longer alkyl chain silane coupling agents.

8.1.3 Applications of Prepared Magnetic Carriers

1. Magnetic carriers with reactive amine groups have been proved to be effective for removal or recovery of heavy metal ions such as Cu^{2+} and Zn^{2+} from aqueous solutions. Selective separation of copper from zinc can be achieved by controlling the solution pH. Loaded metal ions on magnetic carriers can be stripped off effectively using 0.01 N nitric or hydrochloric acid.

2. The recycle of magnetic carriers is feasible, which could offset the high price of magnetic carriers.

3. Magnetic carriers with reactive amine and thiol groups have potential applications in biological cell separation, immobilization of enzyme, magnetic fluids, and waste remediation.

8.2 CONTRIBUTIONS TO ORIGINAL KNOWLEDGE

1. It is the first time that magnetic carriers with reactive thiol groups were prepared using bolaamphiphile such as MHA through molecular self-assembly.

2. A novel approach, i.e., sol-gel process followed by dense liquid silica coating, was developed and used in coating a densely packed, thin silica layer on magnetic particles.

3. Magnetic carriers with reactive amino groups were prepared by silanation of APTES on silica coated magnetic particles.

4. The prepared magnetic carriers were characterized systematically by XPS, DRIFTS, thin film flotation, zeta-potential measurement, leaching test, TGA, and VSM. The issue of film stability was discussed thoroughly.

5. Applications of magnetic carriers in industrial effluent management and metal recovery were demonstrated. The potential uses in waste remediation, immobilization of enzyme, biological cell separation, and magnetic fluids were proposed.

8.3 FUTURE PROSPECTS

1. By controlling the reactivity of functional groups with magnetic particles, magnetic carriers with a variety of reactive functional groups on surface could be prepared using other bolaamphiphiles through molecular self-assembly.

2. The features of porous silica coating by sol-gel and the leaching of magnetic particles in hydrochloric acid could be used to prepare inorganic membrane as schematically shown below:

Thin porous silica layer is first coated on magnetic particles. Then, the core magnetic particles can be dissolved in hydrochloric acid so that a hollow porous silica

membrane can be obtained. By controlling the hydrolysis of TEOS in sol-gel process, a variety of hollow silica membranes with various pore size distributions can be achieved. Further modification of this hollow silica membrane by silanation using silane coupling agents could be of importance in drug delivery and capsulation.

3. Other silane coupling agents with long hydrocarbon chain could be used to prepare more densely packed and stable surface films on magnetic particles.

4. Magnetic carriers with reactive functional groups such as carboxylic, phosphate, thiol could be prepared on silica coated magnetic particles through silanation. These magnetic carriers could be used as a template for further deposition of other thin ceramic films such as alumina, titania, ruthenium oxides, etc.. The magnetic particles prepared as such have unique features: the magnetic core inside and thin metal oxides on the surface. These magnetic carriers used as catalyst can be separated from the system by magnetic separation.

5. Applications of magnetic carriers in toxic species removal, biological cell separation, etc. are wide open and should be further explored.

REFERENCES

Alaerts, G.J., Jitjaturunt, V. and Kelderman, P., **1989,** *Water Sci. Technol.*, 21, 12, 1701.

Albert garcia III, Oh, S., and Engler, C. R., **1989**, *Biotechnology and Bioengineering*, Vol.33, 321-326.

Allara, D. L., Hebard, A. F., Padden, F. J., Nuzzo, R. G. and Falcone, D. R., **1983**, *J. Vac. Sci. Technology*, A1(2), 376-382.

Allara, D. L. and Nuzzo, R. G., **1985**, *Langmuir*, 1, 52.

Angeletti, E., Canepa, C., Martinetti, G. and Venturello, P., **1988,** *Tetrahedron Lett.*, 29, 2261.

Appelbaum, S.B., **1968,** Demineralization by Ion Exchange, Academic Press, New York.

Arkles, B, **1992**, Silane Coupling Agent Chemisty, in Silicon Compounds, Register and Review, Petrarch System Catalogue, p59.

Azzam, R. M. A. and Bashara, N. M., **1977**, Ellipsometry and Polarized Light; North-Holland Publishing Company, Amsterdam.

Bain, C. D., Troughton, E. B., Tao, Yu-Tai, Evall, J., Whitesides, G. M. and Nuzzo, R. G., **1989,** *J. Am. Chem. Soc.*, 111, 321.

Barrow, N. J. and Bowden, J. W., **1987**, *J. Colloid Interface Sci.*, 119, 236.

Battistel, E., Bianchi, D. and Rialdi, G., **1991**, *Pure Appl. Chem.*, 63, 1483.

Battjes, K. P., Barolo, A. M. and Dreyfuss, P., **1992,** In Silane and other coupling agents, (Ed.) K.L. Mittal, Utrecht, The Netherlands, pp 199-213.

Bean, C. P. and Livingston, J. D., **1959,** *J. Appl. Phys.*, 30, 120s.

Berg, E. W. and Downey, D. M., **1980,** *Analytical Chemica Acta*, 120, 273.

Bergna, H. E., **1994,** In The Colloid Chemistry of Silica, American Chemical Society, Ed. by Bergna, H. E., Washington, D.C., pp 1-47.

Bergna, H. E., Firment, L. E. and Swartzfager, D. G., **1994,** In The Colloid Chemistry of Silica, Ed. by Bergna, H. E., American Chemical Society, Washington, D.C., pp 561-578.

Bierbaum, K., Kinzler, M., Woll, Ch. and Grunze, M., **1995,** *Langmuir*, 11, 512.

Birzer, J. O. and Schulzer, H. L., **1986**, *J. Colloid. Polym. Sci.*, 264, 642.

Blitz, J.P., Murthy, R.S.S. and Leyden, D., **1986,** *J. Colloid and Interface Science*, Vol. 121, No. 1, pp 63-69.

Blum, F.D., Meesiri, W., Kang, H.J. and Gambogi, J.E., **1992,** In Silanes and other Coupling Agents, K.L. Mittal (Ed.), Utrecht, The Netherlands, pp181-198.

Bogart, G. R. and Leyden, D. E., **1994,** *J. Colloid and Interface Sci.*, 167, 18-26.

Bolger, J. C., **1983,** In Adhesion Aspects of Polymeric Coatings, Ed by K. L. Mittal, Plenum Press, New York.

Bolto, B.A. and Weiss, D. E., **1977**, In Ion exchange and Solvent Extraction, Eds. by J. A. Marinsky and Y. Marcus, Marcel Dekker, New York.

Bosch, P., Lopez, T., Asomoza, M. and Gomez, R., **1995,** *Langmuir*, 11, 4328-4332.

Briggs, D. and Seah, M.P., Ed., **1990,** Practical Surface Analysis, Vol. 1, Auger and X-ray Photoelectron Spectroscopy, John Wiley & Sons, New York.

Briggs, W. S., et. al., **1977,** U.S. patent 4, 019,995.

Brinker, C. J. and Scherer, G. W., **1990,** Sol-Gel Science, the Physics and Chemistry of Sol Gel Processing, Academic Press, Inc..

Bruning, C. and Grobe, J., **1995,** *J. Chem. Soc.,Chem. Commun.*, 2323.

Bunker, B. C., Rieke, P. C., Tarasevich, B. J., Campbell, A. A., Fryxell, G. E., Graff, G. L., Song, L., Liu, J., Virden, J. W. and McVay, G. L., **1994**, *Science*, Vol. 264, 48-55.

Burns, L.N., Holmberg, K. and Brink, C., **1996,** *J. Colloid and Interface Science*, 178, pp 116-122.

Buszewski, B. and Lodkowski, R. J., **1991**, *Liquid Chromatogr.*, 14, 1185.

Butterworth, M. D., Armes, S. P. and Simpson, A. W., **1994,** J. *Chem. Soc. Chem. Commun.*, 2129-2130.

Cases, J. M. et al., **1993,** *Inter. J. Miner. Process.*, Vol. 38, pp 267-269.

Charewicz, W. and Gendolla, T., **1972,** *Applied Chemistry*, 16, 4.

Chen, T. M. and Braner, G. M., **1982,** *J. Dent. Res.* , 61., 1439.

Colloins, R. J. and Sukenik, C. N., **1995**, *Langmuir*, 11, 2322-2324.

Couzis, A. and Gulari, E., **1993**, *Langmuir*, 9, 3414-3421.

Culler, S. R., Ishida, H., and Koening, J. L., **1984**, *Appl. Spectrosc.*, 38, 1.

Cullity, B.D., **1972**, In Introduction to Magnetic Materials; Addision-Wesley: Reading, MA, p 94.

Davis, W. and Haas, P.A., **1972**, In Adsorptive Bubble Separation techniques, Ornl, L. R. (Ed.) Academic Press, ch. 19.

Demopoulos, G. P., **1994**, Effluent Treatment, Professional Development Seminar at McGill, Montreal.

Dixon, D.R., **1992**, *Chemistry in Australia*, 15, 394-396.

Evans, D. F. and Wennerstrom, H., **1994**, The colloidal domain: where physics, chemistry, biology, and technology meet, VCH Publishers, Inc..

Finch, J. A., **1973**, The Liquid-Vapor Interface and Adhesion in Flotation, Ph.D. thesis, McGill University, Canada.

Finch, J.A., Rao, S.R., Leroux, M., Kuyucak, N. and Wheeland, K.G., **1994**, Proc. 3rd International Conference on the Abatement of Acid Drainage, Pittsburgh, Vol. 1, 223.

Firment, L. E., Bergna, H. E., Swartzfager, D. G., Bierstedt, P. E. and van Kavelaaar, M. L., **1989**, *Surface and Interface Analysis*, Vol. 14, 46-52.

Flinn, D. H., Guzonas, D. A. and Yoon, R. -H., **1994**, *Colloids and Surfaces*, 87, 163-176.

Folkers, J. P., Gorman, L. B., Laibinis, P. E., Buchholz, S., Whitesides, G. M. and Nuzzo, R. G., **1995**, *Langmuir*, 11, 813.

Fornasiero, D., Li, F., Ralston, J. and Smart, R. St. C., **1994**, *J. Colloid and Interface Science*, 164, pp 333-344.

Fowkes, F. M., **1964**, *Ind. Eng. Chem.*, 56 (12), 40.

Fowkes, F.M., Huang, Y.C., Shah, B.A., Kulp, M. J. and Lloyd, T.B., **1988**, *Colloids and Surfaces*, 29, 243-261.

Fowkes, F.M., Dwight, D.W., Cole, D.A. and Huang, T.C., **1990**, *J. Non-Cryst. Solids*, 120, 47.

Fuhrhop, J. H. and Kon, J., **1994**, Membranes and Molecular Assemblies: the Synkinetic Approach, Cambridge University Press.

Furlong, D. N., Sing, K. S. W. and Parfitt, G. D., **1979**, *J. Colloid and Interface Sci.*, 69, 409.

Furlong, D. N., Rouquerol, F., Rouquerol, J. and Sing, K. S. W., **1980**, *Journal of Colloid and Interface Science*, 75, 68.

Furlong, D. N., **1994**, In The colloid Chemistry of Silica, Edited by Horacio E. Bergna, , American Chemical Society, Washington, DC, pp 535-559.

Fyfe, C.A.,Gobbi, G.C. and Kennedy, G. L., **1985**, *J. Phys. Chem.*, 89, 277.

Goelzhaeuser, A., Panov, S., Mast, M., Schertel, A., Grunze, M. and Woell, Ch., **1995**, *Surface Science*, v 334, pp 235-247.

Golden, W.G., Snyder, C. L. and Smith, B. J., **1982**, *J. Phys. Chem.*, 86, p4675.

Goldman, P., **1988**, In Electronic Ceramics: Properties, Devices, and Applications (L. M. Levinson, Ed.), Dekker, New York.

Grenler, R. G., **1966**, *J. Phys. Chem.*, Vol. 44, 1, pp 310-315.

Hair, M. L., **1967**, Infrared Spectroscopy in Surface Chemistry, Marcel Dekker, Inc., New York.

Hair, M. L., **1980**, In Vibrational Spectroscopies for Adsorbed Species; Bell, A. T.; Hair, M. L., Eds.; ACS Symposium Series 137, American Chemical Society: Washington DC.

Hair, M. L. and Tripp, C. P., **1995**, *Colloids and Surfaces*, 105, 95-103.

Heckl, W.M.; Marrassi, F.M.; Kallury, K.M.R.; Stone, D.C. and Thonpson, M.,**1990**, *Anal. Chem.*, 62, 32.

Heywood, B. R. and Mann, S., **1994**, *Advanced Materials*, Vol. 6, pp 9-20.

Hill, C. L., Lamotte, A., Althoff, W., Brunie, J. and Whitesides, G. M., **1976**, *Journal of Catalysis*, 43, pp 53-60.

Hoffman, W. P., Phan, H. and Groszek, A., **1995**, *Carbon*, Vol. 33, pp 509-524.

Hong, H. G., Jiang, Min, Sligar,S.G., and Bohn, P.W., **1994**, *Langmuir*, 10, 153-158.

Horner, M.R., Boerio, F. J. and Clearfield, H., **1992**, In Silane and Other Coupling Agents, Ed. Mittal, K.L., Utrecht, The Netherlands, pp 241-262.

Horr, T. J., Ralston, J. and Smart, R. St. C., **1992**, *Colloids and Surfaces*, 64, 67-85.

Howard, P. B. and Parfitt, G. D., **1977**, *Croatica Chem. Data*, 50, 15.

Huang, S. et al, **1988,** *J. Colloid Interface Sci.*, 124 , p666.

Huang, C.P., et al., **1989**, *J. Colloid Interface Sci.*, 131, 2, 289.

Huang, J. Y., **1990,** U.S. Patent 4, 906,382.

Ihs, A.; Liedberg, B., **1991**, *J. Colloid Interface Sci.*, 144, 283.

Iler, R. K., **1959**, U.S. Patent 2,885, 366.

Iler, R. P., **1979**, The Chemistry of Silica, Solubility, Polymerization, Colloid and Surface Properties, and Biochemistry, John Wiley & Sons, New York.

Ishida, H. and Koenig, J. L.,**1978**, *J. Colloid Interface Sci.*, 64, 555.

Ishida, H., Naviroj, S., Tripathy, S. K., Fitzgerald, J. J. and Koenig, J. L., **1981**, SPI, 36th Tech. Conf. Reinf. Plast. 2-C.

Ishida, H., **1984,** *Polym. Compos.*, 5, 101.

Israelachvili, J., **1992,** Intermolecular & Surface Forces, Second Edition, Academic Press.

Kaas, R. L., and Kardos, J. L., **1971**, *Polym. Eng. Sci.*, 11, 11.

Kallury, K.M.R., Macdonald, P. M. and Thompson, M., **1994**, *Lagmuir*, 10, 492.

Kelebek, S., Wells, P. F., and Heinrich, G. W., **1995**, In 27th Annual Operator's Conference of the Canadian Mineral Processors, Ottawa, Canada, paper 10.

Kellar, J.J., Cross, W.M., Yalamanchili, M. R., Young, C.A. and Miller, J. D., **1993**, *Minerals & Metallurgical Processing*, 5, pp75-80.

Khalfaoui, B., Meniai, A. H. and Borja R., **1995**, *J. Chem. Technol.*, 64 (2), pp 153-156.

Kinney, J. B. and Staley, R. H., **1983,** *J. Phys. Chem.*, 87, 3735.

Klassen, V. I. and Mokrousov, V. A., **1963,** An Introduction to the Theory of Flotation, ButterWorths, London.

Kurth, D.G. and Bein, T., **1995**, *Langmuir*, 11, 3061-3067.

Laibinis, P. E., Hickman, J. J., Wrighton, M. S. and Whitesides, G. M., **1989**, *Science*, 245, 845.

Laskowski, J.S., Yordan. J.L. and Yonn, R. H., **1989,** *Langmuir*, 5, 373-376.

Lee, L. H., **1993,** In Contact Angle, Wettability and Adhesion, Mittal, K. L., Ed.; VSP, Utrecht, p 45.

Leyden, D.E. and Luttrell, G. H., **1975**, *Analytical Chemistry*, Vol. 47, No. 9, pp 1612-1617.

Leyden, D.E., Ed, **1986**, Silanes, Surfaces, and Interfaces, Proceedings of the Silanes, Surfaces, and Interafces Symposium, Snowmass, Colorado, June, 19-21, 1985, Gordon and Breach Science Publishers, New York.

Liu, Q. X. and Friedlaender, F. J., **1994**, *Minerals Engineering*, 7, 449.

Liu, Q. X. and Xu, Z. H., **1995**, *Langmuire*, Vol. 11, No. 12, 4617.

Lloyd, T. B., Li, J., Fowkes, F. M., Brand, J. R. and Dizikes, L. J., **1992**, *Journal of Coatings Technology*, Vol. 64, 91-99.

Lund, C. J. and Murphy, P. D.,**1992,** *J. Adhes. Sci. Techol.* , 6, 33.

Lund, H. and Baizer, M. M., **1991**, Organic Electrochemistry, Marcel Dekker, Inc., New York, pp 581-614.

Mann, S., **1988**, *Nature*, 322, pp 119-124.

Mann, S., **1993,** *Nature*, Vol. 365, 499-505.

Mann, S., Archibald, D. G., Didymus, J. M., Douglas, T., Heywood, B. R., Meldrum, F. C. and Reeves, N. J., **1993,** *Science*, Vol. 261, 1286-1292.

Marinakis, K. I. and Shergold, H. L., **1985,** *Int. J. Mineral. Proce.*, 14, 177.

Markovich, R.J.; Qiu, X; Nichols, D.E.; Pidgeon, C.E.; Invergo, B.; Alvarez, F.M., **1991,** *Anal. chem.*, 63, 1985.

Marsden, J and House, I., **1992,** The chemistry of gold extraction, Ellis Horwood Limitted, London.

Mathews, C. K. and van Holds, K. E., **1990**, Biochemistry, The Benjianmin/Cummings Publishing Company, Inc., Chapter 14, p 500.

Matteucci, M.D. and Caruthers, M. H.,**1981**, *J. Ame. Chem. Soc.*, 103, 3185.

McBride, B.C. and Wolf, R. F., **1971**, *Biochem.*, 10, 4312.

Mehmet, A. and Te Riele, W.A.M., **1984,** In Ion Exchange Technology, D. Naden and M. Streat (Eds.), Ellis Horwood, London.

Menager, C. and Cabuil, V., **1995,** *J. Colloid Interface Sci.*, 169, 251.

Mielczarski, J. A., **1987**, *Surf. Sci.*, Vol. 187, pp 526-538.

Mielczarski, J. A. and Yoon, R. H., **1989**, *J. Phys. Chem.*, Vol. 93, pp 2034-2038.

Mielczarski, J. A., Zachvieja, J. B. and Yoon, R. H., **1990,** In SME Annual Meeting, Salt Lake City, Utah, Preprint, 90174, pp1-8.

Mielczarski, J. A. and Yoon, R. H., **1991**, *Langmuir*, Vol. 7, pp 101-108.

Mielczarski, J. A., **1993**, *J. Phys. Chem.*, Vol. 97, pp 2649-2663.

Miller, J. D. and Ishida, H., **1986**, In Silanes, Surfaces, and Interfaces, Proceedings of the Silanes, Surfaces, and Interface, Ed. by D. E. Leyden, Symposium, Snowmass, Colorado, June, 19-21, 1985, Gordon and Breach Science Publishers, New York, pp 525-544.

Mittal, K.L., Ed., **1992**, Silanes and other Coupling Agents, Utrecht, The Netherlands.

Molday, R. S. and Molday, L. L., **1984,** *FEBS Lett.*, 170 (2) 232-238.

Molday, R. S. and Mackenzie, D., **1982**, *J. Immunological Methods*, 52, 353.

Morrish, A.H., **1980**, In Crystals: Growth, Properties, and Applications, H. C. Freyhardt, Mgr. Eed., Vol.2, pp171-197, Springer-Verlag, New York.

Moses, P.R., Weir, L.M., Lennox, J. C., Finklea, H.O., Lenhard, J. R. and Murray, R. W., **1978**, *Anal. Chem.*, 50, 576.

Moulder, J. F., Stickle, W. F., Sobol, P. E. and Bomben, K. D., **1992,** Handbook of X-ray Photoelectron Spectroscopy, Perkin-Elmer Corporation.

Muramatsu, H., Dicks, J. M., Tamiya, E. and Karube, I.,**1987,** *Anal. Chem.* , 59, 2760.

Nemerow, N. L. and Dasgupta, A., **1991,** Industrial and Hazardous Waste Treatment, Van Nostrand Reinhold, New York, p 155.

Nicol, S. K., Galvin, K.P. and Engel, M.D., **1992**, *Mineral Engineering*, Vol. 5, pp 1259-1275.

Niwa, M., Katada, N. and Murrakami, Y., **1990**, *J. Phys. Chem.*, 94, 6441-6445.

Nordell, E., **1951,** Water Treatment, Reinhold, New York, p. 341.

Nunez, L., Buchholz, B.A. and Vandegrift, G.F.,**1995,** *Separation Science and Technology*, 30, 1455.

Olsvik, O., Popovic, T., Skjerve, E., Cudjoe, K.S., Hornes, E., Ugestad, J. and Uhlen, M., **1994**, *Clin. Microbiol. Rev.*, 7, 43.

Ondrus, D.J., Boerio, F.J. and Grannen, K.J., **1989**, *J. Adhes.*, 29, 27.

Pale-Grosdemange, C., Simon, E. S., Prime, K. L. and Whitesides, G. M., **1991**, *J. Am Chem. Soc.*, 113, 12.

Parekh, B.S., Ed. **1988**, REVERSE OSMOSIS TECHNOLOGY: Application for High-Purity-Water Production, Marcel Dekker, Inc..

Parikh, A. N., Allara, D. L., Azouz, I. B. and Rondelez, F., **1994**, *J. Phys. Chem.*, 98, 7577.

Parks, G. A., **1965**, *Chem. Rev.*, 65, 177.

Patsis, A.V. and Cheng, S. J., **1988**, *J. Adhes.*, 25, 145.

Patterson, J. W., **1995**, Industrial Wastewater Treatment Technology (2nd ed.), Butterworth Publishers, Stoneham.

Philipse, A. P., van Bruggen, M. P.B. and Pathmamanoharan, C., **1994**, *Lagmuir*, 10, 92-99.

Pinfold, T. A., **1972**, Ion Flotation, in Robert Lemlich (Ed.), Adsorptive Bubble Separation Techniques, Academic Press, New York.

Pirkle, W. H. and Pochapsky, T. C., **1989**, *Chem. Rev.*, 89, 347.

Plueddemann, E. P., **1985**, In Silane, surfaces, and Interface, (Ed), D.E. Leyden, Gordon and Breach Science Publisher, New York, pp 1-23

Plueddemann, E. P., **1982**, Silane Coupling Agents, Plenum Press.

Poling, G. W., **1969**, J. *Electrochem. Soc.:Solid State Science*, Vol. 116, No. 7, pp 958-963.

Pomerantz, M., Segmuller, A., Netzer, L. and Sagiv, J., **1985**, *Thin Solid Films*, 132, 153.

Prestidge, C.A., Skinner, W.M., Ralston, J. and Smart, R. St. C., **1995**, *Colloids and Surfaces*, 105, pp 325-339.

Qi, Z. G., **1995**, private communication at Department of Chemistry of McGill University.

Qi, Z. G., **1996,** Synthesis of Conducting Polyner Colloids, Hollow Nanoparticles, and Nanofibers, Ph.D. Thesis, Department of Chemistry, McGill University, Montreal, Canada.

Rao, S. R., Xu, Z. and Finch, J. A., **1995**, In Waste Processing and Recycling in Mineral and Metallurgical Industries II, Eds by S. R. Rao, L. M. Armaratunga, G. G. Richards and P.D. Konodos, CIM, Montreal, pp 69-77.

Rao, S.R., Amaratunage, L.M., Richards, G.G. and Kondos, P.D., Ed, **1995,** Waste Processing and Recycling in Mining and Metallurgical Industries II, Proceedings of the International Symposium, Vancouver, B.C., August.

Rieke, P. C., Marsh, B. D., Wood, L. L., Tarasevich, B. J., Liu, J., Song, L. and Fryxell, G. E., **1995**, *Langmuir*, 11, 318-326.

Rousseau, R. W. Ed, **1987**, Handbook of Separation Process Technology, John Wiley & Sons.

Rozenfeld, O., Koltypin, Y., Bamnoker, H., Margel, S. and Gedanken, A., **1994,** *Langmuir*, 10, 3919.

Rubin, A. J., Johnson, J. D. and Lamb, J. C., **1966**, *Ind. Eng. Chem. Process. Des. Dev.*, 5, 368.

Saito, S. (Ed.), **1988,** *Fine Ceramics*, Elsevier, Amsterdam,.

Sando, M., Towata, A. and Tsuge, A., **1995**, *Advanced Powder Technology*, Vol. 6, pp 149-158.

Sarid, D., **1991**, Scanning Force Microscopy: with Applications to Electronic, Magnetic and Atomic Force, Oxford University Press, Oxford.

Schlotter, N. E., Porter, M. D., Bright, T. B. and Allara, D. L., **1986**, *Chemical Physics Letters*, 132, 93.

Schrader, M. E. and Loeb, G. I. (Ed.),**1992**, *Modern Approaches to Wettability: Theory and Application*, Plenum Press, New York.

Scott, C., Ishida, H. and Maurer, F. H. J., **1991,** J. Reinf. Plast. Compos., 10, 463.

Sebba, F., **1959**, *Nature*, 184, 1062.

Sebba, F., **1960,** *Nature*, 188, 736.

Sebba, F., **1962a**, Ion Flotation, American Elsevier, New York.

Sebba, F., **1962b**, Proc/ Int. Conf. Coordination Chem., 7th, Sweden Paper 7J1.

Sebba, F., **1963**, Belg. Pat. 623,140.

Sebba, F., **1964**, Ger. Pat. 623,140.

Sebba, F., **1965**, Proc. A. I. Ch. E. I. Chem. E. Jiont Meeting, London, 1965 (1) 14.

Seyedmonir, S. R., Abdo, S. and Howe, R. F., **1982**, *J. Phys. Chem.*, 86, 1233.

Shafei, G. M. S. Et and Mokhtar, M., **1995**, *J. Colloid and Interface Sci.*, 175, 518-519.

Shih, W.H., Kisailus, D. and Wei, Y., **1995**, *Materials Letter*, 24, pp 13-15.

Simmons, G.W. and Beard, B.C., **1987**, *J. Phys. Chem.*, 91, 1143-1148.

Sivamohan, R., de Donato, P. and Cases, J. M., **1990**, *Langmuir*, 6, 637.

Skoog, D.A. and Leary, J, J., **1992**, Principles of Instrumental Analysis, Fourth Edition, Harcourt Brace College Publishers, New York, pp 568-571.

Smith, E. L., Alves, L. A., Andergg, J. W., Porter, M. D. and Siperko, L. M., **1992**, *Langmuir*, 8, 2707.

Sonti, S.V. and Bose, A., **1995**, *J. Colloid Interface Sci.*, 170, 575.

Spinke, J., Liley, M., Guder, H. J., Angermaier, L.,and Knoll, W., **1993**, *Langmuir*, 9 , 1821-1825.

Sprycha, R., Oyama, H. T., Zelenev, A. and Matijevic, E., **1995**, *Colloid Polymer Sci.* 273, pp 693-700.

Stumm, W. and Morgan, J. J., **1995**, Aquatic Chemistry, Jon Wiley & Sons, Inc., New York, p 804.

Tada, H., **1995**, *Langmuir*, 11, 3281-3284.

Thomas, T. E., Abraham, S. J. R., Blackmore, E. W. and Lansdorp, P. M., **1992**, *J. Immunological Methods*, 154, 245.

Tsugeki, K., Yan, S., Maeda, H., Kusakabe, K. and Morooka, S., **1994**, *Journal of Materials Science Letters*, Vol. 13, p 43-45.

Ugelstad, J., Berge, A., Ellingsen, T., Schmid, R., Nilsen, T. N., Mork, P. C., Stenstad, P., Hornes, E. and O. Olsvik, **1992**, *Prog. Polym. Sci.*, 17, 87.

Ulman, A. **1991**, An Introduction to Ultrathin Organic Film From Langmuir-Blodgett to Self-Assembly; Academic Press, Boston.

Urbain, O. M. and Stemen, W. R., **1941**, U.S. Patent 2,232,294.

Uvdal, K., Bodo, P. and Liedberg, B., **1992**, *J. Colloid Interface Sci.*, 149, 163.

van Oss, C. J., **1994,** Interfacial Forces in Aqueous Media, Marcel Dekker, Inc., New York.

Vandenberg, E., Elwing, H., Askendal, A. and Lundstom, I., **1991**, *J. Colloid Interface Sci.*, 143, 327.

Vansant, E. F., VanDerVoort, P. and Vrancken, K. C., **1995**, Characterization and Chemical Modification of the Silica Surfaces, Elsevier, Amsterdam.

Vigil, G., Xu, Z. H., Steinberg, S. and Israelachvili, J., **1994,** *Journal of Colloid and Interface Science*, 165, 367-385.

Volmer-Uebing, M. and Stratmann, M., **1992,** *Applied Surface Science*, 55, 19.

Vranchen, K. C., Van Der Voort, P., Gillis-D'Hamers, I., Vansant, E.F.and Grobet, P., **1992,** *J. Chem. Soc., Faraday Trans.*, 88, 3197.

Vrancken, K.C., De Coster, L., Van Der Voort, P., Grobet, P.J. and Vansant, E.F., **1995**, *J. Colloid and Interafce Sci.*, 170, 71-77.

Vrancken, K.C., Possemiers, K., Van Der Voort, P. and Vansant, E.F., **1995,** *Colloids and Surfaces*, 98, 235-241.

Waddel, T.G., Leyden, D. E. and DeBello, M.T., **1981,** *J. Am. Chem. Soc.*, 1981, 103, 5303-5307.

Walczak, M. M., Chung, C., Stole, S. M., Widrig, C. A. and Porter, M. D., **1991**, *J. Am. Chem. Soc.*, 113, 2370.

Wang, W. X., Xu, Z. H. and Finch, J. A., **1996**, *Environmental Science and Technology*, in press.

Whitehead, R. A. et al., **1987**, U.S. Patent 4,695,393.

Whitesides, G. M., Hill, C. L. and Brunie, J., **1976,** *Ind. Eng. Chem., Process Des. Dev.*, Vol. 15, No. 1, pp 226-227.

Williams, M. C. and Fuerstenau, D. W., **1987**, *Int. J. Miner. Proess.*, 20, 153-157.

Wood, R., Kim, D. S., Bsilio, C. I. and Yoon, R.-H., **1995**, *Colloids and Surfaces*, 94, 67.

Wooding, A., Kilner, M. and Lambrick, D., **1992,** *J. Colloid Interface Sci.*, 149, 98.

Xu, Z. H., Liu, Q. X., Ling, J. and Summers, A., **1996**, *Langmuir*, Vol. 12, No.2, pp 547-554.

Yang, J., Friberg, S. E., Sjoblom, J., Paatero, E. and Sundqvist, **1995**, *Colloids and Surfaces*, 104, 223-232.

Yen, S. P. S., Rembaum, A. and Landel, R. F., **1981**, U.S. Patent 4, 285, 819.

Yokoyama, T., Nakazato, T. and Tarutani, T., **1980**, *Bull. Chem. Sco. Jpn.*, 53, 850.

Yoon, R. H., Basilio, C. I., Marticorena, M. A., Kerr, A. N. and Stratton-Crawley, R., **1995**, *Minerals Enginerring*, Vol. 8, No. 7, pp 807-816.

Zhong, C. H. and Porter, M. D., **1994**, *J. Am. Chem. Soc.*, 116, 11616-11617.

Zhuravlev, L. T., **1993**, *Colloids and Surfaces*, 74 (1), 71.

APPENDICES

A-I RECIPES FOR SILICA COATINGS BY SOL-GEL PROCESS

Sol-Gel processing is based on the hydrolysis of TEOS in ethanol and ammonium hydroxides:

$$Si\text{-}(O\text{-}CH_2\text{-}CH_3)_4 + 2H_2O \overset{OH^-}{=} SiO_2 + 4CH_3\text{-}CH_2\text{-}OH$$

Suppose TEOS is fully hydrolyzed, then one mole of TEOS will form one mole of silica. Since the molecular weight and density of TEOS are 208.33 and 0.94, respectively, the weight percentage of added silica to the magnetic particles can be calculated as followings:

$$Wt\%\ (\frac{SiO_2}{Fe_2O_3}) = \frac{60 \times 0.94 \times TEOS(mL)}{Fe_2O_3(gram)} \times 100 = \frac{0.27 \times TEOS(mL)}{Fe_2O_3(gram)} \times 100$$

Coating experiments are conducted in a final volume of 60 mL of TEOS solution. If 0.2 mL of TEOS is used, the final concentration of TEOS will be 0.015 mole/L. The calculated results are summarized in Table A-1.

Table A-1 TEOS concentration and added silica levels[a]

TEOS (ml)	TEOS (mole/L)	γ-Fe_2O_3 (g)	wt% (SiO_2/γ-Fe_2O_3)
0.2	0.015	0.900	6
0.2	0.015	0.518	11
0.2	0.015	0.200	27
0.2	0.015	0.100	54

a: 6 mL ammonium hydroxide and 53.8 mL ethanol is used to make the final volume of 60 mL.

A-II RECIPES FOR DENSE LIQUID SILICA COATING

Aqueous Silica Solution: Take 22.2 mL of 27-wt% aqueous SiO_2, purchased from Aldrich, into a 100 mL volumetric flask, and dilute to 100 mL with Millipore water. This solution contains 1 M SiO_2 (i.e. 6 gram of SiO_2 in 100 mL water) because the molecular weight of SiO_2 is 60. The concentrated aqueous silica is corrosive and should be handled with extreme care. Don't store the concentrated aqueous silica solution in a glass flask for a long time. The gelation of aqueous silica solution may stick the cap onto the top. A fresh aqueous solution of silica should be used for each experiment.

Supersatuartion Level Control: Take 1 mL of 1 M of aqueous SiO_2 solution (0.06 g SiO_2, i.e. 0.001 morality) into a 99 mL aqueous solution containing 1 gram of magnetic particles (γ-Fe_2O_3) gives 1 x 10^{-2} M of SiO_2 in solution. This concentration is close to the solubility regime of aqueous silica in which the heterogeneous nucleation is favored (see Figure 5.3 in chapter 5) at pH around 9.5. In this case, the added silica level (percentage of silica added over γ-Fe_2O_3) is 6% (i.e. 0.06 g SiO_2/L γ-Fe_2O_3).

Silica Level Control: The added silica level is controlled by changing the weight of the magnetic particles used in the coating experiments, while maintaining the same concentration of aqueous silica in solution. As described in the supersaturation level control, the added silica level can be changed to 12 wt % if 0.5 gram of magnetic particles is used when keeping the same supersaturation level. The calculated silica levels are summarized in Table A-2.

Coating Experiments: The coating experiments are conducted in a three neck flask with mechanical stirring. The pH of the solution is monitored by a pH meter. One gram (or 0.55 gram, depending on silica level) of magnetic particles is mixed with 90 mL Millipore water. The slurry pH is about 5.6 but is then adjusted to 9.5 by adding sodium hydroxide solution. Then, the slurry is heated up to 90 ± 3 °C by putting the flask on

mantle. The temperature is controlled by adjusting the voltage adapter connected to the mantle. 1 M of aqueous silica solution is diluted to 0.1 M before being added to the slurry. 10 mL of 0.1 M aqueous silica is added concurrently with 0.3 M H_2SO_4 within 1 hour in order to maintain the slurry pH at 9.5. The reaction continues for one hour. The slurry is cooled to room temperature and centrifuged. The solid product is then washed three times with Millipore water and finally dried in a vacuum oven at 110 °C for 24 hours.

Table A-2 The calculated results of added silica and theoretically silica coating levels in DL process.

initial aqueous silica (M)	amount added (mL)	final volume (mL)	final silica concentr. (M)	γ-Fe_2O_3 added (g)	wt% (SiO_2/γ-Fe_2O_3)	Theoretical coated silica (%) [a]
0.1	10	100	0.01	0.55	10.5	8.10
0.1	10	100	0.01	0.40	15.0	11.25
0.1	10	100	0.01	0.22	27.2	20.45

a: Based on the limiting solubility of aqueous silica ca. 2.5×10^{-3}, the amount of silica that can be coated on magnetic particles theoretically will be (0.01-0.0025)*60/10=0.045 g. The coated silica can then be calculated based on the amount of magnetic particles used.

IMAGE EVALUATION
TEST TARGET (QA-3)

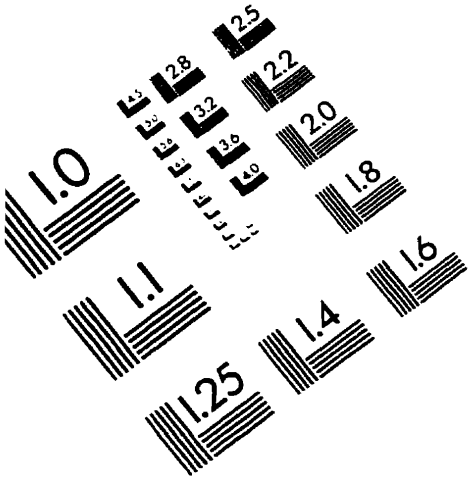

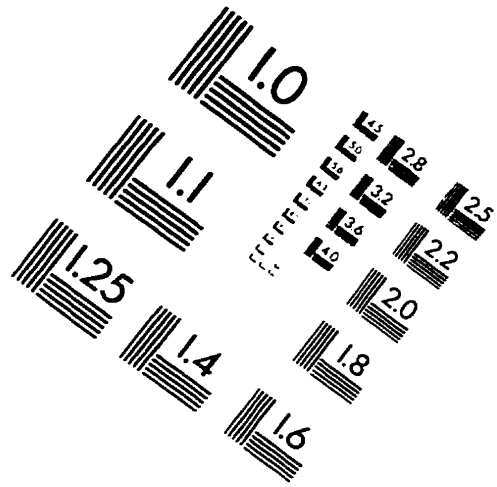

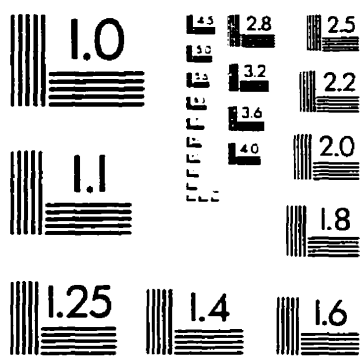

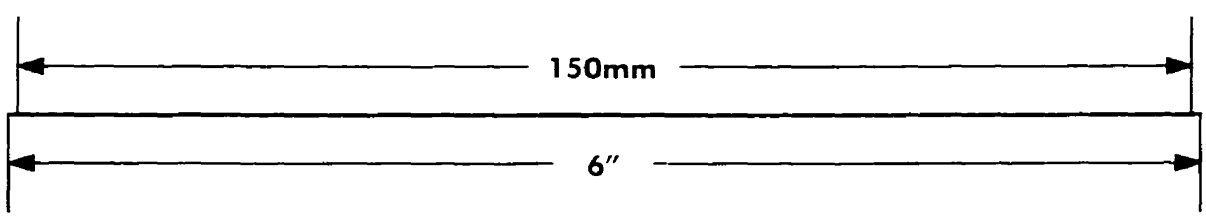

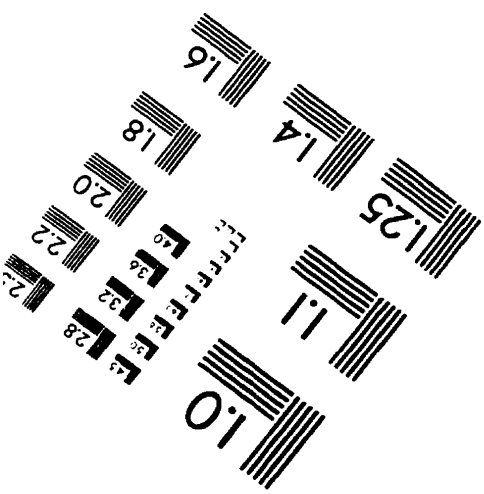

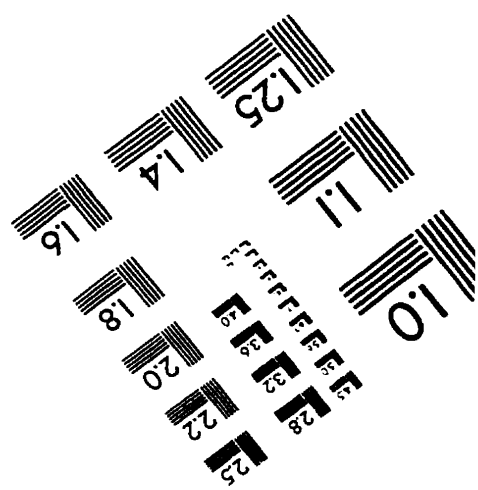

APPLIED IMAGE, Inc
1653 East Main Street
Rochester, NY 14609 USA
Phone: 716/482-0300
Fax: 716/288-5989